Norwegian University of Science and Technology

Master Thesis

Atomic force microscopy measurements of the surface and the interaction characterization to optimize the surface patterning for bacterial micro arrays

Author:
Ian Damm Muri

Supervisor:
Professor Bjørn Torger Stokke

A thesis submitted in fulfillment of the requirements for the degree of Master of science (Siv.ing) in Bionanotechnology

in the

Biophysics and Medical Technology research group
Department of physics

June 30, 2013

"Knowledge of what is, does not open the door directly to what should be. For every door that is being opened, two more will appear. Is the smallest thing in the world a little curl on nothing?"

Unknown

Acknowledgements

This thesis is submitted to the Department of Physics in the Norwegian University of Science and Technology (NTNU) in partial fulfillment of the requirements for the Master of Science in Nanotechnology. The work was carried out from January to June 2013. First of all I would like to thank supervisor Bjørn Torger Stokke for giving me the possibility to carry out the work presented in this thesis. I am grateful for all the information, assistance, and help that I've received during this work. Inspiring advices and helpful tricks has been a significant factor in the completing of my work that is being present in this thesis. I would also like to thank Astrid Bjørkøy, Gjertrud Maurstad, and Tatyana Sherstova for all the technical support and advices about the laboratory and the microscopy techniques. I am also indebted to researcher Katarzyna Maria Psonka-Antonczyk that have inspired to very helpful discussions, advices and comments that have helped me to explore this project fully. Constructive discussions and comments have inspired me to push the limits in this work. Next, I would like to thank Phd. candidate Nina Bjørk Arnfinnsdottir that are working in the field of this thesis presented. Thank you for all the given information, nice advices, discussions and common nanolab work. I have really appreciated our cooperation during this project and the open discussions about challenges or opportunities.

Then I would also like to thank to the nanolab people for inspiring nanolab courses and advices that have always been appreciated and taken into consideration when fabricating and characterizing samples. Last but not least, I also want to thank the people from Department of Physics for the nice socializations and nice lunch arrangements on Thursdays were cake or other types of meals were enjoyed.

Ian Damm Muri
Trondheim, June 2013

Contents

List of Figures

List of Tables

NORWEGIAN UNIVERSITY OF SCIENCE AND TECHNOLOGY

Abstract

The Faculty of Natural Sciences and Technology
Department of physics

Master of science (Siv.ing) in Bionanotechnology

Atomic force microscopy measurements of the surface and the interaction characterization to optimize the surface patterning for bacterial micro arrays

by Ian Damm Muri

This Master project was done in the Department of Physics at NTNU in the spring 2013. The project focus on the optimization of micro patterning techniques to produce micro arrays for single bacterial cell studies. The micro arrays are produced by controlling the surface chemistry and the spatial resolution of the two dimensional (2D) patterns in the micro or nanometer range. Such micro arrays of bacteria consist of a high number of spots of bacterial adhering molecules on a flat surface having a size that allows a single bacteria to be immobilized. Patterned surfaces that allows controlled and patterned adhesion of single bacteria can serve in a great number of applications. Studies of bacterial interactions are important to understand the mechanisms behind formation of biofilms, that is highly relevant for e.g. implants of medical devices. Understanding the bacterial interactions in heterogeneous populations are also relevant in the development of homogeneous populations that are engineered to respond to certain patterns in the environment. Micro arrays of homogeneous bacterial populations could then also function as e.g. cell based sensor device to detect pathogenic agents or toxins. It has also been an increasing interest for making single cell arrays of motile bacteria to be used as biomotors for micro or nanoscale systems.

This project explores the application of soft lithography for the preparation of patterned supports designed for the monitoring of bacterial population at the individual bacterial cell level. The surface functionalization are optimized in order to allow efficient transfer of anchoring molecules, as well a strong and stable bacterial immobilization, combined with high bacterial viability. The optimization are performed by measuring the interactions between the bacteria *DH5alfa* and bacterial adhesive or repulsive surfaces with atomic force microscope (AFM). The bacterial interactions with glass, bovine serum

albumine (BSA), poly-L-lysine (PLL), polydopamine (PDA), and Cell-Tak surfaces are assessed to find proper adhesive or repulsive molecules for the bacterial micro arrays. BSA are defined as bacterial repulsive molecule, while PLL, PDA, and Cell-Tak are characterized as bacterial adhesive molecules.

PLL and Cell-Tak were incubated on the glass surfaces while PDA and BSA were printed on the glass surface by the use of a flat poly(dimethysiloxane) (PDMS) stamp. The bacterial interactions with glass, BSA, PLL, PDA and Cell-Tak surfaces were found to have mean rupture forces of 0.13nN, 0.28nN, 1.22nN, 1.73nN, and 1.91nN, respectively. The mean rupture lengths were found to be 32nm, 24nm, 58nm, 65nm, and 108nm for glass, BSA, PLL, PDA and Cell-Tak surfaces, respectively. The immobilization of bacteria on the AFM tip were validated before and after AFM experiments by the use of fluorescence microscopy and scanning electron microscopy (SEM). The bacteria *DH5alfa* show to interact stronger with PLL, PDA and Cell-Tak surfaces than for glass and BSA surfaces. The bacterial interactions with Cell-Tak and PDA surfaces show to exhibit mean rupture forces that is higher than the mean rupture force for PLL surfaces. The bacterial interactions with Cell-Tak surfaces show also to have a mean rupture length value that is close to or larger than twice the mean rupture length value of bacterial interactions with glass, BSA, PDA, and PLL surfaces. PDA or Cell-Tak can then be defined optimal bacterial adhesive layers in bacterial micro arrays because of their larger mean rupture forces and lengths values than the PLL values. BSA can be characterized as bacterial inert or repulsive layer because of its small mean rupture force and length. The bacterial viability on PDA or Cell-Tak surfaces can be assessed by the use of the LIVE/DEAD Baclight Viablility Kit (Invitrogen, kit L7012) supplied by the company Life Technologies.

Since a cluster of bacterias are interacting with the bacterial adhesive or repulsive surfaces, it is unknown if the bacterial interactions with surfaces are dependent on the number of bacterias being immobilized on the tip. A higher accuracy of the AFM force measurements of the bacterial interactions with surfaces can be obtained by modifying the AFM tip with a colloidal glass bead as demonstrated by Beaussert et al. (Beaussart et al. 2013). This way of immobilizing and validating the presence of bacterias on the AFM tip minimize time consuming procedures of control measurements and SEM investigations of the AFM tip after the force measurements. The use of a simple, less time consuming and accurate AFM technique for bacterial force measurements would open up for the possibility to explore the bacterial interaction with the bacterial adhesive or repulsive surfaces as a function of the liquid medium, contact time or loading rate.

Lastly, the bacterial interactions with the Cell-Tak surface show to have extended rupture lengths with multiple force peaks obtained that indicates stretching and unfolding of the Cell-Tak proteins or the bacterial cell surface proteins. The combination of non-covalent interactions behind this bacterial adhesion is not clear, but it is assumed to involve electrostatic and hydrophobic interactions. As the AFM images shows that the Cell-Tak layer is non-uniform, further force measurements of bacterial interactions with Cell-Tak surfaces are suggested to be investigated. The investigation of bacterial interactions with the Cell-Tak surface should also consist of using alternative preparation methods of Cell-Tak proteins glass surfaces as micro contact printing or other incubation methods. To further optimize bacterial micro arrays and to investigate the factors involved in bacterial adhesion to bacterial adhesive or repulsive surfaces, characterization techniques like PeakForce QNM AFM mode supplied by the company Bruker, mapping using accumulated probe trajectories (MAPT) technique, or bacterial AFM force measurements would have the possibility to facilitate such investigations.

Sammendrag

Dette Master prosjektet ble utført ved Institutt for fysikk ved NTNU våren 2013. Prosjektet fokuserer på å optimalisere mikro strukturerings teknikker for å produsere micro mønstre for single bakterielle celle studier. Mikro mønstre er produsert ved å kontrollere overflatekjemien og den romlige oppløsningen av de to dimensjonale (2D) mønstrene i området mikro eller nanometer. Slike mikro matriser av bakterier består av et høyt antall flekker av bakterielle attraktive molekyler på en overflate som har en størrelse som tillater at enkle bakterier blir immobilisert. Mønstrede overflater som tillater kontrollert og mønstret hefting av enkle bakterier kan bli anvendt i mange sammenhenger. Studier av bakterielle interaksjoner er viktig for å forstå mekanismene bak dannelsen av biofilmer, som også er svært relevant for medisinske implantater. Forståelsen for bakterielle interaksjoner i heterogene populasjoner er også relevant i utviklingen av homogene populasjoner som er konstruert for å reagere på visse mønstre i miljøet. Mikro matriser av homogene bakterielle populasjoner kunne da også fungere blant annet som celle baserte sensorer som kan oppdage smittestoffer eller giftstoffer. Det har også vært en økende interesse for å anvende matriser av individuelle bevegelige bakterielle celler som biomotorer for mikro eller nanoskala systemer.

Dette prosjektet utforsker anvendelsen av myk litografi for å utarbeide mikro mønstrede plattformer utformet for å overvåke bakterie populasjoner på et individuelt bakterielt celle nivå. Funksjonaliseringen av overflaten optimaliseres for å tillate effektiv overføring av forankrings molekyler, samt en sterk og stabil bakteriell immobilisering, kombinert med høy bakteriell levedyktighet. Optimaliseringen er gjennomført ved å måle interaksjoner mellom bakterier av typen *DH5alfa* og bakterielle attraktive eller frastøtende flater med atom kraft mikroskopi (AFM). Bakterielle interaksjoner med glass, Bovine Serum Albumin (BSA), poly-L-lysin (PLL), polydopamine (PDA), og Cell-Tak overflater har blitt tolket for å finne passende attraktive eller frastøtende molekyler for bakterielle mikro mønstre. BSA er definert som bakterielt frastøtende molekyler, mens PLL, PDA, og Cell-Tak er karakterisert som bakterielt attraktive molekyler.

PLL og Cell-Tak ble inkubert på glassflater mens PDA og BSA ble stemplet på glassflaten ved hjelp av et flatt poly (dimethysiloxane) (PDMS) stempel. Bakterielle interaksjoner med glass, BSA, PLL, PDA og Cell-Tak overflater ble funnet å ha gjennomsnittlig brudd krefter på 0.13nN, 0.28nN, 1.22nN, 1.73nN og 1.91nN, henholdsvis. De gjennomsnittlige brudd lengdene ble funnet å være på 32nm, 24nm, 58 nm, 65 nm, og 108Nm for glass, BSA, PLL, PDA og Cell-Tak flater, henholdsvis. Immobiliseringen av bakterier på AFM spissen ble bekreftet både før og etter AFM eksperimentene ved bruk

av fluorescens mikroskopi og scanning elektron mikroskopi (SEM). Bakterien *DH5alfa* viser å intereagere sterkere med PLL, PDA og Cell-Tak overflater enn for glass og BSA overflater. De bakterielle interaksjonene med Cell-Tak og PDA overflater vise å utstille gjennomsnittlige brudd krefter som er høyere enn den gjennomsnittlige brudd kraften for PLL overflater. De bakterielle interaksjonene med Cell-Tak flater viser også å ha en gjennomsnittlig brudd lengde verdi som er nær eller større enn det dobbelte av de gjennomsnittlige brudd lengde verdiene av de bakterielle interaksjonene med glass, BSA, PDA, og PLL overflater. PDA eller Cell-Tak kan bli definert som optimale bakterielle attraktve lag i bakterielle mikro matriser på grunn av deres gjennomsnittlige brudd kraft og lengde verdier som er større enn PLL verdier. BSA kan karakteriseres som et bakteriell inert eller frastøtende lag på grunn av liten gjennomsnittlige brudd kraft og lengd. Den bakterielle levedyktigheten på PDA eller Cell-Tak overflater kan vurderes ved bruk av LIVE / DEAD Baclight Viablility Kit (Invitrogen, L7012 kit) levert av selskapet Life Technologies.

Siden en klynge av bakterier er i samspill med bakterielle attraktive eller frastøtende overflater, er det ukjent om de bakterielle interaksjoner med overflatene er avhengig av antall bakterier som blir immobilisert på spissen. Høyere nøyaktighet kan oppnås fra AFM kraft målingene av de bakterielle interaksjoner med overflatene ved å modifisere AFM spissen med en kolloidal glass perle (Demonstrert av Beaussert et al. (Beaussart et al. 2013)). Denne måten å immobilisere og bekrefte tilstedeværelsen av bakterier på AFM spissen minimiserer tidskrevende prosedyrer som kontrollmålinger og SEM undersøkelser av AFM spisser etter kraft målingene. Bruk av en enkel, mindre tidkrevende og nøyaktig AFM teknikk i bakterielle kraft målinger ville åpne opp for muligheten til å utforske bakterielle interaksjoner med bakterielle attraktive eller frastøtende overflater som en funksjon av innholdet i mediumet, kontakt tid eller trekk-hastighet.

Så til sist, bakterielle interaksjoner med Cell-Tak overflaten viser å ha forlenget brudd lengder med flere kraft topper som indikerer strekking og utfoldelse av Cell-Tak proteiner eller proteiner på overflaten av bakterie cellen. Kombinasjonen av ikke-kovalente interaksjoner bak denne bakterielle adhesjonen er ukjent, men det antas å involvere elektrostatiske og hydrofobe interaksjoner. Ettersom AFM bildene viser at Cell-Tak overflaten ikke er uniform, foreslåes det at ytterligere kraft målinger av bakterielle interaksjoner med Cell-Tak overflater blir undersøkt. Undersøkingen av bakterielle interaksjoner med Cell-Tak overflaten bør også bestå av å bruke alternative prepareringsmetoder for Cell-Tak proteiner på glassflater, som blant annet mikro kontakt printing eller andre inkubasjon metoder. For å ytterligere optimalisere bakterielle mikro mønstrer og undersøkingen av hvilke faktorer som er involvert i den bakterielle heftingen til bakterielle attraktive eller frastøtende overflater, kan karakterisering teknikker

som PeakForce QNM AFM modus levert av selskapet Bruker, mapping med akkumulert probe baner (MAPT) teknikker, eller bakterielle AFM kraft målinger gi mulighet til å utforske slike undersøkelser.

Chapter 1

Introduction

The field of micro- and nanotechnology has been widely used to develop tools for disciplines of sciences as biochemistry, biology and microbiology to gain knowledge about biomolecules, cell interactions, and their properties. Single cell studies are necessary to understand the fundamental issues in cell biology concerning cell-cell, cell-medium and cell surface interactions. Factors involved within the heterogeneity of cell colonies and the cells influence on each other can be uncovered by studying these fundamental issues.

Micro patterning techniques have shown promising possibilities in single cell studies by producing large two dimensional (2D) patterned surfaces of different chemical composition. Today such micro arrays are often used to screen large arrangement of antibodies, proteins or DNA [1]. The use of such screening has been applied in disease diagnosing, and drug development by performing genotyping and detecting sequence variations [1]. By controlling the surface chemistry, and the spatial resolution of the 2D patterns in the micro or nanometer range, micro patterning can be a practical tool to pattern viable bacterias on surfaces for single cell studies. These techniques can for instance be used to produce micro arrays of bacterias. Such micro arrays consist of a high number of spots of bacterial adhering molecules on a flat surface having a size allowing a single bacteria to be immobilized. Patterned surfaces that allow for controlled and patterned bacterial adhesion, even down to the level of a single bacterial cell, can serve in a great number of applications. Studies on bacterial interactions are particularly important for investigating the formation of biofilms that is highly relevant for implants of medical devices. Understanding the bacterial interactions in heterogeneous populations is also needed to develop homogeneous populations engineered for responding to certain patterns in the environment. Bacteria micro arrays of homogeneous bacterial populations could then function as e.g. cell based sensor device to detect pathogenic agents or toxins [2–4]. It has also been an increasing interest for making single cell arrays of motile bacteria

to be used as biomotors for micro and nanoscale systems. These motile bacterias are often involved in microfluidics to function as pumps or rotational biomotors to mix or transport fluids [5–7].

This presented project explores the application of soft lithography for the preparation of patterned supports designed for the monitoring of bacterial populations at the individual bacterial level. Micro contact printing is used to pattern surfaces with arrays of "islands" of bacterial adhering chemicals surrounded by chemicals that resist bacterial adhesion in order to produce single bacterial arrays. These arrays are intended to be used as a tool for the study of gene expression of attached bacteria by using genetically modified bacteria that produce green fluorescent proteins (GFP) when the expression of a certain gene is turned on. Absence or presence of fluorescence in the microarray can be continuously monitored by a confocal microscope, and the degree of gene expression can thus be studied. The elastomeric stamps are produced in the NTNU Nanolab using lithographic techniques. **The aim of this project is to optimize the surface functionalization in order to allow efficient transfer of anchoring molecules, as well a strong and stable bacterial immobilization, combined with high bacterial viability.** In order to optimize the bacterial adhesion in bacterial micro arrays Atomic Force Microscope (AFM) is used to both characterize printed micro arrays and to determine the interactions between the surface and live bacteria. The interaction between the surface and live bacteria can be quantified or measured by using AFM in a force spectroscopy mode, i.e. by measuring forces between surface and live bacteria attached to the AFM tip. By characterizing the printed micro arrays as well studying the interactions between live bacteria and the surface, it is possible to optimize the bacterial attachment and the bacterial mobility in micro arrays by choosing the proper bacterial adhesive or repulsive molecules. The bacterial adhesive molecules used in this project is of poly-l-lysine (PLL), polydopamine (PDA), and Cell-Tak^{TM}(Cell-Tak). The bacterial repulsive molecule used in this project is bovine serum albumine (BSA). An illustration of the bacterial microarray that is being optimized and the experimental setup can be seen in figure 1.1

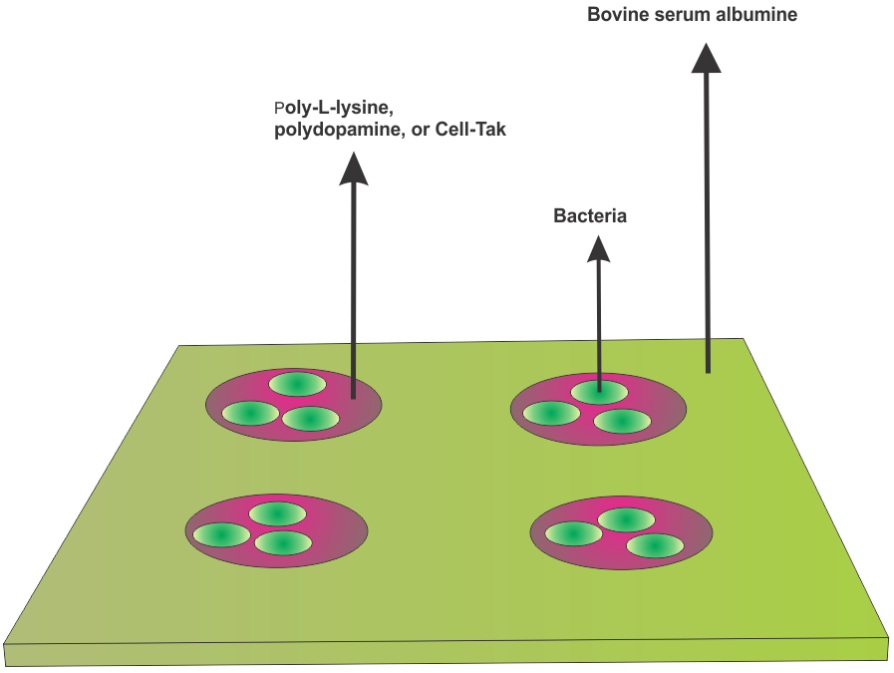

(A) Illustration of micro contact printed surfaces for bacterial micro arrays. Bovine serum albumine (BSA) represent the bacterial repulsive molecules and poly-l-lysine (PLL), polydopamine (PDA), or Cell-Tak represent the bacterial adhesive molecules. The micro arrays aim to attach 1 bacterias per "island"

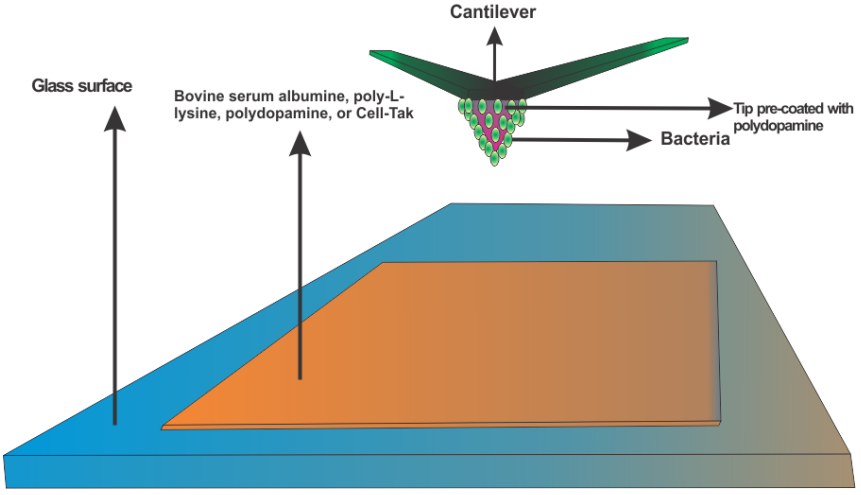

(B) Illustration of the experimental setup to optimize the bacterial attachment in microarrays by choosing the proper bacterial adhesive or repulsive molecules. The AFM operates with a PDA coated tip with multiple bacterias attached to it. The tip with immobilized bacteria is approaching the PLL, PDA, Cell-Tak or BSA surface until it is in contact making it possible for the bacteria and surface to interact via making bonds. After contact, the cantilever is retracting and forcing the interaction bonds to rupture. The AFM setup is measuring the interaction forces between the bacteria and the surface

FIGURE 1.1: Illustration of a bacterial micro array, and an experimental AFM setup to investigate how different protocols of bacterial attachment occurs

Chapter 2

Micro array technology; pattern biomolecules or cells

2.1 Photolithographic techniques

Geometrical shapes can be transferred to the surface of a wafer or substrate by the use of the photolithographic process. It is widely used in semiconductor industry for the patterning of metals in electronic circuits. It has also been used for micro patterning of proteins [1, 8–10]. The patterns are generated by using light, a photo mask, and a light sensitive photoresist that is able to either depolymerize or polymerize when exposed to light. The photoresist is applied as a thin layer on the surface of the substrate and selectively exposed to ultraviolet (UV) light through photo mask containing patterns. After exposure the photoresist is developed, exposing a pattern on the surface that is either a positive or a negative of the photo mask depending on the type of resist used. Positive photoresist depolymerize when exposed to UV-light and becomes more soluble in a developer solution than the unexposed areas of photoresist. For negative photoresist, the exposed areas polymerizes and becomes more insoluble in developer solution than the unexposed areas of the photoresist.

Patterned photoresist can be used to fabricate Poly(dimethysiloxane) (PDMS) stamps used for soft lithography (See section 2.2). The patterned photoresist can also be used to fabricate micro patterns of molecules by using a lift-off process. This involves a deposition of a material on the surface of the patterned photoresist. Lift-off follows after deposition. The lift-off is a process where the sample of photoresist and deposited materials undergoes sonication in a solvent to remove the photoresist, that is leaving the deposited molecules on the surface only [1, 8–10]. This is illustrated in figure 2.1.

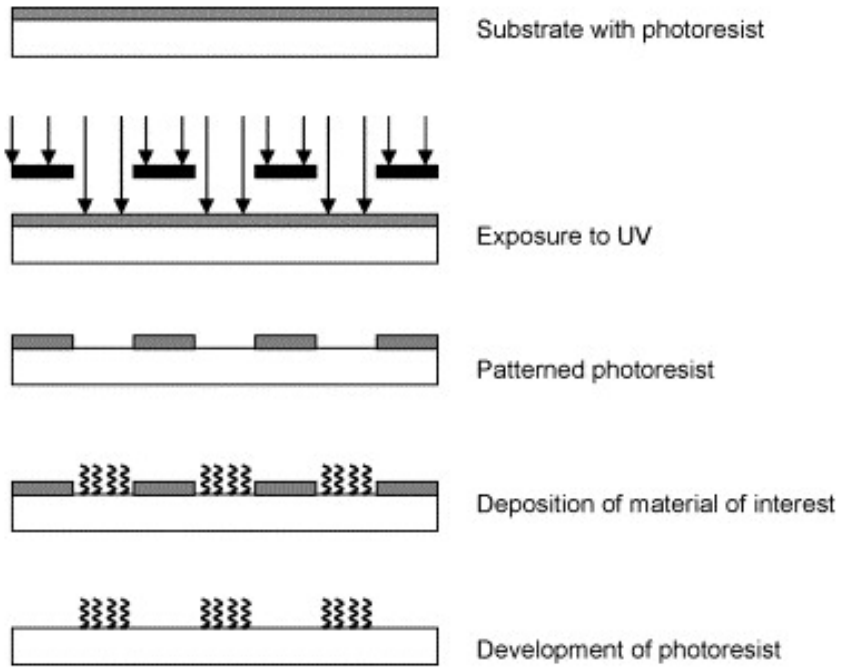

FIGURE 2.1: Schematic of photolithography procedure[8]

Lithography techniques can produce patterns with submicron resolution and have the possibility to achieve nanometer resolution by the use of electron beam lithography (EBL) [8, 11]. Instead of UV-light, an electron beam can be used to pattern the resist on the substrate. The patterns of nanometer resolution is achievable since the wavelength of electrons is smaller than the wavelength of UV-light. EBL is mostly used to make replica molds but has also been reported to pattern polyethylene glycol (PEG) hydrogels on microscope slides [11, 12]. Some drawbacks of EBL is high costs, low throughput, complicated experimental conditions, and incapability of direct patterning of a surface with biomolecules because of the high energy in the electron beam. Photolithography, gives a high throughput, even though it needs cleanroom techniques and chemicals that can denature biomolecules as well be toxic to cells [9].

2.2 Soft lithography and Micro contact Printing

Soft lithography is a lithography technique that involves the use of a patterned elastomer as the mask, stamp, or mold. A master mold is made using UV or electron beam lithography and this mold is used to produce patterned elastomer surfaces. This patterned elastomer surface can be used for e.g. in micro contact printing, where the elastomer stamp is used to transfer chemicals onto surfaces in order to pattern them.

Poly(dimethysiloxane) (PDMS) is usually used as the elastomer since it is commercially available, cheap, flexible, transparent, and a thermally curable elastomer. The patterned elastomer is produced by mixing a prepolymer and a cross linking agent that is then poured into a master mold and incubated at high temperature for curing. When cured, the stamps are peeled off the mold ready to be used for soft lithography. This process is illustrated in figure 2.2b. Both the master mold and the PDMS stamps are reusable which minimizes the use of cleanroom techniques. Soft lithography is used without toxic additives or denaturing chemicals, and serves in general as an effective, cheap and convenient method to produce micro arrays of molecules or cells. Typical soft lithography techniques are microfluidic pattering, stencil pattering and micro contact printing (μCP) [8, 9]. These soft lithography techniques can be seen in figure 2.2.

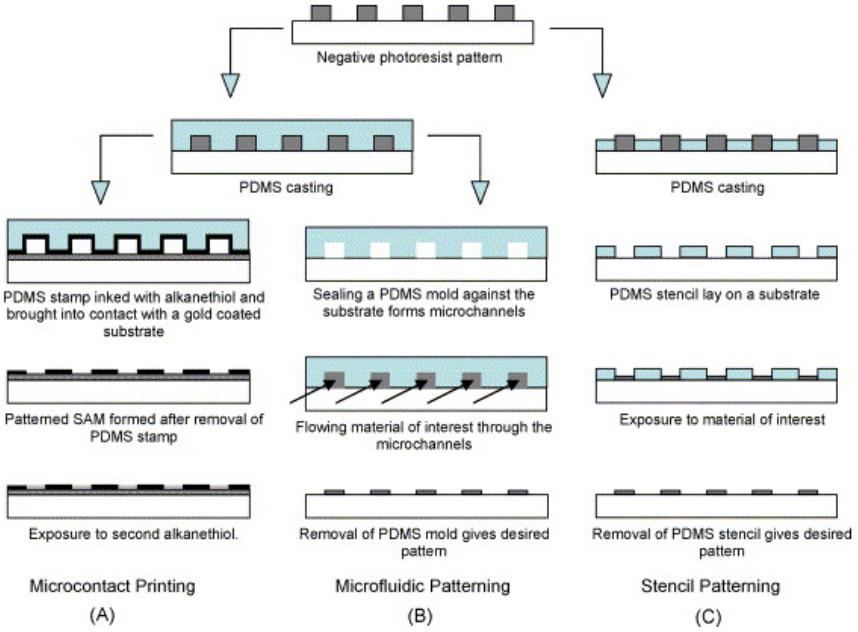

(A) Procedure of Soft lithography techniques [9]

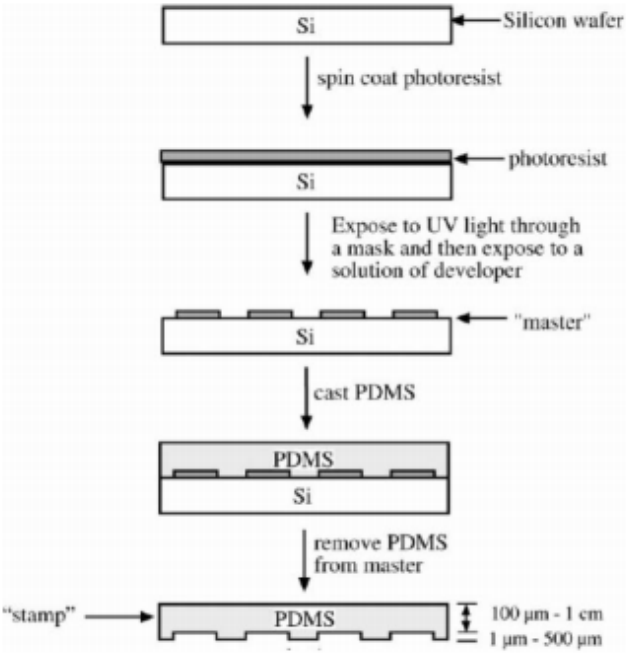

(B) Fabrication of PDMS stamp for μCP[8]

FIGURE 2.2: Schematics of the fabrication of PDMS stamps to be used in soft lithography, and the procedure of μCP, microfluidic patterning, and stencil patterning [8, 9]

In microfluidic patterning, the process of transferring molecules is performed by sealing the patterned PDMS to the substrate surface making microfluidic channels or networks with the substrate. Fluid is injected in the channels to make patterns on the surface. In stencil patterning, PDMS is spun on the mold not fully covering the upper structure of the mold. Holes will be created in the thin film of PDMS and after curing the holed PDMS can be placed on the substrate surface. The holed PDMS leaves part of the substrate exposed, making it possible to pattern biomaterials of interests. This is illustrated in figure 2.2a. The exposure of cells or biomolecules on the holed PDMS will appear as spots on the substrate after the PDMS is removed. In μCP, the patterned surface of the PDMS stamp is incubated in a solution of certain molecules of interests and stamped on a substrate. From figure 2.2a the incubated solution is the "ink". The molecules ability to assemble on the surface of the substrate is dependent on the chemical composition of the "ink", chemical composition of the stamp, and the stamping time. The stamp is dried before it is pressed onto the substrate surface. When the stamp is removed, the molecules are left as a pattern on the substrate. A great variety of molecules have been successfully patterned with μCP. Among others, molecules like antibodies, DNA, self assembled monolayers (SAM), and polycationic (co)polymers have been successfully transferred from the stamp to the substrate[8, 9]. The hydrophobic nature of PDMS has limitations in binding certain molecules or "ink" with hydrophilic tendencies. To enhance the binding ability between the PDMS and the "ink", PDMS can be treated with oxygen plasma to reduce the hydrophobicity of its surface. In general, soft lithography technique has shown to be a versatile method for patterning biomolecules, since a variety of molecules and substrates is compatible with this technique.

2.2.1 Printed micro arrays of bovine serum albumine (BSA) and poly-l-lysine (PLL) made by μCP

Some produced micro arrays of bacterial adhesive and repulsive surfaces are presented in this section as a supplement to the idea of assessing how different protocols of bacterial attachment occurs. In a project carried out at the Biophysics and Medical Technology research group at the Norwegian University of Science Technology-Department of Physics, μCP have been used to print bacterial adhesive and repulsive molecules as PLL and BSA. BSA and PLL have been tagged with fluorescent probes so they become visible in a fluorescent microscope. AFM has also been used to characterize the of topography printed surfaces. Figure 2.3 shows some images obtained of the printed patterns of BSA and PLL made by μCP

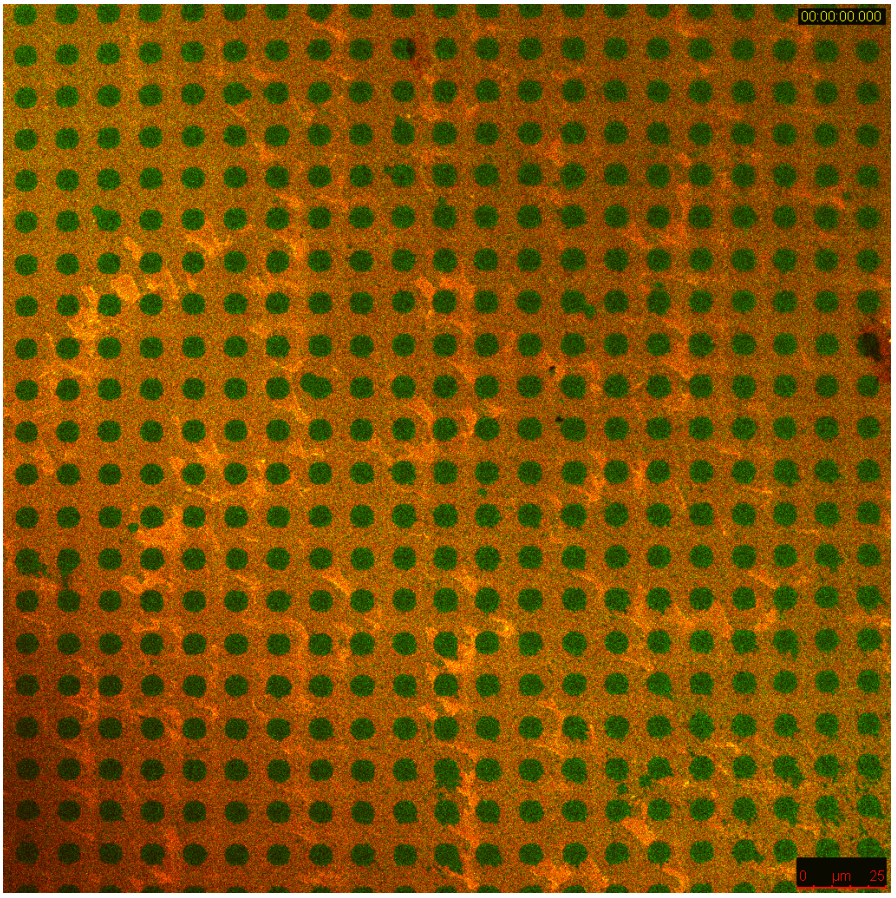

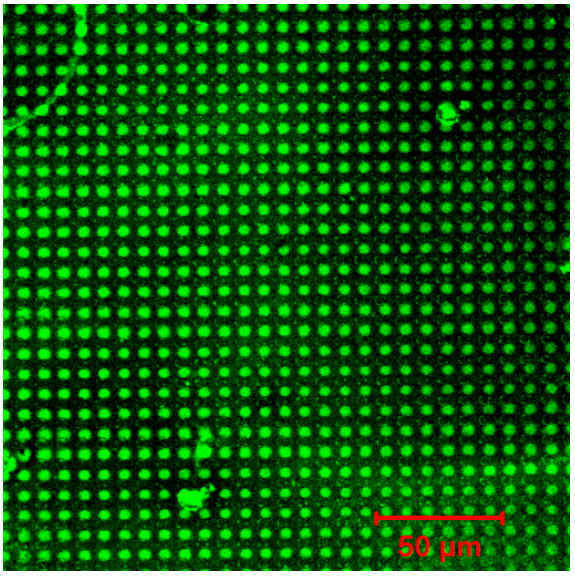

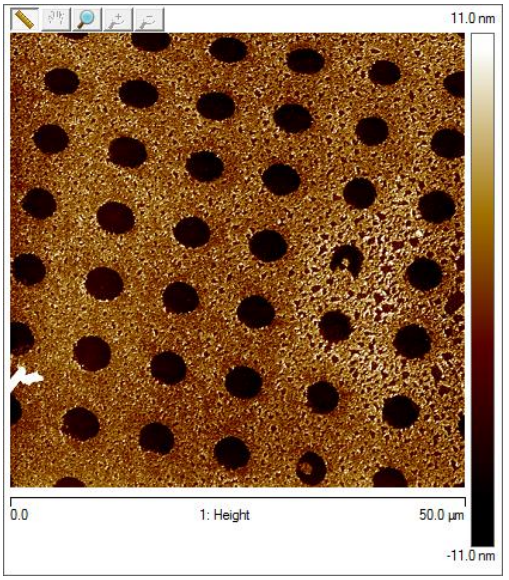

FIGURE 2.3: Images of printed BSA on a PLL layer made by μCP. The image at the top and bottom left were obtained with a fluorescent microscope, while image to the bottom right were obtained with an AFM. The printed surfaces were made within the Biophysics and Medical Technology research group at the Norwegian University of Science and Technology-Department of Physics [13, 14]

Chapter 3

AFM for assessing bacterial interactions and characterizing surfaces to optimize bacterial micro arrays

3.1 AFM setup for imaging and force measurements:

As mentioned in Chapter 1 and 2, μCP can be used to print bacterial repulsive molecules on a layer of bacterial adhesive molecules with intention to produce bacterial micro arrays. BSA molecules would then function as a bacterial repulsive layer, while Cell-Tak, PDA, or PLL molecules would function as a bacterial adhesive layer. To investigate the bacterial interactions to these bacterial adhesive or repulsive surfaces, AFM serves as an ideal tool with intention to characterize interactions and surfaces. AFM is a technique with possibilities to detect attractive and repulsive forces between a sharp or biofunctionalized tip and the surface of a sample. The forces measured are in the nanonewton range and are due to the interaction between a cloud of electrons in the atoms that constitutes the sample and the tip. These forces include mechanical forces, Van der Waals forces, capillary forces, chemical bonding forces, electrostatic forces, magnetic forces, brush interactions, elastic interactions, or specific binding forces. Information about the topography of the surface, the texture, and the viscoelastic properties is also possible to obtain. Main parts of the AFM design are; 1.The piezoelectric scanner responsible for moving the sample or the tip, depending on the AFM configuration, in a very accurate and defined manner. 2.The cantilever with attached tip that is moved over the sample surface that is influenced by the attractive or repulsive forces between its apex and the

surface itself resulting in the tip deflection. 3.The optical detection setup with the feedback system[15]. The AFM parts and feedback system are illustrated in figure 3.1.

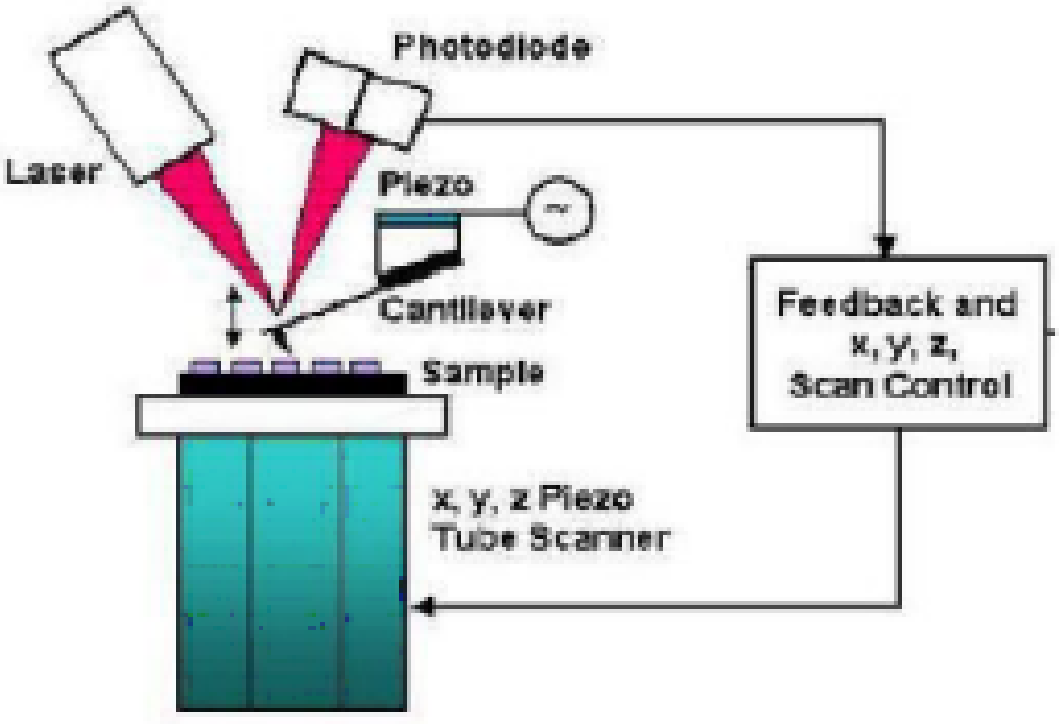

FIGURE 3.1: Illustration of the main parts of an AFM system [15]

The tip is raster scanning the surface and while scanning it is influenced by the interactions that cause its deflection. Laser path changes and this change is recorded in the photodiode. This change is also used in a feedback system to correct the position of the piezo scanner stage. AFM instruments usually have a setup were the feedback system is connected with either a movable piezo tube scanner or a movable piezo cantilever holder. Considering the deflection of the cantilever as a result of the interactions with the sample surface in figure 3.2, in position 1, at relatively large distances attractive forces are too small to exert a significant force between the clouds of electrons in the atoms of the tip and the sample. When reaching position 2 at a relatively smaller distance, the force is increasing rapidly. At very small distances, force still increases until actual contact is reached in position 3. In the contact region in position 4 the cantilever bends out and straightens again, unless the sample is very rigid and easily deformed. In position 5 the force between the sample and tip is close to zero. The tip is forced further towards the sample in position 6, and the cantilever starts to bend in the opposite direction.

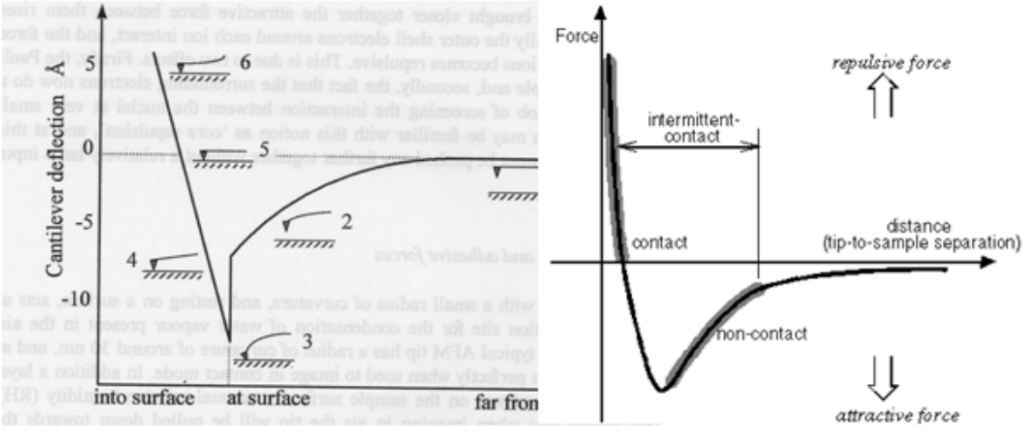

FIGURE 3.2: Graph of attraction and repulsion interactions as a function of the distance between tip and sample [15]

The relationship between the deflection of cantilever as a result of its interactions with the sample surface can be described by Hooks law,

$$F = -kd \tag{3.1}$$

where F is the force, k is the spring constant of the cantilever, and d is the deflection of the cantilever. The spring constant can be calculated based on the dimensions of a cantilever and the mechanical properties of the material it is made of [15].

3.1.1 Imaging modes

AFM can operate in contact, oscillating non-contact and oscillating tapping mode. In contact mode, the tip is in physical contact with the sample separated only by a few Ångstrøm within an interactive region as indicated in figure 3.2. Contact mode can be performed with a constant force exerted by the cantilever or a constant height of the piezoelectric scanner. Constant force conditions can obtain topography images by detecting the deflection of the cantilever and the feedback system by moving the piezoelectric scanner in the z-direction to maintain a constant force between tip and sample. The z-values being collected by the piezoelectric scanner determines the image. With a constant height of the piezo electric scanner, the deflection of the cantilever gives information about the topography of the samples. Figure 3.1 illustrates the AFM system and the feedback loop.

In oscillating mode, the cantilever is forced to oscillate at an operated controlled frequency that is close to its resonance frequency. The tuning of this operated control frequency is performed by using the piezo stack to excite the cantilever at different

frequencies to find its resonance frequency domain. When the tip is approaching the specimen, the topography of the sample can be determined by the change in the oscillations made by the force fields that is altering the oscillating amplitude, phase or frequency. The measurements can be performed with constant height or constant resonance frequency similar to that being used in the contact mode with its feedback system. Using the frequency modulation, changes in the oscillation frequency gives information about the tip-sample interactions. While using the amplitude modulation, changes in oscillating amplitude or phase provide the feedback signal for imaging. In the case of oscillating non-contact mode, the distance between tip and sample is of several hundreds of Ångstrøm with a frequency slightly above its resonance frequency. The forces measured are in range of piconewtons, where changes in the resonance frequency or vibration amplitude is detected. In the case of oscillating tapping mode, the tip is oscillating with its resonance frequency in air and is positioned above the surface so it only taps the surface for a very small fraction of its oscillating period. The short time that the tip is in contact with the sample reduces the lateral forces exerted during the raster scanning. The phase or amplitude error contrast images as well the topography of the height of the specimen can be obtained while using oscillating tapping mode. This mode has the possibility to detect variations in the composition, adhesion, friction, viscoelasticity, and other properties. The AFM feedback loop is operated so that the phase or amplitude error is monitored while the topographic image is being taken, i.e. the images of topography, phase, and amplitude error can be collected simultaneously[15, 16]. The mechanism of the oscillating tapping mode with a phase monitored signal is illustrated in figure 3.3.

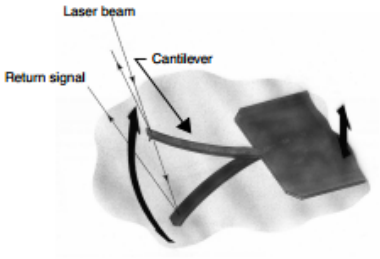

(A) Tapping cantilever in free air

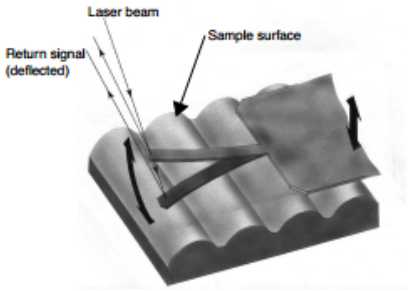

(B) Tapping cantilever on a sample surface

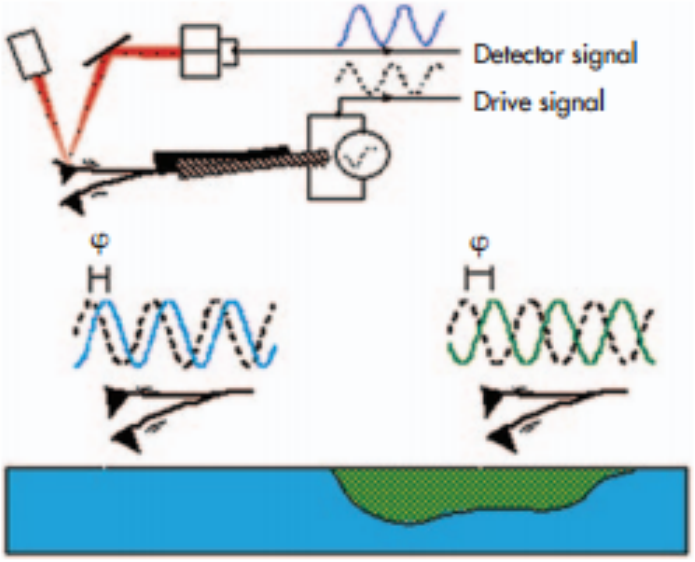

(C) Phase imaging

FIGURE 3.3: Schematic of tapping cantilever and phase or amplitude error imaging [16]

The vertical resolution is limited by the thermal noise generated by the cantilevers vibration, and therefore the minimum height or force differences that can be detected by a cantilever depends on its spring. The lateral resolution depends on the geometry of the tip, the elastic properties of the sample, and the eventual height differences. Scanning with a sharp tip having a high aspect ratio is important to obtain high and optimal lateral resolution that are real images.

3.1.2 Surface roughness analysis with AFM:

Surface roughness analysis are statistical values calculated according the relative heights, phase or other values of each pixel in the AFM image. Most commonly used roughness statistics are average roughness (Ra) or root mean square averages (Rq) of the AFM

image values. Ra and Rq are represented in equation 3.2a and 3.2b,

$$R\mathrm{a} = \frac{1}{N}\sum_{i=1}^{N}|Z\mathrm{i}| \tag{3.2a}$$

$$R\mathrm{q} = \sqrt{\sum_{i=1}^{N}\frac{Z\mathrm{i}^2}{N}} \tag{3.2b}$$

where N is number of points in the image or the selected region in the image, and Zi is the current Z value[17].

3.1.3 The piezo electric scanner

The scanners used in AFM are made from a piezoelectric material which expands and contracts proportionally to an applied voltage. The piezoelectric actuators in the scanner are being used to move the sample relatively to the stationary tip or to move the tip relatively to the stationary sample and requires high resolution movements of the position in three orthogonal directions in a cartesian coordinate system. The scanner is constructed by combining independently operated piezo electrodes for X, Y, and Z into a single tube. The schematic of the scanner and the piezo electric effect of the material can be seen in figure 3.4.

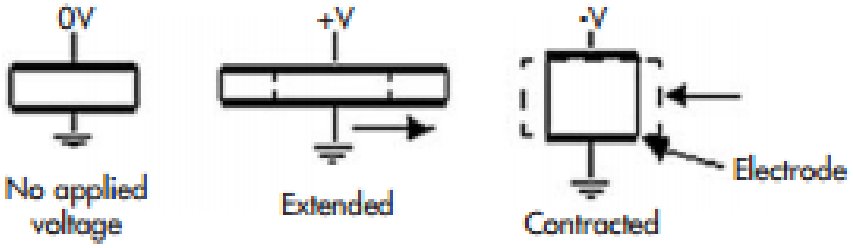

(A) The effect of applied voltage on a piezoelectric material

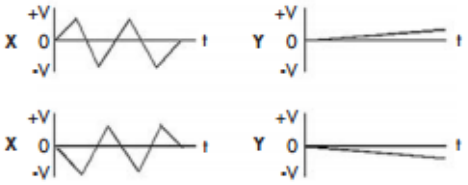

(B) Waveforms applied to the piezo electrodes during a raster scan with X-axis as the fast axis

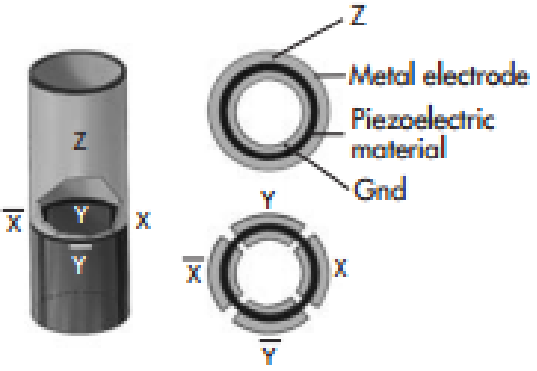

(C) The piezoelectric scanner with X-Y-Z configurations. AC signals applied to conductive areas of the tube piezo movement along the three major axes

FIGURE 3.4: Illustrations of the mechanisms in the piezoelectric scanner [15, 16]

The AFM Multimode manufactured by Bruker have usually three types of piezo electric scanners used called the J, E and A scanner that refers to the maximum scan size of 125μm x 125μm, 10μm x 10μm and 0.4μm x 0.4μm respectively [15, 16].

3.2 Dynamic force measurements with AFM and the calibration process

AFM as a force probe for dynamic force measurements can be conducted in liquid, which makes it suitable for live cells experiments. Force-distance curves can be acquired by ramping the piezo along the axis perpendicular to the surface. The smallest force to be measured is dependent on having a small spring constant of the cantilever, but this is also limited by the noise introduced on the cantilever that is a result of thermal fluctuations. De-adhesion and bond strengths of the force-distance curves can be displayed by operating a software made for analyzing the output signals. Force-distance curves are often obtained in contact mode where the tip is approaching and retracting on a sample with a certain loading rate, loading force and contact time with the surface. Considering the approach and retract schematics in figure 3.5, the force curves consist

of a non-contact region were the probe is off the sample and a contact region where the probe is in contact with the surface.

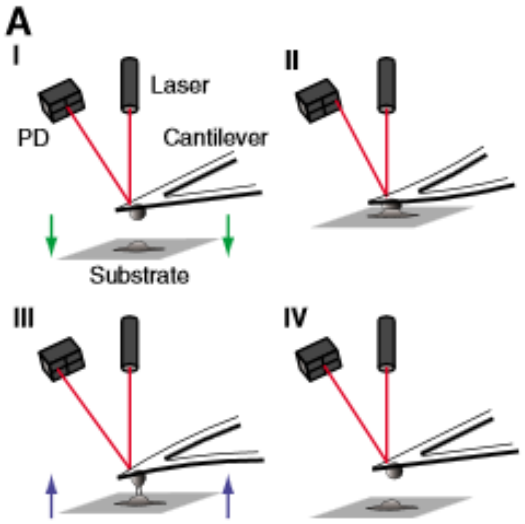

(A) Illustration of approach and retract mechanism with a cell attached to the cantilever

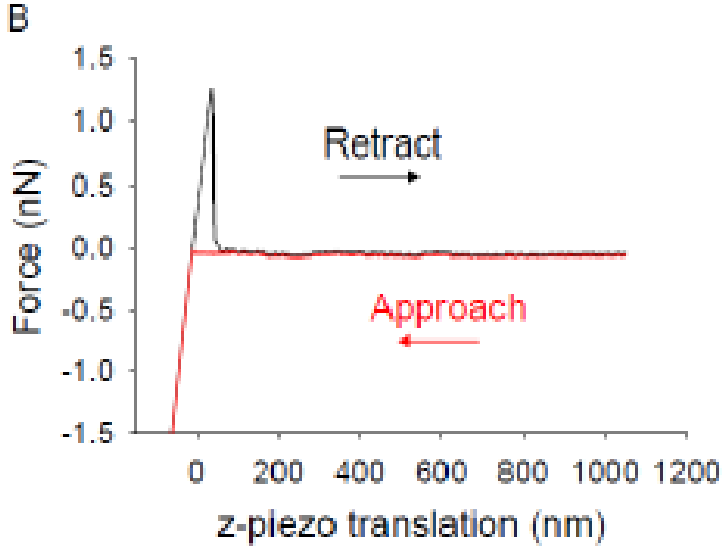

(B) Illustration of force-distance curves for approach and retract

FIGURE 3.5: Schematic illustration of approaching and retracting with AFM [15, 18]

The interactions for the approach curve are similar to what is described for figure 3.2. In the contact region, the probe is under a certain loading force for a certain contact time. Loading force is the force applied when indenting a certain sample surface (from figure 3.5b loading force is 1.5nN), and contact time is the time the tip is in contact with the surface under a certain loading force. When retracting the probe the cantilever exceeds the tip-sample adhesion force, and the probe jumps out of contact. The magnitude of this jump is used as a measure of the adhesion force or the rupture force. Multiple

jumps occurring in these force-distance curves can be explained as specific interactions in certain dynamic force measurements. The use of different loading rates influences the unbinding events and the magnitude of the force-jumps since this is changing the energy landscape of the unbinding processes [19]. The loading rate can be described as a linear rise of force with time having an expression of,

$$r_{\mathrm{f}} = kv_{\mathrm{t}} \tag{3.3}$$

where r_{f} is the loading rate, v_{t} it the separation speed, and k the transducer spring constant [15]. To obtain quantitative force-distance curves the spring constant has to be known, as well as the relationship between the photo-diode output voltage and the force obtained as a result of the cantilever deflection. As mentioned above, the relationship between the deflection of the cantilever and the sample can be described by Hooks law,

$$F_{\mathrm{z}} = -k\alpha V_{\mathrm{deflection}} \tag{3.4}$$

where F_{z} is the force that causes cantilever deflection in z direction (perpendicular to the surface), k is the spring constant of the cantilever, α is the deflection sensitivity in nm/volt and $V_{\mathrm{deflection}}$ is the measured deflection of the cantilever in volt. The cantilevers spring constant can be obtained by using its thermally driven fluctuations, and can be described by using the equipartition principle that forms equation 3.5,

$$\frac{1}{2}k < z^2 >= \frac{1}{2}k_{\mathrm{B}}T \tag{3.5}$$

where $< z^2 >$ is the deflections in the frequency domain around resonance, k_{B} is the Boltzmanns constant, and T is the temperature in Kelvin [15]. The deflection sensitivity involved in equation 3.4 is obtained by bringing the cantilever in contact with a hard substrate that is flat and observing the linear relation in the readout of the split photo-diode and the z-displacement of the calibrated scanner. This allows a conversion from the electrical signal to the deflection in nm of the cantilever. An illustration of the photo-diode system is shown in figure 3.6. The electrical signal of the cantilever deflection can be described by measuring differences in the signal from the photodetector segments,

$$F_{\mathrm{deflection}} = \beta[(I_{\mathrm{upperleft}} + I_{\mathrm{upperright}}) - (I_{\mathrm{lowerleft}} + I_{\mathrm{lowerright}})] \tag{3.6}$$

where $F_{\mathrm{deflection}}$ is the electrical signal in voltage from the deflection, β is the displacement coefficient, and I_{segment} is the laser intensity in volts of the different segments of the photodetector [15].

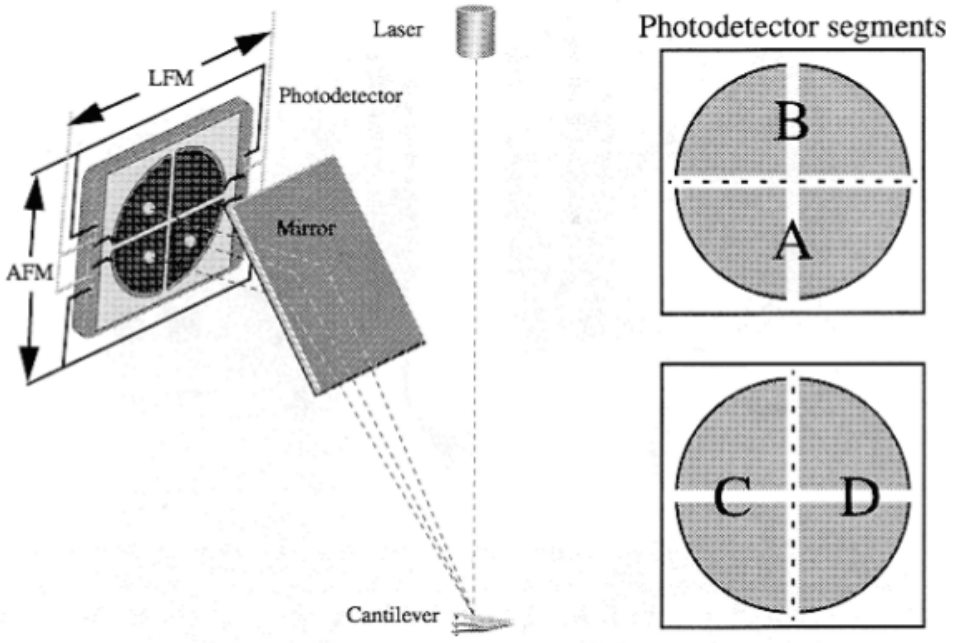

FIGURE 3.6: Illustration of detector system with four segments of photo-detectors. Upperleft, upperight, lowerright, and lowerleft [15]

3.2.1 Assessing dynamical force measurements of bacterial interactions

As mentioned above, the jumps in the force-distance curve are characterized as a adhesion forces or rupture forces, and the adhesion rupture force of the binding can be measured by the magnitude of the jump in the curve. The unbinding events are a stochastic processes, and the reliable quantification of the adhesion forces requires obtaining multiple individual force curves. The quantification of rupture force requires multiple individual force-distance curves because of the kinetics of bond dissociation where the thermal impulses in liquids are at a smaller scale ($< 10^{-12}$s) than the processes that are observed in the force-distance curves (experiment process with period of 10^{-4}s to minutes will have thermal impulses influencing the dissociation events). The collecting of the interaction forces of the multiple force-distance curves in a histogram will provide the main output data for the force spectroscopy measurements. Bacterial interactions are usually measured in AFM by having bacteria immobilized on the sample surface or having bacteria immobilized on the tip. The latter configuration makes it possible to use a single bacterial cell to probe different sample surfaces [20]. This probing can also be performed as a function of environmental conditions as temperature, pH, or ionic strength. As the resolution of force measurements for AFM is in

range of 10pN to nN, it has shown to be a useful technique for many microbial related experimental investigation. Typical investigations consist of bacterial adhesion to pig gastrin mucin, or other (bio)material surfaces of interests. These investigation are with intention to engineer or to enhance bacterial adhesion or repulsion to certain surfaces for medical or industrial use. The most suitable molecules used for functionalizing the tip for bacterial immobilization has reported in these experiments to be poly-L-lysine (PLL), polyethyleneimine (PEI), or polydopamine (PDA) [21–26]. These molecules are suitable in a way that the bacteria are viable under the experimental conditions as well as the interaction force between bacteria and AFM tip are stronger than the bacteria interaction with the surface, which also depends on the bacteria interactions with the surface.

Concerning the study of bacterial interaction to optimize the bacterial attachment in micro arrays, the main output used as an indicator to assess the bacterial interactions is focused on the rupture force or the rupture length. Microbial cell development, cell viability, and metabolic activity have shown to be strongly affected by cell adhesion, which also represents the initial step in the formation of a biofilm [27]. A few novel techniques that are using a viable cell as a probe in dynamic force measurements have recently been explored. In a single-cell force spectroscopy (SCFS) technique called fluid force microscope (FluidFM) demonstrated by Potthoff et al.[28] the pace of force measurements was accelerated up to 200 yeast and mammalian cells per probe. This high-throughput SCFS technique recorded statistically relevant data in a rapid manner. They showed adhesion force to be linearly correlated with the performed work throughout 9 hours of adhesion measurements, which is consistent and expected for conventional SCFS [28]. As this is generalized to be universal for most cell adhesions, the adhesion force or adhesion work can individually be used as indicators of the bacterial interactions with certain surfaces. In another SCFS demonstrated by Beaussart et al.[29] a colloidal glass bead was glued to a cantilever and then coated with polydopamine. A single bacterium was then immobilized on the polydopamine coated glass bead to be used for SCFS experiments. The immobilized bacterium on the glass bead was facing the body towards the surface where its presence including its viability could be observed by assessing its fluorescence state. These live or dead bacterial assays have fluorescent states where green fluorescent bacterias are indicating alive bacterias and red fluorescent bacterias are indicating dead bacteria [28, 29].

Chapter 4

Bacterial adhesion in micro arrays; spatial resolution and surface chemistry

4.1 Specific and non-specific interaction in bacterial adhesion

Bacterial adhesion to surfaces is dominated by either specific or non-specific interactions, and these interactions occur between the outer cell wall of the bacteria and the surface. Specific interaction consists of covalent chemical bonds, electrostatic interactions, Van der Waals forces, hydrogen bonds and hydrophilic or hydrophobic interactions over short distances. The specific interactions can also be characterized of having a recognizing macromolecule with its complementary that is dependent on the geometry and the fractional occurrences of the non-covalent or the covalent interactions. The non-specific interactions consist of electrostatic, hydrophobic, and Van der Waals interactions over long distances. Short distance is meant as extremely short were a substratum can distinguish between the molecules on the cell surface, and large distance is meant as a distance were a substratum cannot distinguish between individual molecules on the cell surface. The non-specific interactions are associated with the physiochemical properties of the cells, surface, and solution conditions in the surrounding environment [15]. Non-covalent interactions appear in specific and non-specific interaction. The different bacterial interaction mechanisms are illustrated in figure 4.1.

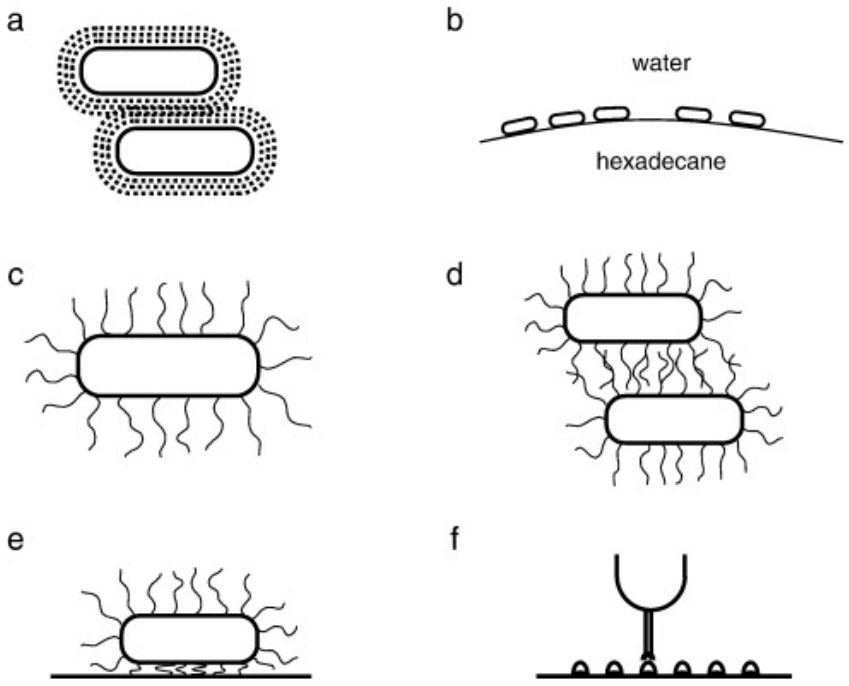

FIGURE 4.1: Various types of bacterial interactions. a. (Screened) electrostatic interaction. b. Adhesion of hydrophobic bacteria to the hexadecane - water interface by a combination of hydrophobic and other colloidal interactions (including electrostatics). c. Entropic repulsion by bacterial surface polymers. d. Bridging interaction by surface bacterial surface polymers. e. Non-specific interaction between bacterium and substrate. f. Specific interaction between pathogenic bacterium and host cell [30]

The size of individual bacterium is usually in range of 0.5-2 μm which is close to the size of colloidal particles. As bacteria can be considered as colloidal particles with a surface, the bacterial interactions with a substratum can been be theoretically described by applying the Derjaguin-Landau-Verwey-Overbeek (DLVO) theory and a thermodynamic approaching model that includes an extended DLVO theory. Since bacteria usually are negatively charged in aqueous solutions, the DLVO theory can describe the bacterial adhesion as a two step phase. DLVO theory is a summation of van der Waals and Couloumb interactions between a surface and a particle, leading to attractive and repulsive forces illustrated in figure 4.2b. From the illustrations in figure 4.2a, the first cell adhesion phase (non-specific interactions) is reversible and is initiated by the motility or the Brownian motion of the bacteria. The repulsive barrier is a result of electrostatic energy that is caused by an overlap of the electrical double layers of bacterial cells and the substratum. The electric double layer is formed as the substratum or bacteria attract counter ions because of the charge of their surface. From the illustrations in figure 4.2b, the repulsive energy increases as the ionic strength of the aqueous solution decreases. The next phase in figure 4.2a (specific interactions) is followed by the bacteria ability to use nanofibers as pili and flagella or to produce exopolymeric substances (EPS) that can pierce the energy barrier because of their small radii. The nanofibers or EPS are then

bridging the cell and the substrate surface forming an irreversible adhesion. For low ionic strengths bacteria will adhere less than for high ionic strengths. This adhesion is dependent on the nanofibers, including the EPS inability or ability to pierce the energy barrier for low or high ionic strengths, respectively. The charge of the substrate surface will also influence the long range interaction with the bacteria. Positively charged substrates will result in a relatively small distance to the repulsive energy barrier and a relatively large depth of the secondary energy minimum outside the energy barrier, while negatively charged substrates result in a relatively large distance to the repulsive energy barrier and relatively small depth of the secondary energy minimum outside the energy barrier [31, 32].

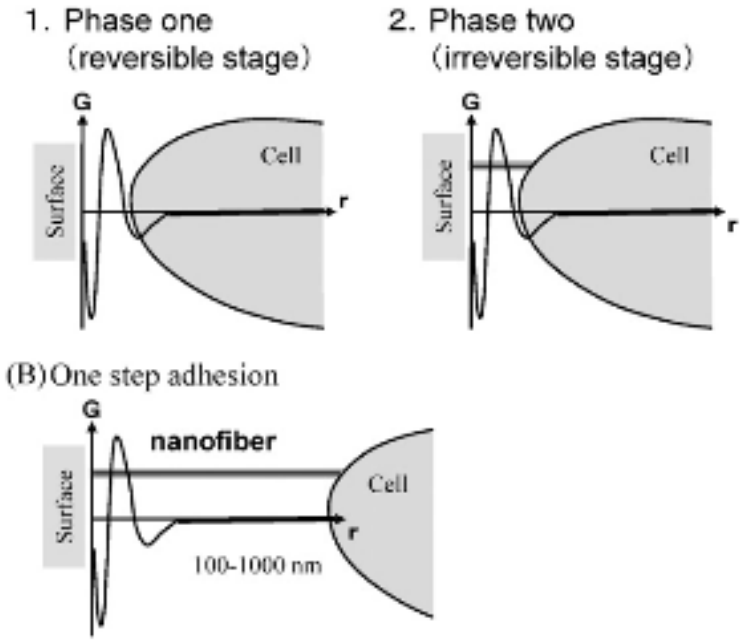

(A) Illustration of bacterial adhesion mechanisms. (A) Two step adhesion. (B) Long fibers mediating a one step process. Have been seen in *Acinetobacter* sp.Tol 5.

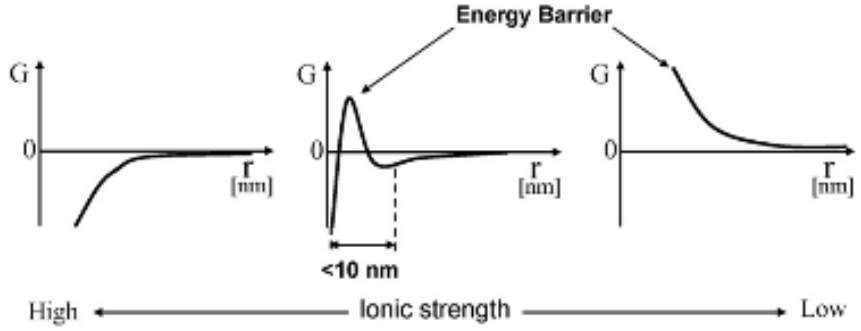

(B) The total interaction energy between a bacterial cell and a surface depending on the ionic strength.

FIGURE 4.2: Schematic of the bacterial adhesion mechanism to a surface, and the dependency on ionic strength [32]

The thermodynamical approach considers the surface free energies of the interacting surfaces, and can be calculated by using the equation of the extended DLVO theory that was proposed by van Oss,

$$\Delta G_{\mathrm{Total}}(H) = \Delta G_{\mathrm{EL}}(H) + \Delta G_{\mathrm{LW}}(H) + \Delta G_{\mathrm{AB}}(H) \tag{4.1}$$

where $\Delta G_{\mathrm{LW}}(H)$ is the Lifshitz-van-der-Waals interaction, $\Delta G_{\mathrm{EL}}(H)$ is the electric double layer interaction, and $\Delta G_{\mathrm{AB}}(H)$ relates to acid-base interactions. Negative free energy $\Delta G_{\mathrm{Total}}(H)$ would favor bacterial adhesion to the substrate surface [31, 32]. More detailed explanation of these variables are presented in Appendix A. This approach helps to explain experimental observations where bacteria with hydrophobic cell surfaces prefer hydrophobic material surfaces whereas bacteria with hydrophilic cell surfaces prefer hydrophilic material surfaces. It also explains the two phase adhesion process by introducing the surface free energies for hydrogen bonding named Lewis acid-base interactions, and electrostatic interactions as the electric double layer or the Coulomb interactions. Calculations have shown that the distance between the interacting surfaces of less than 5 nm is required before acid-base interactions can become operative. Researchers have also found experimental observation where there is a link between decreasing bacterial adhesion and decreasing ionic strength that is consistent with the DLVO theory [31, 32]. Measurements methods related to this model consist typically of assessing Zeta potential measurements for the electrostatic interactions and assessing the contact angle measurements for the hydrophobic interactions of bacterias [33]. However, the capacity of bacteria to remove vicinal water to form the short-range interactions are often strain-dependent which also highlights the importance of the specific cell surface components on the bacterial surface as well as the substrate surface. The one phase adhesion observed for the bacterium *Acinetobacter* sp. Tol 5 (illustrated in figure 4.2b) deviates from the DLVO theory due to the long nanofibers on the outer cell wall. The actual adhesion of bacterias have often shown to be a complicated process that is often deviating from the DLVO theory. Considering the assumption of the bacteria as a colloidal particle, a bacterium differs from the colloidal particle having a surface that is chemically and structurally heterogeneous [32]. An illustration of the cell wall, outer membrane and typical cell appendages on Gram-negative and Gram-positive bacterial cells can be seen in figure 4.3. The properties of the cell surface components are also described below.

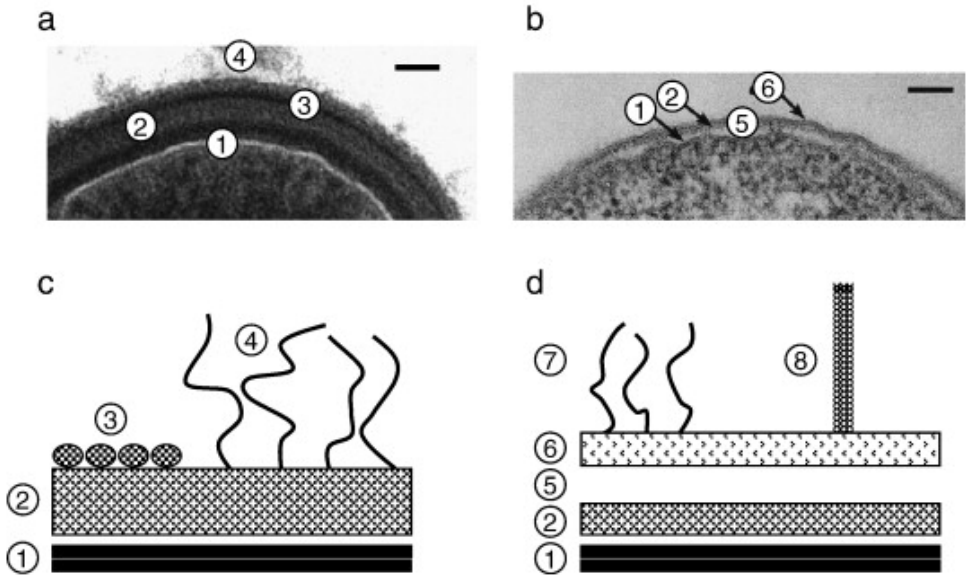

FIGURE 4.3: Electron micrographs (a, b) and schematic structure of the bacterial cell wall (c,d). a,c: Gram-positive cell wall; b,d: Gram-negative cell wall. 1. Plasma membrane; 2. Peptidoglycan; 3. S-layer; 4. Exopolysaccharides; 5. Periplasmic space; 6. Outer membrane; 7. Lipopolysaccharides; 8. Pilus. The schemes c, d are not to scale. Bar in a, b is 100 nm [30]

Polysaccharides involved in viable bacterial adhesions consist typically of lipopolysccharide (LPS) and exopolymeric substances (EPS). LPS is hypothesized to bind a surface from a distance about 20 nm. Hydrogen bonds is also then assumed to be formed with the substrate. The tightly bounded, loosely bounded or soluble EPS produced by the bacteria are composed of primary polysaccharides and other macromolecules as proteins, DNA, lipids, and humic substances. An EPS matrix keep microorganisms together in biofilms and enhance bacterial adhesion to a given surface. The interaction consists mainly of non-covalent bonds as electrostatic and hydrogen bonds[32].

Bacterial nanofibers have shown to function as bacterial adhesin, mediating cell adhesion to abiotic surfaces and biofilm formation, and binding specifically to host cells or extracellular matrices (ECM) such as collagen or fibronectin. Most well known proteinous adhesin of Gram-negative and Gram-positive bacteria is the pilus or fimbria. Among many properties, it is involved in non-specific adhesion to abiotic surfaces for biofilm and colonization as well the binding to specific targets of the ECM [32].

Non-fimbrial adhesins are called autotransporter adhesins (ATADS). They have short monomeric or oligomeric nanofibers of polypeptides often seen in Gram-Negative bacteria. The common function of ATADS is to adhere to host cells, and to bind ECM proteins as fibronectin, laminin, collagen, as well as mediate self agglutination of cells [32]. Considering the complexity of cell interactions that involve multiple binding sites,

i.e. specific or non-specific interaction, it is reasonable to use single cell techniques and experimental observations to reveal the complexity of the bacterial interactions with surfaces in great detail.

4.2 Controlled bacterial adhesion or repulsion

The physiochemical properties of the bacterial cell, substrate surface, solution conditions in the surrounding environment and the spatial resolution of the bacterial adhesive or repulsive micro array of molecules affect the specific or non-specific interactions of bacterial adhesions. All above mentioned factors must be taken into consideration when designing a patterned surface for selective bacterial adhesion. An area of spots on which the bacteria can be attached on is often produced by the μCP technique mentioned in section 2.2. This is done by producing a micro array of adhesive or repulsive molecules. For bacterial adhesion, most functionalizing molecules are polymers that exhibit cationic properties, which binds the negatively charged surface of the bacteria electrostatically. Common cationic polymers used for bacterial adhesion are poly-L-lysine (PLL), polyethyleneimine (PEI), and polyelectrolyte multilayers (PEL) [10, 22, 24, 34, 35]. Reports have also shown that antibodies, biotin-streptavidin complexes, polydopamine (PDA) or Cell-Tak (protein from mussel *Mytilus edulis)* have been used for bacterial adhesion [2, 36, 37]. Figure 4.4 illustrates bacterial cells being immobilized by electrostatic interactions, polyphenolic protein adhesive interactions, as well immobilizations by covalent interactions and a physical trap.

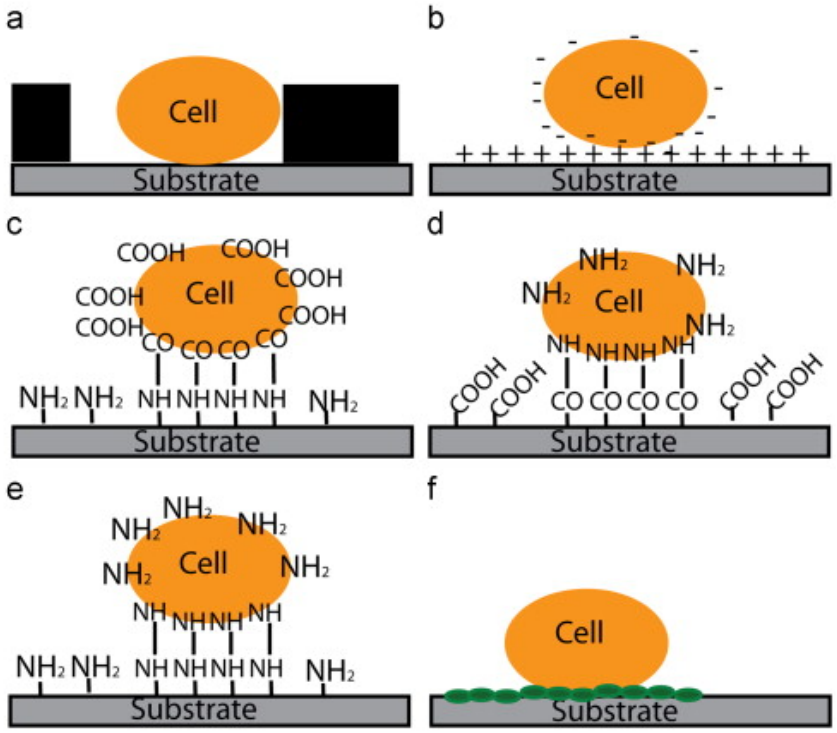

FIGURE 4.4: Schematic representation of the different immobilization methods. (a) physical confinement by capturing in microwells, (b) attractive electrostatic interactions, (c) covalent binding to amine-functionalised surfaces by 1-ethyl-3-(3-dimethylaminopropyl) carbodiimide hydrochloride (EDC) - N-hydroxysuccinimide (NHS), (d) covalent binding to carboxyl-functionalised surfaces by EDC-NHS, (e) covalent binding to amine-functionalised surfaces by glutaraldehyde, and (f) attachment to polyphenolic adhesive protein of the Cell-Tak [37]

For bacterial repulsion, the functionalizing molecules are exhibiting inert properties to not form specific or non-specific bindings to the bacterial surface or biomolecules (as EPS) involved in bacterial adhesions. Reports on commonly used functionalizing molecules for a bacterial passivated array are hexamethyldisilazane (HMDS), polyethylene glycol (PEG), octadecyltrichlorosilane (OTS), and bovine serum albumin (BSA) [10, 12, 36, 38, 39].

4.2.1 Examples of bacterial micro arrays

The spatial resolution of the patterned areas with activating or passivating molecules have shown to affect the bacteria ability to bind and form an array [33]. Printed BSA on glass made by μCP with a lattice of 1-3μm and monolayer of 5-6nm have shown the bacteria to adhere rapidly on the bare glass with a minimized adhesion to the BSA patterns [39]. Patterns of PLL or PEI molecules on a surface with spots size of 2μm have shown to become occupied by 2 or 3 viable cells [10]. Other reports have shown cells being spatially controlled by constructing physical traps or wells to capture the bacteria

[40]. Physical traps produced for single bacterial micro arrays can also be improved by adhering the bacteria nose to the bottom of a well by having PLL on the bottom of it. The bacterias in this micro array showed to be viable for 4 hours [35]. Instead of using PLL, certain elastin like polypeptides (ELP) with the hydrophobicity dependent on the temperature can be applied to bind or unbind the bacteria from the wells or holes by adjusting the temperature of the environment [41]. Figure 4.5 shows the different approaches to the immobilizations mentioned above.

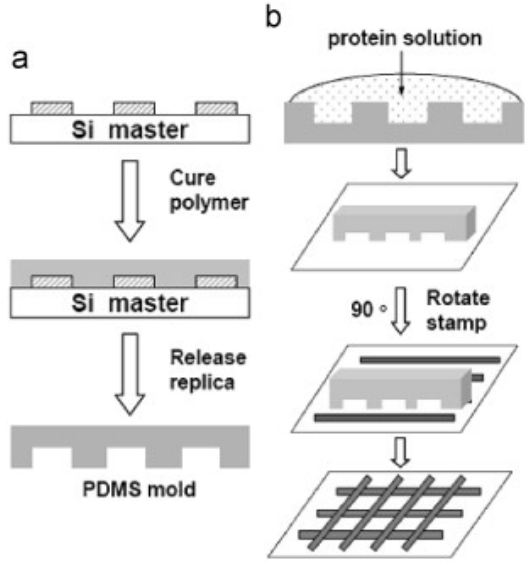

(A) μCP of BSA on glass surface [39]

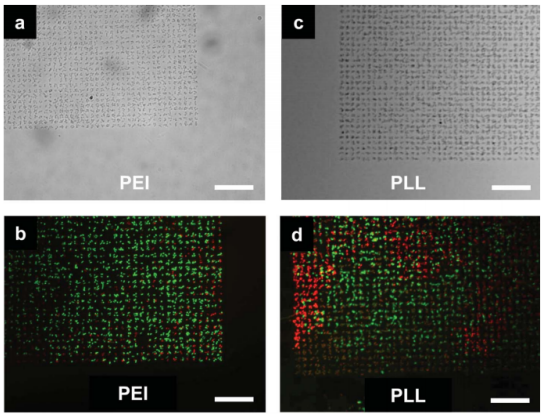

(B) Spots of PLL or PEI arrays with GFP bacteria. Arrays of PLL or PEI are produced by lift-off lithography technique [10]

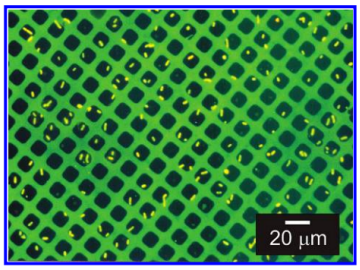

(C) Bacterial adhesion in corral. The adhesive array are produced by μCP [40]

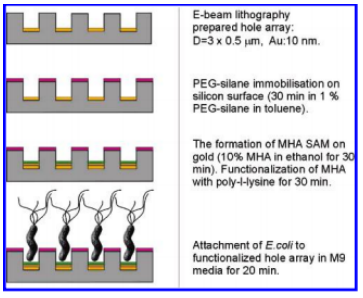

(D) Bacterial adhesion in corral. The corrals are produced by the E-beam lithography technique [35]

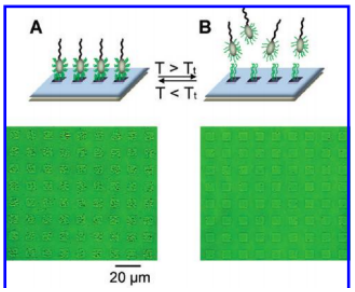

(E) ELP patterns with attachment or detachment of bacteria. ELP arrays are produced by μCP [41]

FIGURE 4.5: Different approaches to immobilize bacteria in micro arrays

The spatial resolution of the physical trap, the adhesive or the repulsive spots of the functionalizing molecules show to have a significant impact on the ability of bacteria to become attached and viable in a micro array. Viable attachment of bacteria is considered as of sustaining its normal functions on the outer cell membrane as proton pumps or other biomolecular motors, transport through porins, and proliferation. A viable attachment is dependent on the interaction strength between the bacteria and the adhesive spots

in the micro array that needs to be carefully balanced, where a large interaction force would lead to bacterial inactivation and a small interaction force would lead to unstable attachment of the bacteria. Choosing the proper micro array with a proper spatial size and molecules for activation or passivation is important to engineer a micro array of stable and viable bacterial cells.

4.3 Chemical and structural properties of the bacterial adhesive and repulsive molecules used in this project

This project focuses on assessing the use of poly-L-lysine (PLL), polydopamine (PDA), Cell-Tak and bovine serum albumin (BSA) as bacterial adhesive and repulsive molecules in micro arrays made by μCP. PLL, PDA and Cell-Tak have been shown to exhibit suitable properties to function as a bacterial adhesive molecules, while BSA has shown to be a suitable candidate for an inert bacterial repulsive molecule. Controlled bacterial adhesion was mentioned in section 4.2.

4.3.1 Chemical and structural properties of poly-L-lysine (PLL)

PLL is a homo-poly-amino acid with L-lysine as a monomer unit. The peptide bonds in PLL can be arranged between the carboxyl and the amino α or the amino ε carbon group in the L-lysine. The arrangement of the peptide bond can have consequences considering cell adhesions and antimicrobial activity. Chemical structure of α and ε PLL can be seen in figure 4.6.

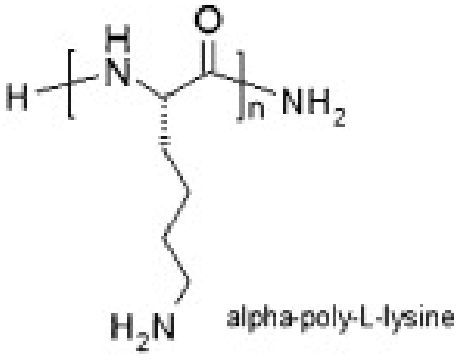

(A) Chemical structure of α PLL

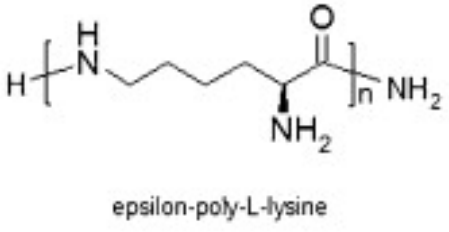

(B) Chemical structure of ε PLL

FIGURE 4.6: Chemical structure of α and ε PLL [42]

PLL usually has a pKa above 7.0 and is therefore soluble in water as a cationic polymer. The PLL is soluble in water because of the protonated amine groups that are positively

charged[42–44]. The PLL used for coating in this project are an aqueous solution of PLL with the molecular weight (wt) of 15000-30000 Da. It is fluorescently labeled on the amine groups with fluorescein isothiocyanate (FITC), with an excitation/emission wavelength of 490/525nm.

4.3.2 Chemical and structural properties of polydopamine and Cell-Tak

Cell-Tak or polydopamine (PDA) is a mixture of polyphenolic proteins secreted from the mussell *Mytilus edulis*. These proteins consist mainly of L-3,4-dihydroxyphenylalanine (L-DOPA) and the dimeric amino acid cystine [45–47]. L-DOPA consists of an amine group, a carboxyl group and a cathecol ring. It is assumed that L-DOPA can exhibit zwitterionic properties dependent on the pH, although when formed as a peptide, its interaction potentials will mostly rely on the phenylene ring via its hydroxyl groups. The aromatic ring may play a twofold role in the adhesive mussel protein as a surface anchor and as curing adhesive proteins in wet environments by the substituted hydroxyl groups. L-DOPA can be arranged as L-L-DOPA or L-D-DOPA as indicated in figure 4.7 [48].

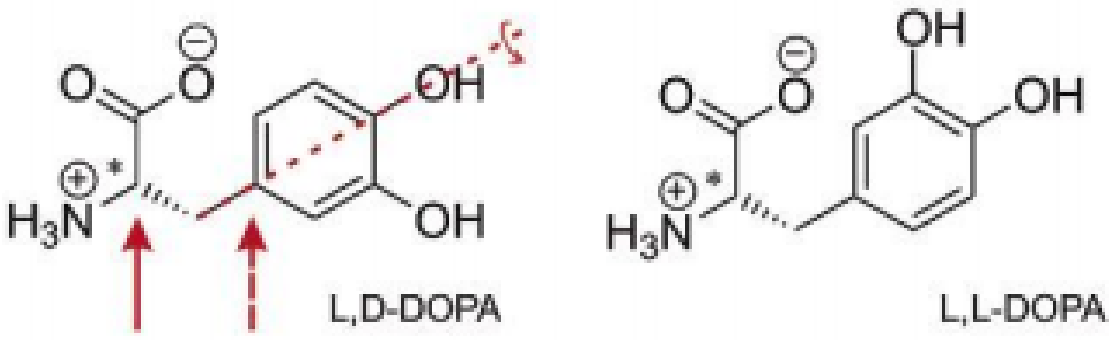

FIGURE 4.7: Chemical structure of L-L-DOPA and L-D-DOPA [48]

The polydopamine (PDA) used for coating in this project is an oxidative self polymerization of dopamine (2-(3,4-dihydroxyphenyl)ethylamine) that is diluted in a Tris-buffered solution with pH of 8.5. The oxidative self polymerizing process is a result of the dopamine being oxidized, deprotonated, rearranged, and protonated in several steps forming the PDA that have crosslinked dopamine in two configurations. The possible mechanisms are illustrated in figure 4.8.

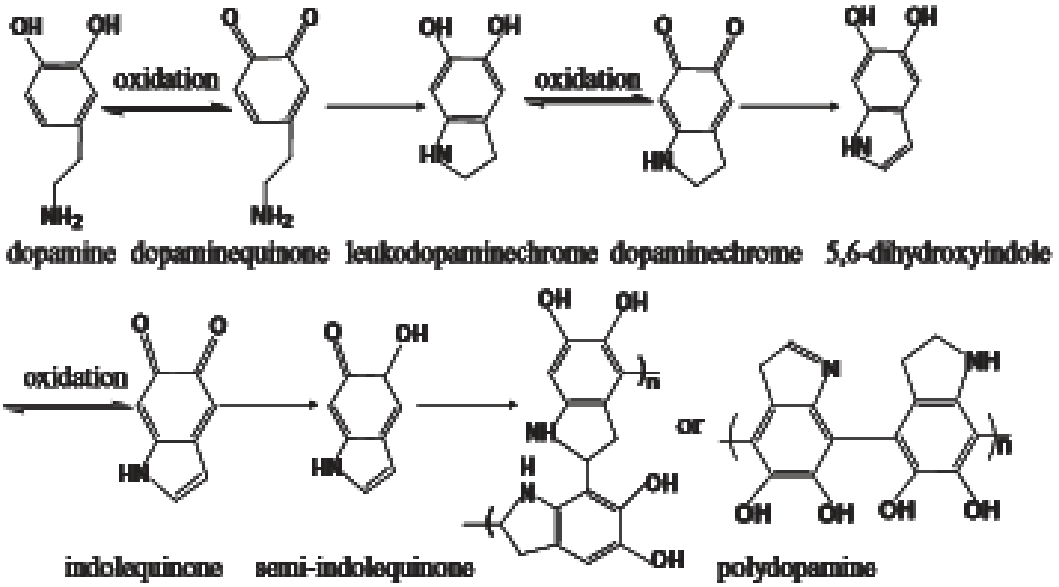

FIGURE 4.8: Possible mechanism for oxidative polymerization of dopamine [49]

The Cell-Tak^{TM}(mentioned often only as Cell-Tak in this project) proteins used for coating in this project are commercially available product that has a wt of 110-140kD and a DOPA protein ratio above 0.05. The Cell-Tak protein solution is diluted in a buffer of sodium bicarbonate and sodium hydroxide to obtain a pH of 8.0. Cell-Tak proteins disperse in the solution as the pH raises up to pH 8.0 and adsorb to the first surface they encounter [47].

4.3.3 Chemical and structural properties of bovine serum albumin (BSA)

BSA is a single polypeptide chain consisting of about 583 amino acid residues. The carbohydrates are absent in these amino acid residues. Albumins themselves are a group of acidic proteins that occur in body fluids, in tissues of mammals, and some plant seeds. At pH range of 5.0-7.0, the BSA contains 17 intrachain disulfide bridges and 1 sulfhydryl group. BSA is readily soluble in water and can be precipitated in high concentrations of neutral salts such as ammonium sulfate. It has a good solution stability, but when heated above 50 °C it rapidly forms hydrophobic aggregates that is not reversible upon cooling [50]. Molecular structure of BSA can be seen in figure 4.9.

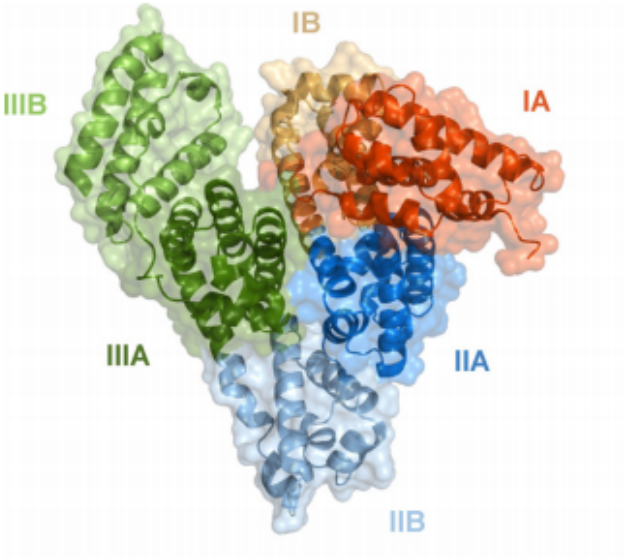

FIGURE 4.9: Molecular structure of BSA [51]

The BSA used in this project has a wt of 66kDa and is diluted in a phosphate buffered saline solution with a pH of 7.4.

4.3.4 Protein interactions with relevance to bacterial micro arrays

The adsorption of proteins on substrate surfaces has been shown to be physiochemical and entropically driven. The protein adsorption is a result of the gain of entropy by the dehydration and the configuration that is being changed and produced by the protein adsorption. It is assumed that a high adsorption of polypeptides should occur on a surface with a large interfacial free energy [52]. Adsorption process between glass and PLL, BSA, PDA or Cell-Tak is also a function of the electrostatic, hydrophobic or hydrophilic, and Van der Vaals interactions as well as hydrogen bonds. The binding constant for the PLL, BSA, PDA or Cell-Tak interaction with the glass can be quantified by using a model that is called the Langmuir model [53]. The physiochemical properties of these molecules printed on a surface concerning bacterial interactions can also be assessed with a relatively new technique called mapping using accumulated probe trajectories (MAPT). MAPT is expanding the concept of super-resolution surface mapping by the use of total internal reflection fluorescence microscopy (TIRFM). In short, this technique can map intermolecular interactions (such as hydrogen bonding, electrostatic, π-stacking, surface charge or diffusion coefficient) between a surface and an appropriate selection of one or more probe molecules [54–56]. Such surface characterization of bacterial adhesive or repulsive surfaces are relevant in the optimization of bacterial micro arrays since the underlying nature of bacterial adhesion and type of interactions can be uncovered.

Chapter 5

Materials and Methods

5.1 Bacterial Strain and suspension samples

Throughout this project the bacteria *DH5alfa* have been used as a model for the interaction measurements. These bacteria are engineered with fluorescent proteins (transcribed and translated by the mCherry gene) with excitation/emission wavelength of 587/610nm. The mCherry gene is under the control of a constitutive T5 phage promotor N25. All the T5 phage promotor N25 elements are residing on a low copy mini-RK2 plasmid with kanamycin resistance marker. The mCherry gene is transcribed and translated in the intracellular part of the bacterial cell. Under stringent response the amount of mCherry gene being transcribed and translated is assumed to decrease, i.e. the presence of fluorescence of the bacteria in an optical microscope is also assumed to decrease. The suspension samples of the bacteria *DH5alfa* were kindly provided by a Postdoctoral fellow Rahmi Lale from the Department of Biotechnology, NTNU.

5.2 Preparation and characterization of bacterial attractive or repulsive surfaces

Materials used to prepare bacterial attractive surfaces included Cell-Tak proteins (BD Biosciences), poly-L-lysine (PLL) wt 15000-30000 with labeled fluorescein isothiocyanate with excitation/emission wavelength of 490/525nm (Sigma-Aldrich Norway AS), and dopamine hydrochloride (Sigma-Aldrich Norway AS). Materials used to prepare bacterial repulsive surfaces included bovine serum albumine (BSA) (Sigma-Aldrich Norway AS).

Materials used as substrates for the adsorption of bacterial repulsive or attractive molecules included clean and sterile "WillCo-dish" glass bottom dishes (WillCo Wells), and glass coverslips. The glass coverslips were cleaned with a mixture of hydrochloric acid (HCl) 1 Molar (Sigma-Aldrich Norway AS) and methanol-96% (Sigma-Aldrich Norway AS) with a ratio of 1:1 for 10 minutes, rinsed with miliQ water (resistivity of 18.2 Ω, Millipore-Simplicity 185) and dried with a stream of compressed nitrogen gas. Micropipette Biohitm200 or Mettler Toledo MT5 were used to measure and transfer solutions in the procedures of this chapter.

BSA and polydopamine (PDA) were individually μCP on the substrate surfaces by the use of non patterned and flat PDMS stamps, since this have shown to produce a surface layer that is relatively smooth [13, 39, 57]. The flat PDMS stamps were kindly provided by Phd. student Nina Bjørk Arnfinnsdottir from the Biophysics and Medical Technology research group, Department of Physics, NTNU.

5.2.1 Preparation of a layer of Cell-Tak

The Cell-Tak solution was prepared by first mixing the stock solution of Cell-Tak proteins in 0.1M sodium bicarbonate (pH 8.0) (Sigma-Aldrich Norway AS), and then adding a solution of 1M sodium hydroxide (Sigma-Aldrich Norway AS) with a ratio of 2:57:1 [Cell-Tak]:[sodium bicarbonate]:[sodium hydroxide]. Sodium hydroxide was added into the Cell-Tak solution immediately prior coating the substrate surface. The substrate surface of glass coverslips or WillCo dishes were incubated with the Cell-Tak solution for 25 minutes at 4°C. The substrate was then rinsed with milliQ water to remove excess Cell-Tak solution and dried with a stream of compressed nitrogen gas. The samples with Cell-Tak layers were stored at 4°C until further use to ensure that the Cell-Tak proteins contains their original shape and function. Storage period of these samples was limited to one week.

5.2.2 Preparation of a layer of PLL

PLL was diluted in milliQ water to a concentration of 1 mg/mL and stored at 4 °C until further use. The PLL solution was then incubated on the substrate surface of glass coverslips or WillCo dishes for 10 minutes at room temperature. The substrate was then rinsed with milliQ water to remove excess PLL solution and dried with a stream of compressed nitrogen gas. The samples with PLL layers were stored at 4°C. Storage period of these samples was limited to 4 months.

5.2.3 Preparation of a layer of PDA

To facilitate future depositions of polydopamine layers, the dopamine hydrochloride was diluted in miliQ water and stored at -20°C to slow down the polymerization process of the dopamine. Dopamine hydrochloride of 20mg was diluted in 200μL milliQ water and equally divided to 20 eppendorf tubes (Eppendorf). The dopamine hydrochloride solutions were then stored at -20°C until further use. The solution to be used for coating was prepared by mixing the dopamine hydrochloride of one of the eppendorf tube of with with 250μL 10 mM TRIS buffer (pH 8.5) (Sigma-Aldrich Norway AS) to reach a final concentration of 4 mg/mL. The dopamine hydrochloride TRIS solution was deposited on a non patterned and flat PDMS stamp and incubated for one hour at room temperature. Due to the hydrophobic surface of the PDMS stamp, the droplet tend to maintain a high water contact angle, the surface of the flat PDMS stamp will not be covered fully by the solution. A small sheet of ultrafine paper (UFpaper) was then used to force the droplet to spread onto the PDMS surface that is minimizing above-mentioned behavior. After the incubation the paper was removed from the PDMS stamp, and the latter was rinsed with milliQ water to remove the excess PDA solution. The PDMS stamp was then blow dried with a stream of compressed nitrogen gas (0.34 bar) perpendicular to the surface for 15 seconds. The distance between nozzle and surface was maintained higher than 50 mm, while the focus of the gas stream was directed over the entire PDMS surface. Next, the PDMS stamp was brought in contact with a substrate surface of glass coverslip or WillCo dish. A mechanical device "Squeezer"(In house built) was used to apply a uniform weight pressure of 100gram on the PDMS stamp. A paper between the PDMS stamp and the knob applying the pressure should be used to avoid unwanted adhesion between them. The PDMS stamp was in contact with the substrate surface for 7 minutes under 100gram weight pressure and then peeled carefully off with a tweezer. Samples with PDA layers were stored at 4°C until further use. Storage period of these samples were also limited to one week.

5.2.4 Preparation of a layer of BSA

BSA was diluted in PBS of with pH 7.4 (Sigma-Aldrich Norway AS) to a concentration of 1mg/mL and stored at 4°C until further use. The PBS was prepared according to the manufacturer instructions by diluting a PBS tablet in milliQ water, and filtrating through a 0.2μm filter (Pall Corporation). The BSA was μCP in the same way as described in section 5.2.3 for PDA. The incubation time on the non-patterned and flat PDMS stamp was 15 minutes at room temperature. The PDMS surface was then rinsed with milliQ water to remove excess BSA-PBS solution and dried with a stream

of compressed nitrogen gas. BSA was then printed on the substrate surfaces of glass coverslips or WillCo dishes and stored at 4°C until further use. Storage period of these samples was limited to 4 months.

5.2.5 Characterizing the surfaces of the bacterial repulsive or attractive layers

AFM multimode from Bruker was used to characterize manufactured surfaces of bacterial adhesive or repulsive layers on the glass substrate. The AFM was operated in tapping mode for all measurements and E-scanner was used having the ability to scan surfaces up to 10μm in x and y direction. The parameters for proportional gain, integral gain, amplitude setpoint, and drive amplitude were manually adjusted for each image separately to optimize the raster scanning. Overlapping of trace and retrace signal was used as a prerequisite for adequate and high-quality image acquisition. The scan rate was set to 0.996 Hz, scan size was set to 5μm, and the number of lines was 512. The drive frequency was automatically determined by the autotune function in the acquisition in NanoScope Analysis software to find a drive frequency corresponding to the resonance frequency of the cantilever. The adjustment of laser and photo-diode detector was performed as instructed in the user manual. The sum voltage was in range between 2 and 3V. Topography, phase and amplitude error images were obtained and analyzed in the NanoScope Analysis software. The flattening function was used to fit each line individually to center data to remove tilt or bow artifact [16]. The clean image function was used to enhance the contrast in the images.

5.3 Cell probe design and characterization

A triangle shaped cantilever made of non-conductive silicon nitride (Si_3N_4) (Bruker, Model: OTR4-10) with spring constant in range of 0.02-0.035 N/m (calibrated by the use of thermal tune method) were used to prepare cell probes similar as described in literature [22, 24, 29]. The cantilever was cleaned in a 1:1 vol/vol mixture of 37% HCl (Sigma-Aldrich Norway AS) and methanol-96% (Sigma-Aldrich Norway AS) with a ratio of 1:1 for 25 minutes, rinsed with milliQ water and dried with a stream of compressed nitrogen gas. Next, the cantilever was exposed to 4 mg/mL dopamine hydrochloride in 10mM TRIS buffer (pH 8.5) (PDA solution was prepared as described in section 5.2.3) for 1 hour to coat its inner surface with PDA. The cantilever was then washed with milliQ water and left to dry under room temperature. The immobilization of bacterial cells was performed by depositing a bacterial cell suspension of (from section

5.1) on the cantilever so it covers it fully for 40 minutes. The cantilever was then rinsed with Luria-Bertani (LB) medium (The LB medium was kindly provided by a Postdoctoral fellow Rahmi Lale from the Department of Biotechnology, NTNU), and kept immersed in the LB medium until further use for maximum 6 hours to ensure that the bacteria immobilized on the tip stays viable. The cantilever was then washed with PBS immediately prior the AFM force measurements. The coating of the bacterial-cell tip was confirmed both before and after the AFM force measurements. This can be seen in figure 5.1. The bacterial coating was confirmed before AFM force measurements by imaging the epifluorescence from the tip by the use of the inverted Zeiss microscope (Zeiss Axio Observer) that is integrated as a part of the Bioscope Catalyst (Bruker). After the AFM force measurements, the presence of immobilized bacteria on the tip was checked with scanning electron microscopy (SEM; Hitachi TM3000). The Volts used for imaging were in range between 15kV to 25 kV. The bacteria were fixed for SEM imaging by immersing the cantilever in 3% glutaraldehyde (Sigma-Aldrich Norway AS) in PBS for 4 hours. After the fixation the cantilever was rinsed with PBS, and left to dry under room temperature. Next, the cantilever was sputter coated with 10nm layer of gold with Cressington 208 HR, model 2009. The SEM imaging and sputter coating were performed in the ISO7 area of the nanolab at NTNU. A bare AFM tip and polydopamine coated AFM tip was used as a control for both SEM imaging and AFM force measurements.

5.4 The experimental setup for the bacterial AFM force measurements

The AFM tip was coated with PDA to function as a "glue" for the bacteria. The bacteria was then attached to the PDA coated AFM tip as a result of the bacterial adhesive nature of the PDA. Next, the presence of bacteria on the tip was validated by the use of epifluorescence microscopy. The fluorescence is a result of the mCherry gene that being transcribed and translated to red fluorescent proteins as mentioned in section 5.1. Then, the AFM tip attached with bacteria is used to measure the interactions between the bacteria and the bacterial adhesive or repulsive surfaces to access the adhesion force. The presence of bacterias was then validated after the AFM experiment by the use of SEM. The cell probe design and characterization were mentioned in section 5.3. The illustration of bacterial force measurements and the validation of bacteria present on the AFM tip before and after AFM experiments are presented in figure 5.1.

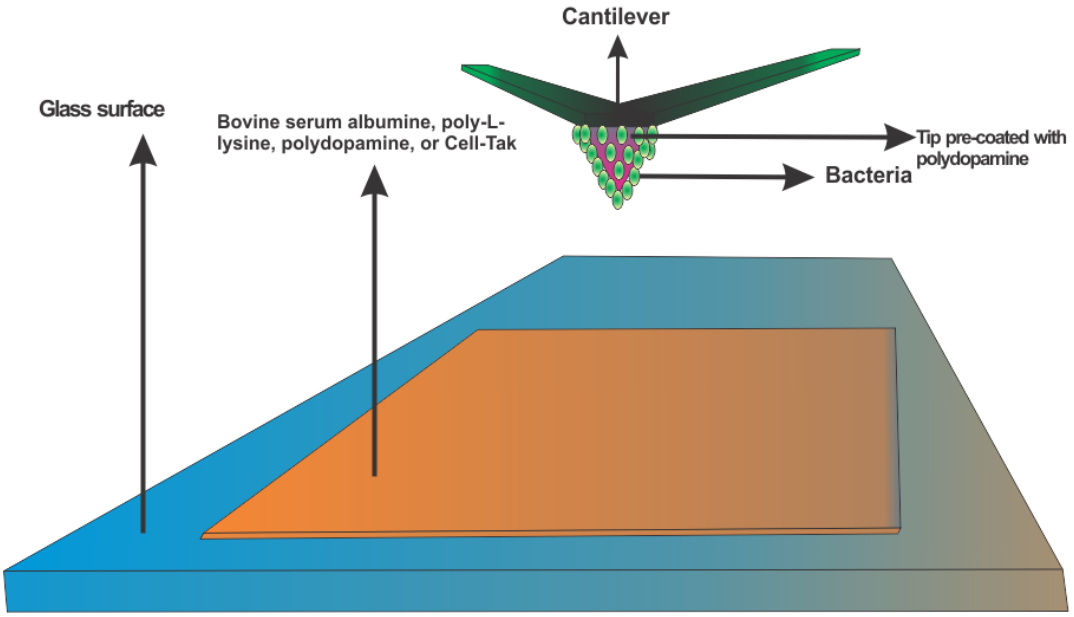

(A) Illustration of the experimental setup under AFM force measurements

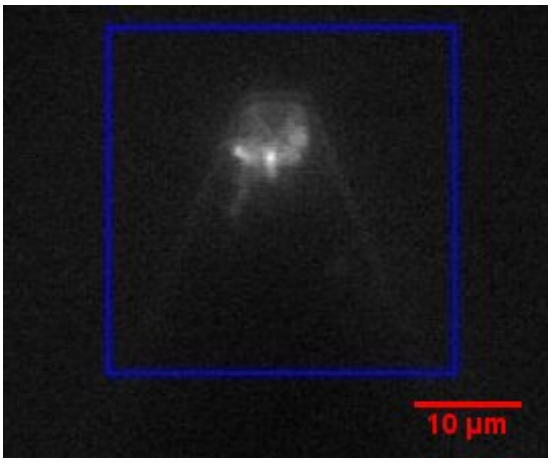

(B) Checking the presence of bacteria before AFM force measurements by observing the fluorescence

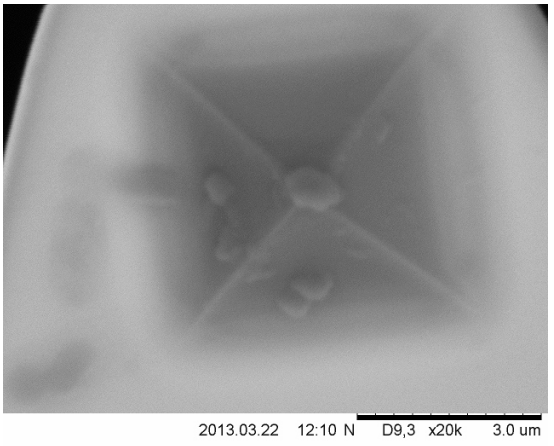

(C) Checking the presence of bacterias after AFM force measurements by scanning electron microscope (SEM) imaging

FIGURE 5.1: Illustration of the experimental setup to validate the presence of bacteria on the AFM tip before and after the AFM measurements[58]

Figure 5.1a illustrates bacteria attached to the tip under the AFM measurements for the different bacterial adhesive or repulsive surfaces. Figure 5.1b illustrates the investigation of the bacteria immobilization on the tip before each AFM experiment by the use of epifluorescence microscopy and figure 5.1c illustrates the investigation of bacteria immobilization on the tip after the AFM experiments by the use of SEM. Control measurements were performed to further validate the presence of PDA and bacteria on the AFM tip. To further validate the presence of PDA on the AFM tip control measurements was performed by obtaining force interactions between bare or PDA coated AFM tip and the bacterial adhesive or repulsive surfaces, including glass surfaces as illustrated in figure 5.2a and 5.2b. To further validate the presence of bacterias on the

AFM tip control measurements were performed by obtaining force interactions between the bacterial coated AFM tip and glass surface as illustrated in figure 5.2c.

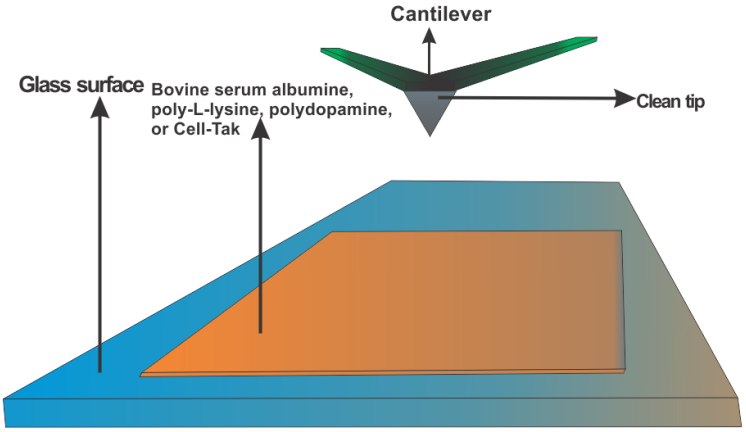

(A) Illustration of control AFM force measurements with a bare AFM tip

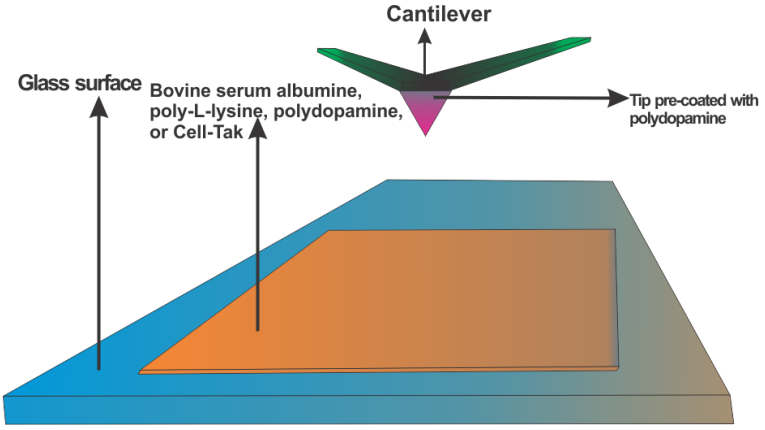

(B) Illustration of control AFM force measurements with a polydopamine coated AFM tip

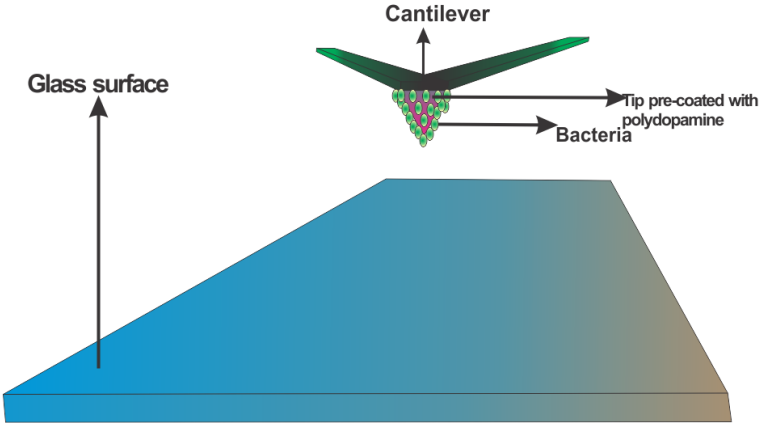

(C) Illustration of control AFM force measurements with a bacterial coated AFM tip

FIGURE 5.2: Illustration of the control AFM force measurements performed for the different AFM tip coatings for glass, BSA, PLL, PDA, and Cell-Tak surfaces

The characteristics of the force-distance curves including the force ruptures obtained

between the bare, PDA coated, or bacterial coated AFM tip and the bacterial adhesive, bacterial repulsive or glass surfaces helps to assess the presence of PDA and the bacteria attached to the AFM tip.

5.5 Force spectroscopy using AFM

The AFM force measurements were performed at room temperature using the BioScope Catalyst (Bruker, USA). All measurements were conducted in milliQ water to avoid any modification of the cell wall due to desiccation. Single force-distance curves and a matrix of 20x20 force-distance curves on 5x5μm^2 squares were recorded. This gave 400 force curves that were analyzed for each experiment. The spring constant of the tips was measured for each probe by the thermal-tune method. The spring constants were in the range of 0.02-0.035 N/m. The calibration procedure on BioScope Catalyst is explained in Appendix B. All force measurements were recorded with a loading rate of 96 nN/s, contact time of 0 s, and a loading force of 1 nN. The approaching and retraction velocity were determined by the use of equation 3.3 in section 3.2 to set a velocity that gives the proper loading rate. The sum voltage on a photo-diode varied between 3 and 6 V. The horizontal and vertical voltage varied between -0.10 to 0.10V and -1.8 to -2.5V, respectively. The duration on each experiment was less than one hour to ensure viable bacteria under the AFM force measurements. Other parameters as the loading force was also set to 1 nN for the same reasons. A bare AFM tip and polydopamine coated tip was used as a control for the AFM force measurements.

5.6 Analysis

The programs used to analyze the obtained force-distance curves were developed in IDL and Matlab. Functions and scripts written in Matlab were used to produce plots and histograms of the data obtained from the IDL analysis. The IDL program and Matlab codes are further described in Appendix B. The programs used for SEM and fluorescence image analysis were Hitachi TM3000 and Andor Solis, respectively. The Hitachi TM3000 program had a built-in auto focus, brightness and contrast that adjusted the proper imaging parameters. In the Andor Solaris program the gain and exposure time of the CCD camera integrated with the BioScope Catalyst were manually adjusted to achieve optimal contrast. The image analysis program ImageJ was used to label the length scale on the optical images.

5.6.1 Data processing

The IDL program used for the analysis of the raw force-distance curves data (program; difordisveeco3.pro) recorded with BioScope Catalyst was kindly developed by Professor Bjørn T. Stokke, from the Biophysics and Medical Technology research group, Department of Physics, NTNU. Each force-distance curve was manually analyzed in the IDL program in order to extract valid rupture forces and rupture lengths. The individual curves analyzed contain one, several, or no force jumps. In essence, the IDL program enabled analysis of rupture forces and rupture lengtsh from the de-adhesion interactions. Each uploaded file included data points for a force-distance plot, and the plot was created when the text file was opened. Included in this plot a derivative of the force-distance curve were plotted in the same figure. The baseline for the curve was also created to determine the force magnitudes. The parameters for calculating the derivative, baseline and other factors are further explained in Appendix B. For every curve a force jump and associated rupture length was collected. The collection of rupture force and lengths were written to a separate text file. Next, histograms were made of the obtained data by the use of Matlab scripts which are also described further in Appendix B. The optimal number of bins were chosen for the histograms by picking out the middle value of the single integer returned from the Freedman-Diaconis, Scott and Sturge's methods [59–61]. These are regular built-in functions in Matlab, but the function "calcnbins" was distributed from the Matlab central [62]. The mean and standard deviation were derived from the histograms in Matlab based on the Gaussian distribution by the use of the "fitdist" function. The "fitdist" function were also used to evaluate the lambda values from the histograms that is based on the Poisson Distribution. The force interactions versus time for each AFM force experiment were also plotted.

Chapter 6

Results

Interactions between the fluorescent bacteria *DH5alfa* and Cell-Tak, PDA, PLL and BSA layers were investigated by performing AFM force spectroscopy measurements. The results indicates that bacteria are interacting with the different bacterial adhesive or repulsive layers with different rupture mean rupture forces and lengths. The force-distance curves contained one, several, or no rupture force jumps and the number of analyzed rupture force or rupture length data varied between 350 and 450 for each AFM force experiment. Statistical histograms of the obtained rupture forces and rupture lengths are presented for the different bacterial adhesive or repulsive layers. Rupture force were also plotted with rupture length to observe the correlation. The force interactions versus time obtained during each AFM force measurements were plotted to examine whether the interactions change with time during each AFM experiment. Control measurements are also presented in same manner. The validation of immobilized bacteria on the AFM tips are shown by presenting SEM images of bare, PDA, and bacterial AFM tips. The SEM images obtained after each bacterial AFM experiment are shown in Appendix C. The characterizations of prepared bacterial adhesive and repulsive surfaces are presented as AFM images of topography and phase.

6.1 Characterizing the bacterial cell probe and the prepared bacterial adhesive or repulsive surfaces

The bacterial cell probes as well as the control samples of bare and PDA coated AFM probes were characterized in SEM to validate the presence of bacteria. Further, AFM images of the bacterial adhesive or repulsive surfaces were recorded to show the degree of homogeneity of the different surfaces.

6.1.1 Characterizing the immobilization of bacteria *DH5alfa* on the PDA pre-coated AFM tip with SEM

Figure 6.1 shows the SEM images obtained at each step of the bacterial immobilization process.

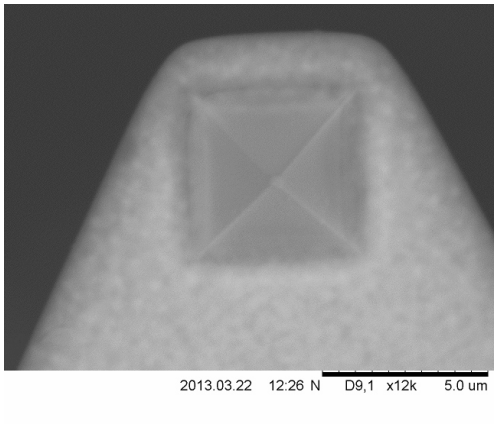

(A) SEM images of bare AFM tip

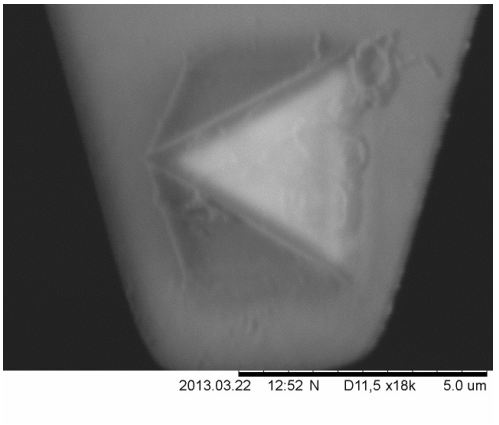

(B) SEM images of bare AFM tip

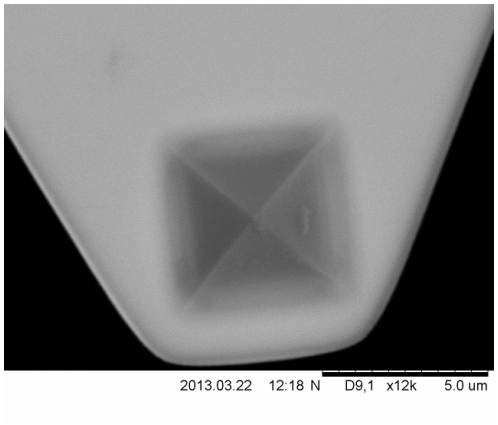

(C) SEM images of polydopamine coated AFM tip

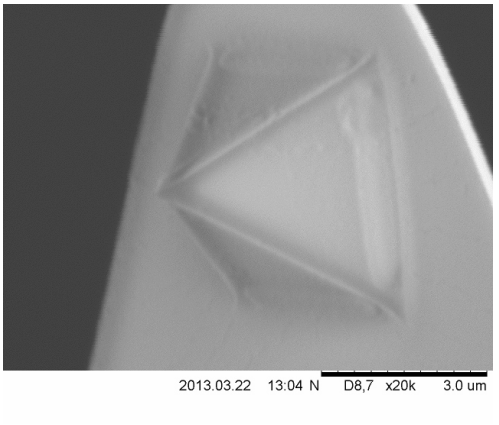

(D) SEM images of polydopamine coated AFM tip

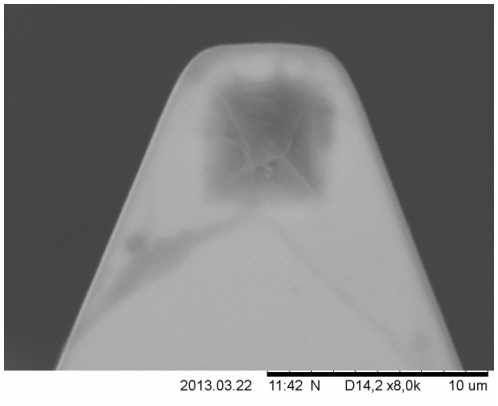

(E) SEM images of polydopamine coated tip immersed with a bacterial suspension

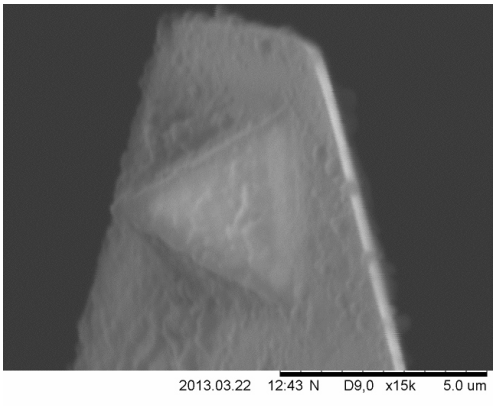

(F) SEM images of polydopamine coated tip immersed with a bacterial suspension

FIGURE 6.1: Representative SEM images of the PDA coated AFM tip, for immobilization of *DH5alfa* bacterial cells onto AFM tip and cantilever

In figure 6.1a and 6.1b, the Si_3N_4 tip was first cleaned with a mixture of HCL and methanol and then treated with glutaraldehyde as described in section 5.3. The bare tip was used as a control and it can be characterized to be absent of debris or other materials on the tip surface. Figure 6.1c and 6.1d shows a bare AFM tip coated with PDA and then glutaraldehyde-treated as described in section 5.3. The PDA coated tip is used as a control and it can be characterized to have few or little materials present on the tip surface. Figure 6.1e and 6.1f shows AFM tip coated with PDA that has been immersed with a bacterial suspension and treated with glutaraldehyde as described in section 5.3. The PDA coated AFM tip that have been immersed with bacteria can be characterized to have biological materials on the tip surface. The biological materials on the AFM tip indicates that bacterias have been present. The immobilizing of a single cell on the probe could not be achieved, and based on the SEM images, cluster of bacterial cells seems rather to be attached.

6.1.2 Characterization of the bacterial adhesive or repulsive surfaces with AFM

Surfaces of BSA, PLL, PDA, and Cell-Tak were prepared as described in section 5.2. The surfaces in figure 6.2, 6.3, 6.4, and 6.5 were AFM scanned in tapping mode. Images of height and phase were obtained including their roughness parameters in table 6.1. The theory behind the roughness parameters was described in section 3.1.2.

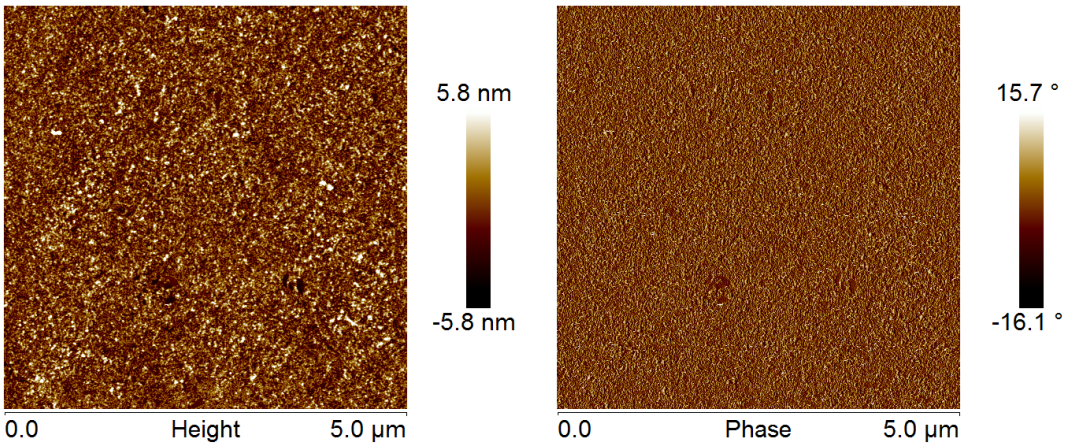

(A) AFM topography (B) AFM phase image

FIGURE 6.2: AFM images of printed bovine serum albumine on glass

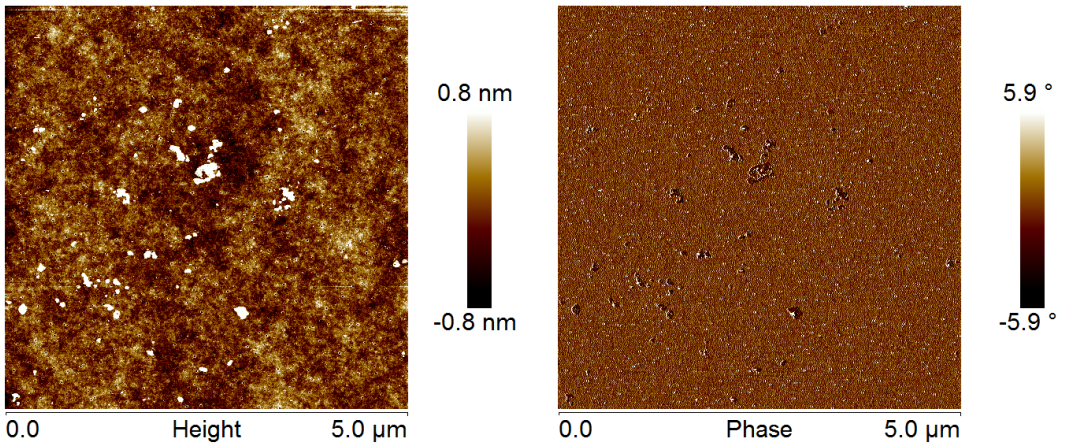

(A) AFM topography (B) AFM phase image

FIGURE 6.3: AFM images of poly-L-lysine incubated on glass

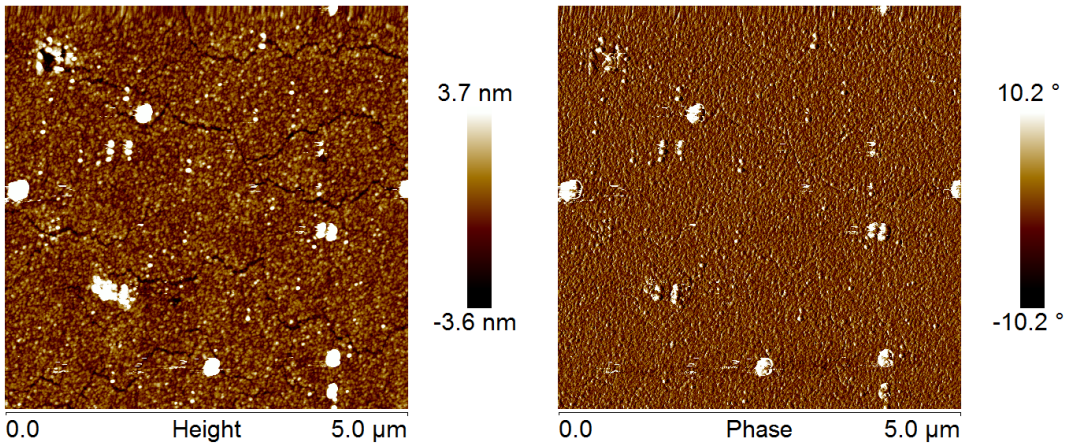

(A) AFM topography (B) AFM phase image

FIGURE 6.4: AFM images of polydopamine printed on glass

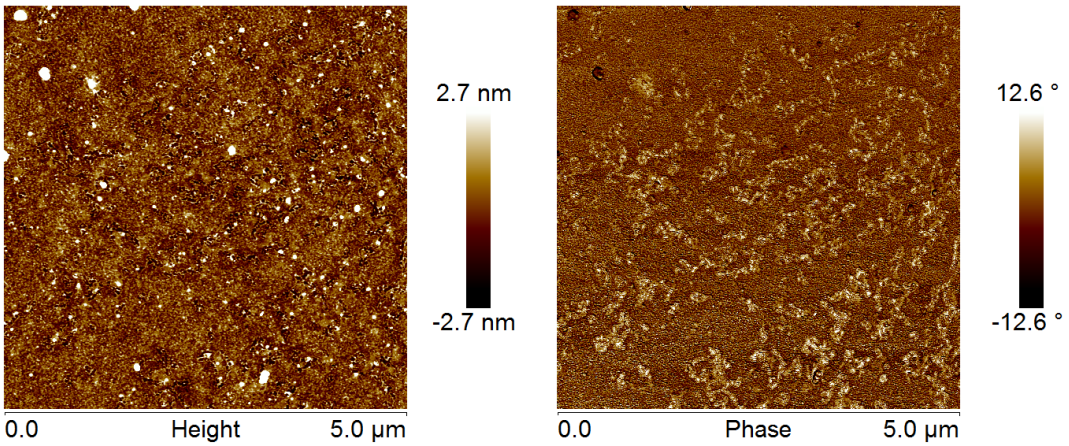

(A) AFM topography (B) AFM phase image

FIGURE 6.5: AFM images of Cell-Tak incubated on glass

Layers	Poly-L-lysine	Polydopamine	Cell-Tak	Bovine serum albumin
Ra	0.20nm	0.76nm	0.65nm	1.51nm
Rq	0.26nm	1.03nm	0.84nm	1.91nm

(A) Roughness analysis of the height images of PLL, PDA, Cell-Tak and BSA layers

Layers	Poly-L-lysine	Polydopamine	Cell-Tak	Bovine serum albumin
Ra	1.47 °	2.57 °	3.24 °	4.48 °
Rq	1.89 °	3.32 °	4.19 °	5.35 °

(B) Roughness analysis of the phase images of PLL, PDA Cell-Tak and BSA layers

TABLE 6.1: Roughness analysis of the height and phase images of PLL, PDA, Cell-Tak and BSA layers. Ra represent the arithmetic value of the absolute values of the surface height deviation measured from the mean image data plane. Rq represent the root mean square average of height deviations measured from the mean image data plane

The AFM topographies in figure 6.2a, 6.3a, 6.4a, and 6.5a indicate that bacterial adhesive or repulsive surfaces have a uniform and flat layers with few aggregates. AFM phase images of BSA, PLL, and PDA surfaces in figure 6.2b, 6.3b, and 6.4 shows to indicate change in phase of the cantilever and tip interactions to be relatively small. The AFM phase image of the Cell-Tak surface in figure 6.5b shows to indicate change in phase of the cantilever and tip interactions to be relatively higher than for the phase images of BSA, PLL, and PDA surfaces. Table 6.1 shows height roughness values to be largest for BSA and PDA surfaces, while the phase roughness values show to be largest for BSA and Cell-Tak surfaces. Height and phase roughness value for the PLL surface are smaller the than the height and phase roughness values for PDA, Cell-Tak and BSA surfaces. Contrast and image quality were optimized as described in section 5.5.

6.2 Measuring the interaction forces between the bacterial *DH5alfa* cell probe and the bacterial adhesive or repulsive surfaces

Force-distance curves were recorded in milliQ water with a loading rate of 96nN/s, a contact time of 0 s, and a loading force of 1 nN for all AFM force measurements. Force-distance curves are presented in a gallery to show the absence or presence of one or multiple force jumps from the bacterial interaction, including the control measurements. The bacterial measurements and control measurements of rupture force and rupture length are presented in histograms. The mean average and standard deviation of the rupture forces and lengths are presented in tables. Rupture force and length were plotted observe their correlation. Force interactions versus time for each AFM force experiment is also plotted to observe the change of interactions with time during each AFM force experiment.

6.2.1 Force-distance curves

A gallery of the force-distance curves obtained of the bacterial interactions with the bacterial adhesive or repulsive surfaces, including the control measurements, are showed in figure 6.6, 6.7, 6.8, 6.9 and 6.10.

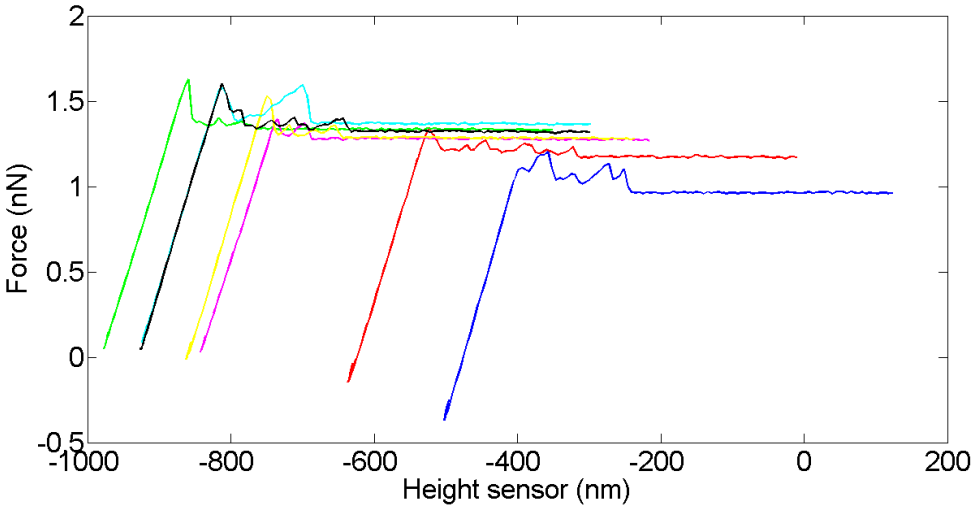

(A) Force-distance curves from the interactions between the bacterial *DH5alfa* coated AFM tip and the glass surface

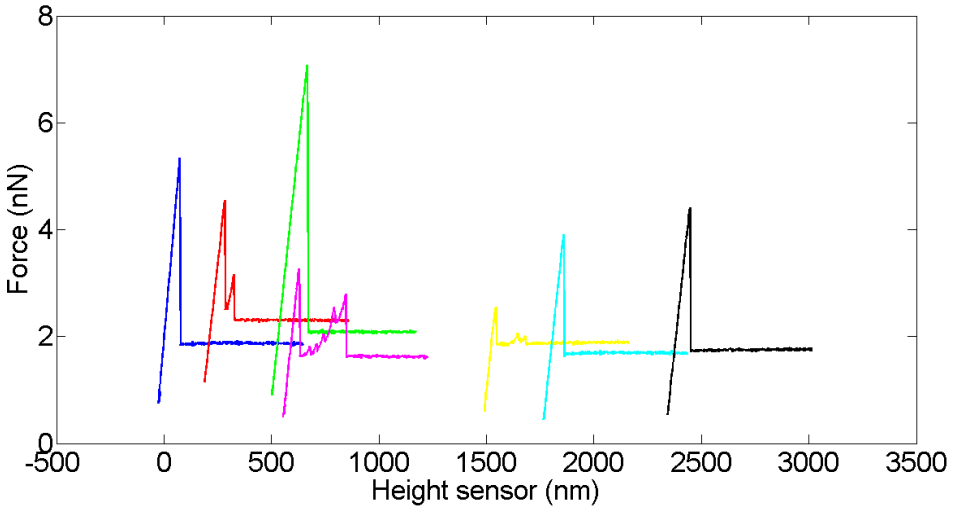

(B) Force-distance curves from the interactions between the PDA coated AFM tip and the glass surface

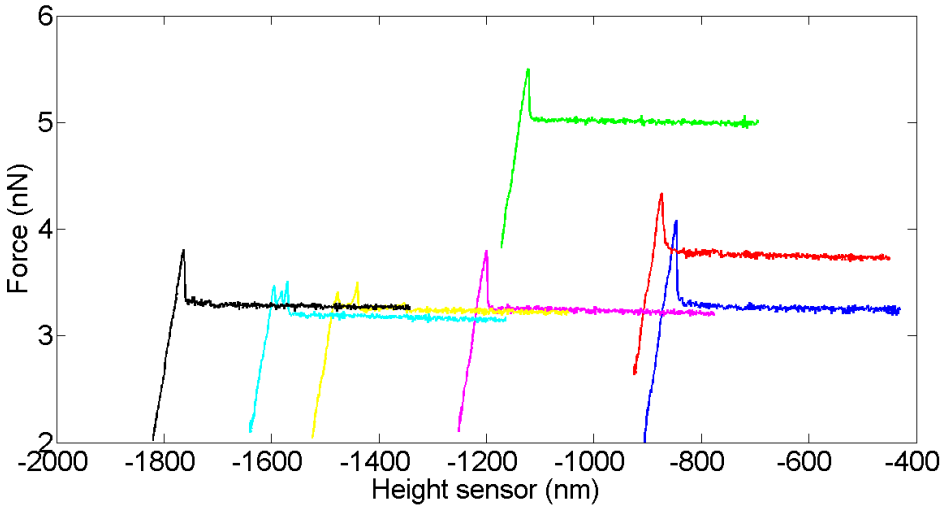

(C) Force-distance curves from the interactions between the bare AFM tip and the glass surface

FIGURE 6.6: Representative plots of the force-distance curves from the interactions between the bacterial *DH5alfa* coated AFM tip and glass surface including the control measurements

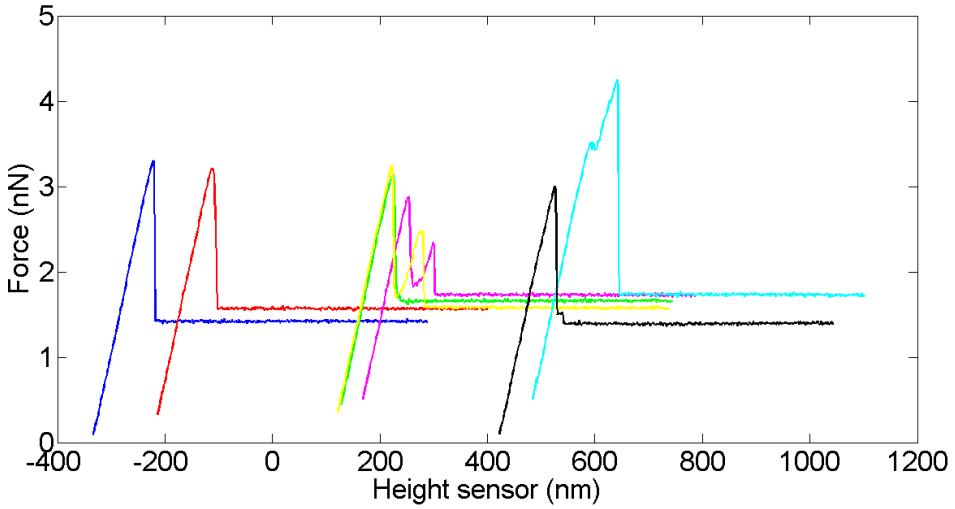

(A) Force-distance curves from the interactions between the bacterial *DH5alfa* coated AFM tip and the PLL surface

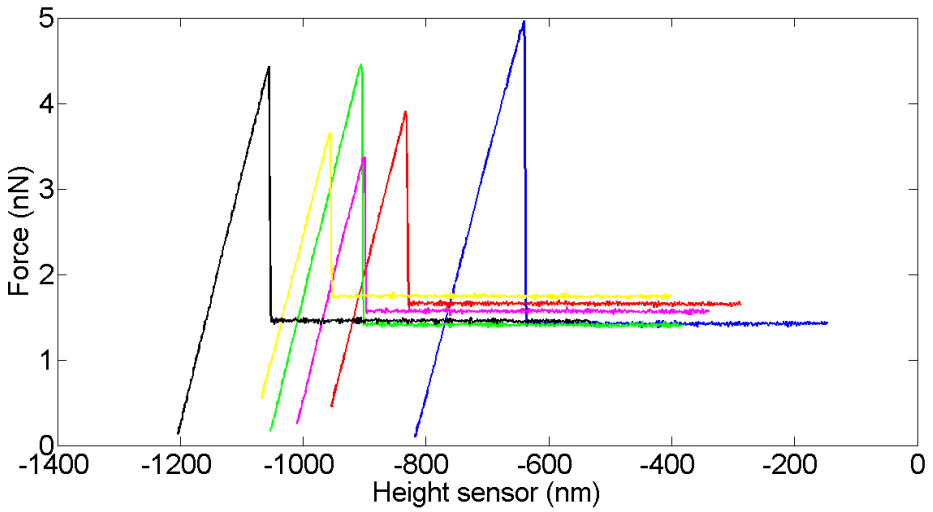

(B) Force-distance curves from the interactions between the PDA coated AFM tip and the PLL surface

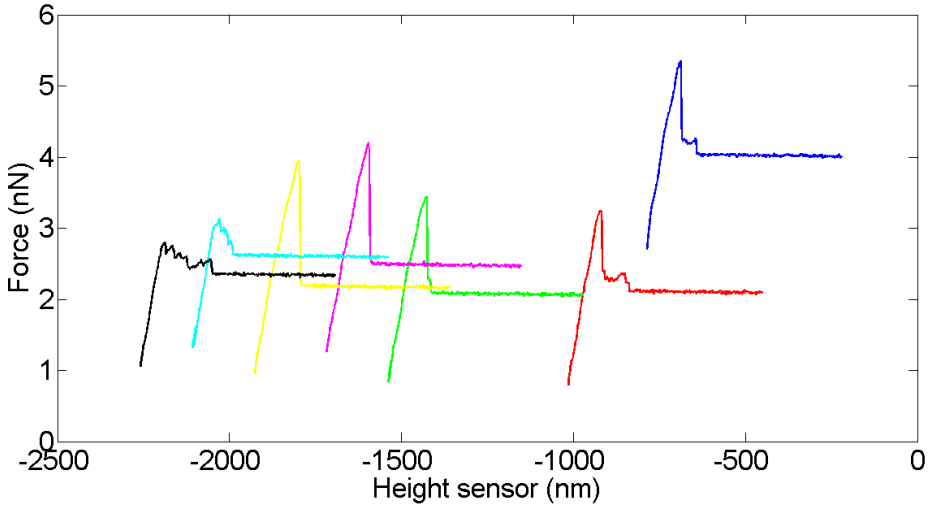

(C) Force-distance curves from the interactions between the bare AFM tip and the PLL surface

FIGURE 6.7: Representative plots of the force-distance curves from the interactions between the bacterial *DH5alfa* coated AFM tip and PLL surface including the control measurements

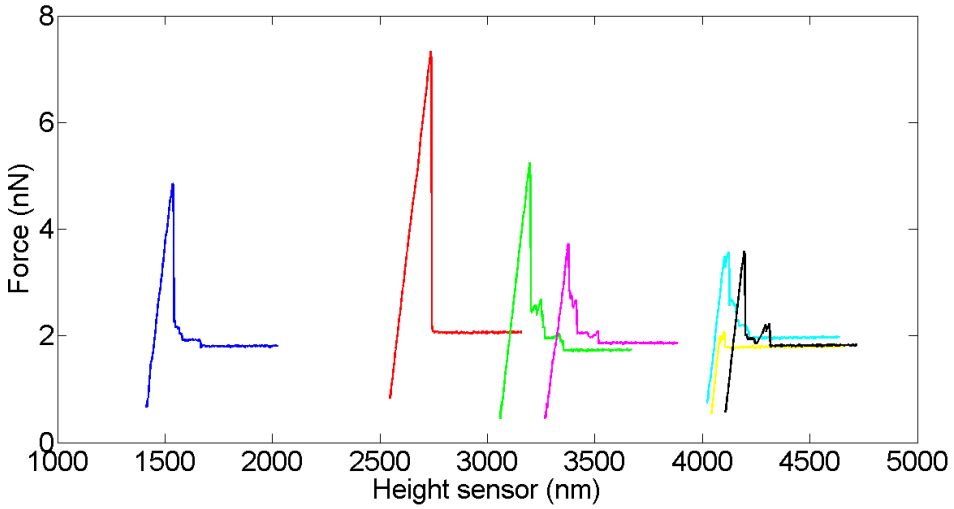

(A) Force-distance curves from the interactions between the bacterial *DH5alfa* coated AFM tip and the PDA surface

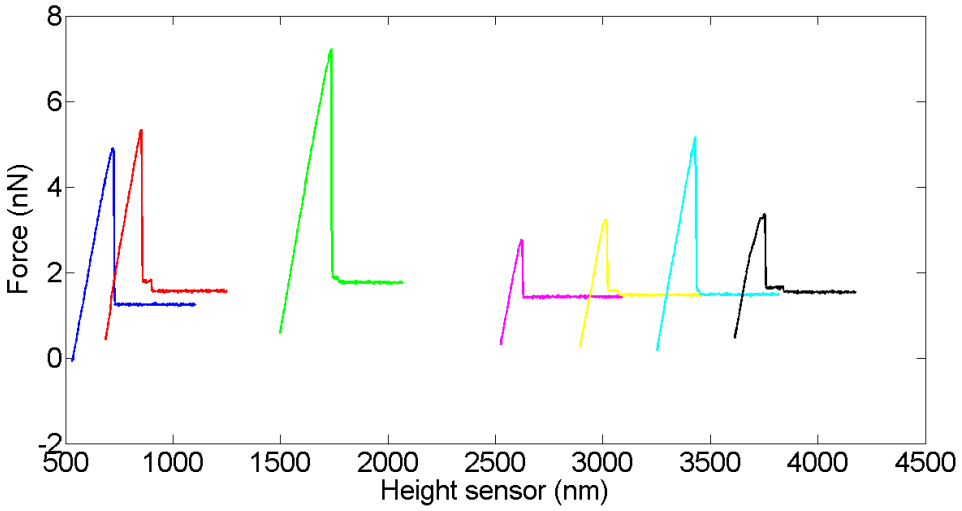

(B) Force-distance curves from the interactions between the PDA coated AFM tip and the PDA surface

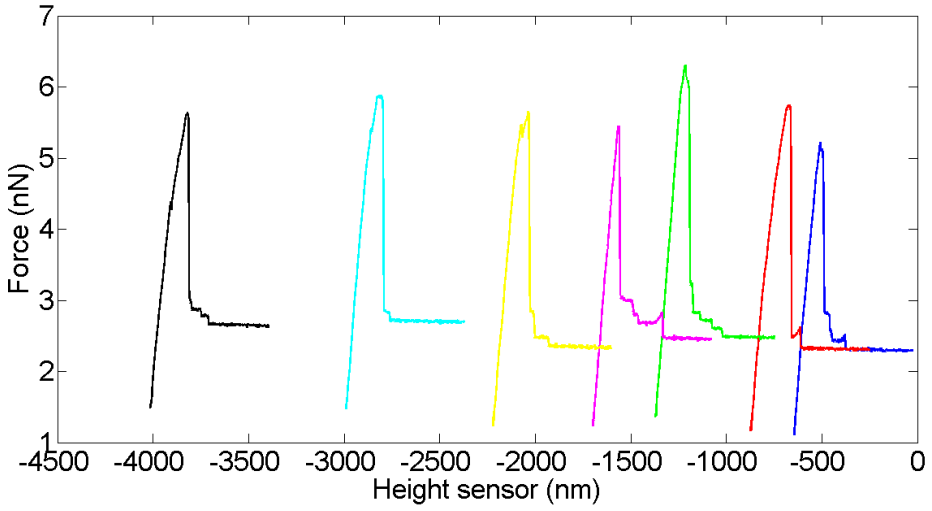

(C) Force-distance curves from the interactions between the bare AFM tip and the PDA surface

FIGURE 6.8: Representative plots of the force-distance curves from the interactions between the bacterial *DH5alfa* coated AFM tip and PDA surface including the control measurements

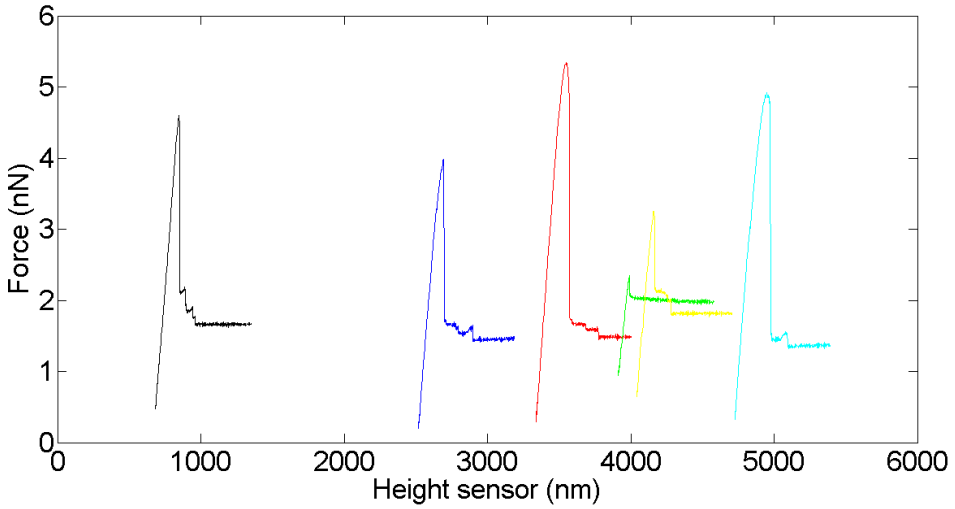

(A) Force-distance curves from the interactions between the bacterial *DH5alfa* coated AFM tip and the Cell-Tak surface

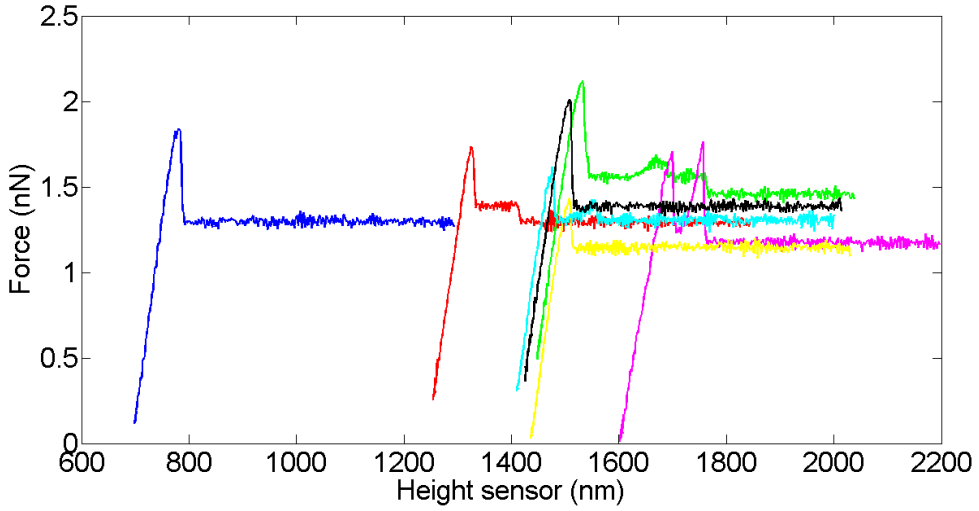

(B) Force-distance curves from the interactions between the PDA coated AFM tip and the Cell-Tak surface

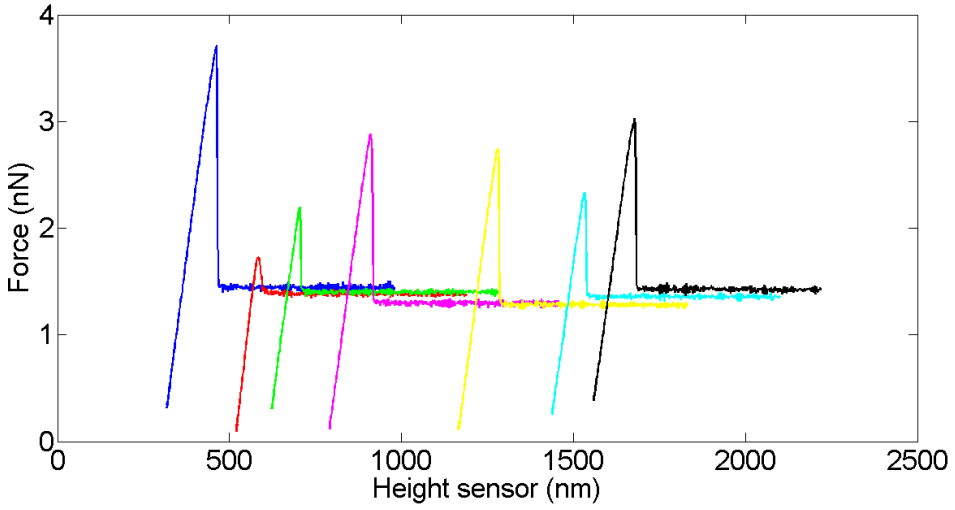

(C) Force-distance curves from the interactions between the bare AFM tip and the Cell-Tak surface

FIGURE 6.9: Representative plots of the force-distance curves from the interactions between the bacterial *DH5alfa* coated AFM tip and Cell-Tak surface including the control measurements

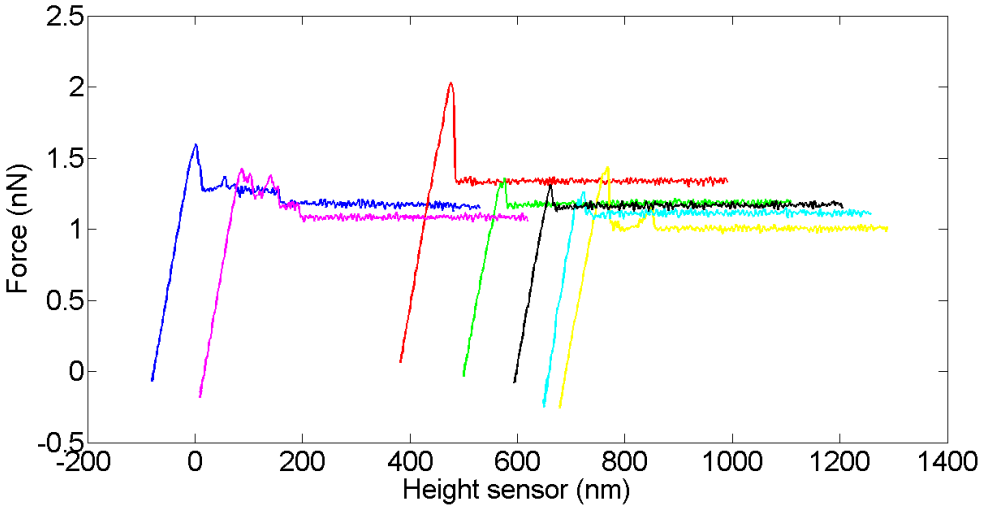

(A) Force-distance curves from the interactions between the bacterial *DH5alfa* coated AFM tip and the BSA surface

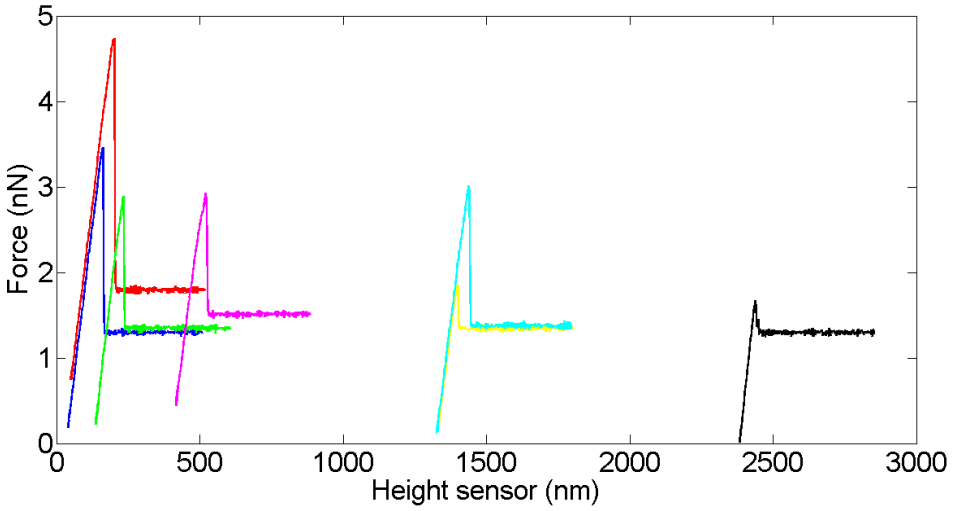

(B) Force-distance curves from the interactions between the PDA coated AFM tip and the BSA surface

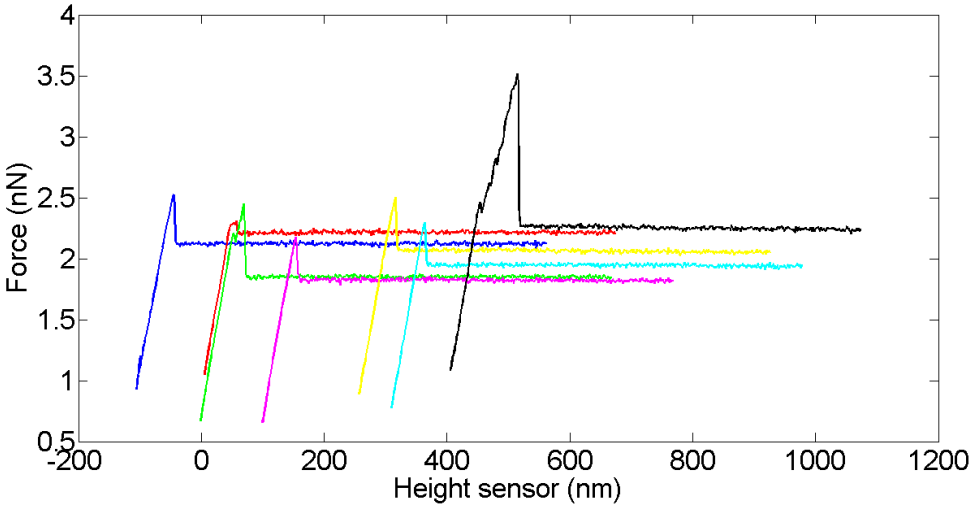

(C) Force-distance curves from the interactions between the bare AFM tip and the BSA surface

FIGURE 6.10: Representative plots of the force-distance curves from the interactions between the bacterial *DH5alfa* coated AFM tip and BSA surface including the control measurements

6.2.2 Rupture forces, and control measurements

The rupture forces are presented below in table 6.2 as well as in figure 6.11, 6.12, 6.13, and 6.14.

Glass	Poly-L-lysine	Polydopamine	Cell-Tak	Bovine serum albumin
0.13 +/− 0.05	1.22 +/− 0.25	1.73 +/− 1.00	1.91 +/− 0.68	0.28 +/− 0.23

(A) Mean rupture force (nN) between the bacterial *DH5alfa* coated AFM tip and the bacterial adhesive or repulsive surfaces

Glass	Poly-L-lysine	Polydopamine	Cell-Tak	Bovine serum albumin
1.46 +/− 0.88	1.79 +/− 0.48	1.98 +/− 0.91	0.30 +/− 0.18	1.22 +/− 0.48

(B) Mean rupture force (nN) between the polydopamine coated AFM tip and the bacterial adhesive or repulsive surfaces

Glass	Poly-L-lysine	Polydopamine	Cell-Tak	Bovine serum albumin
0.42 +/− 0.28	1..00 +/− 0.38	2.48 +/− 0.43	0.83 +/− 0.53	0.27 +/− 0.15

(C) Mean rupture force (nN) between the clean and bare AFM tip and the bacterial adhesive or repulsive surfaces

TABLE 6.2: Mean and standard deviation of the rupture forces between the bacterial *DH5alfa* coated AFM tip and the bacterial adhesive or repulsive surfaces including the control measurements. (+/−) Represents the standard deviation over the 350-450 force ruptures obtained of the different measurements

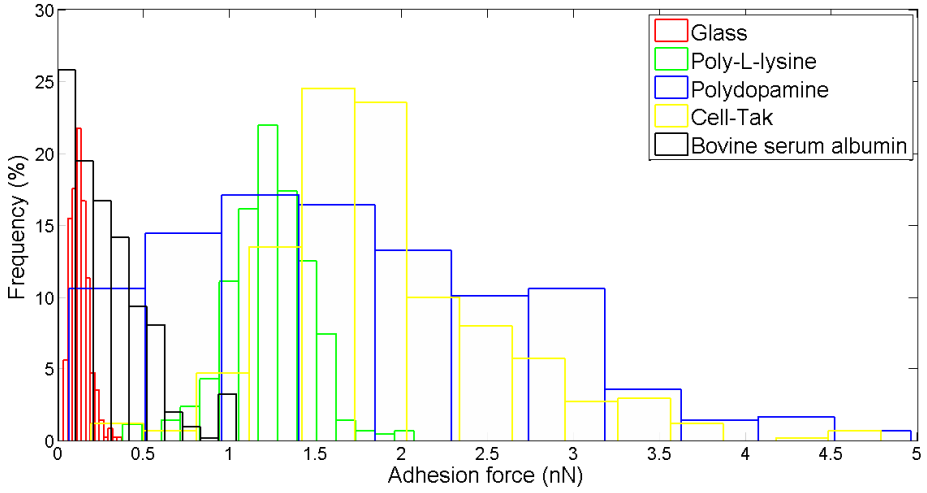

(A) Rupture force measurements between the bacterial *DH5alfa* coated AFM tip and the bacterial adhesive or repulsive surfaces

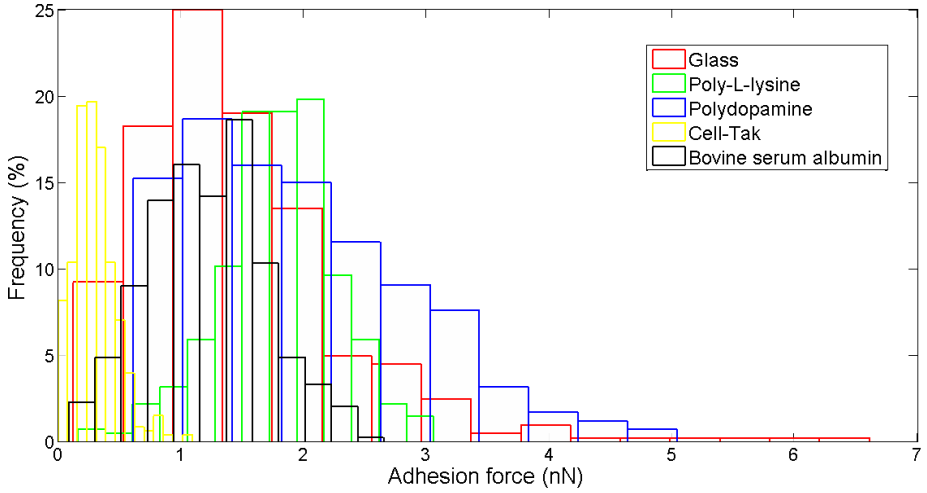

(B) Rupture force measurements (control) between the polydopamine coated AFM tip and the bacterial adhesive or repulsive surfaces

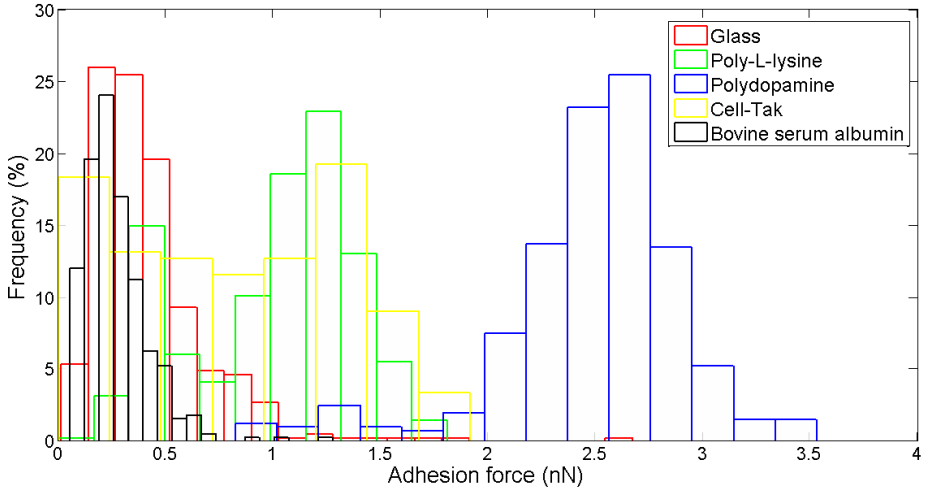

(C) Rupture force measurements (control) between the bare and clean AFM tip and the bacterial adhesive or repulsive surfaces

FIGURE 6.11: Representative histograms of the AFM rupture force measurements between bacterial *DH5alfa* coated AFM tip and the bacterial adhesive or repulsive surfaces including the control measurements

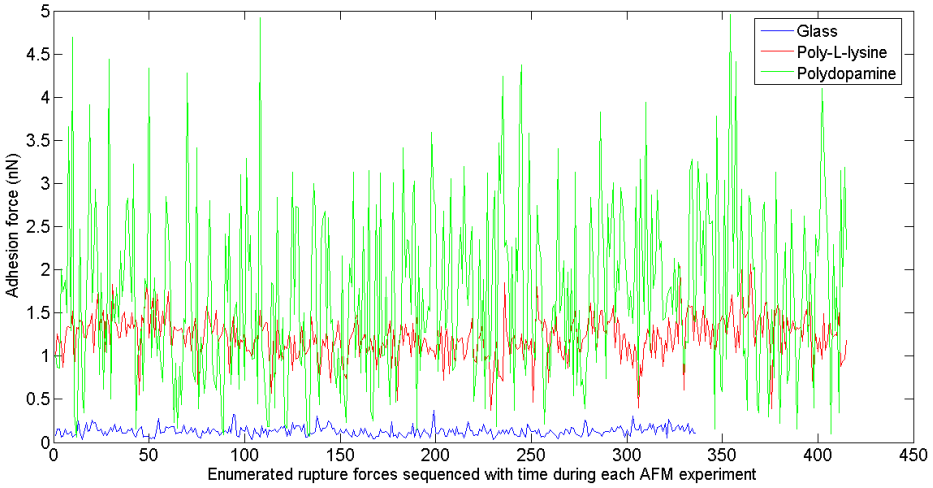

(A) Rupture forces varying with time between the bacterial *DH5alfa* coated AFM tip and glass, PLL, or PDA surfaces

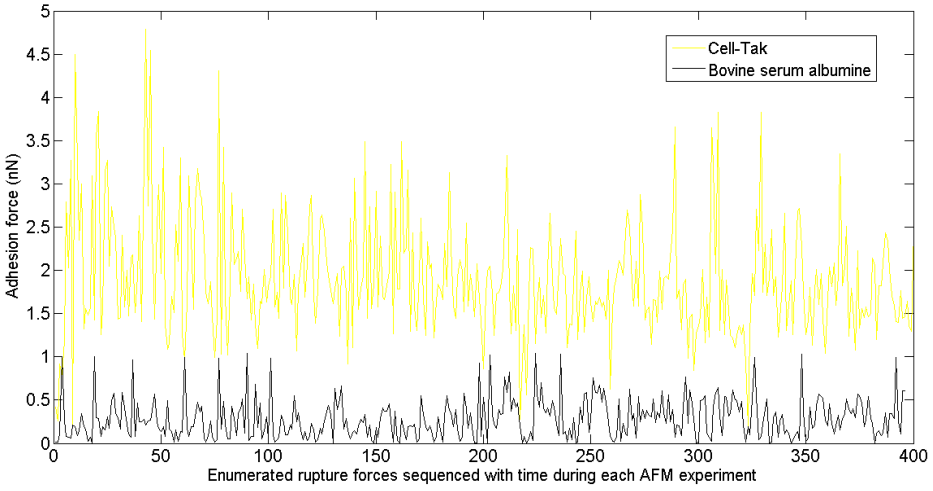

(B) Rupture forces varying with time between the bacterial *DH5alfa* coated AFM tip and BSA or Cell-Tak surfaces

FIGURE 6.12: Representative plots of the rupture forces varying with time between bacterial *DH5alfa* coated AFM tip and the bacterial adhesive or repulsive surfaces

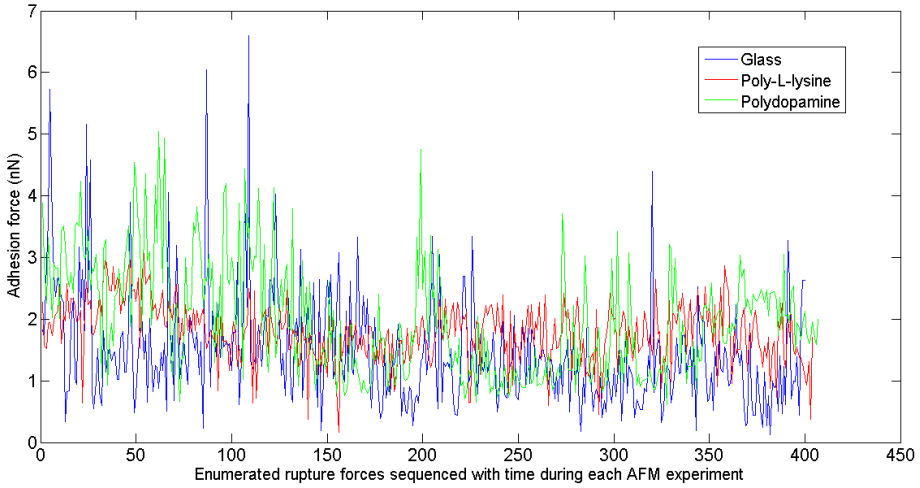

(A) Rupture forces (control) varying with time between the PDA coated AFM tip and glass, PLL, or PDA surfaces

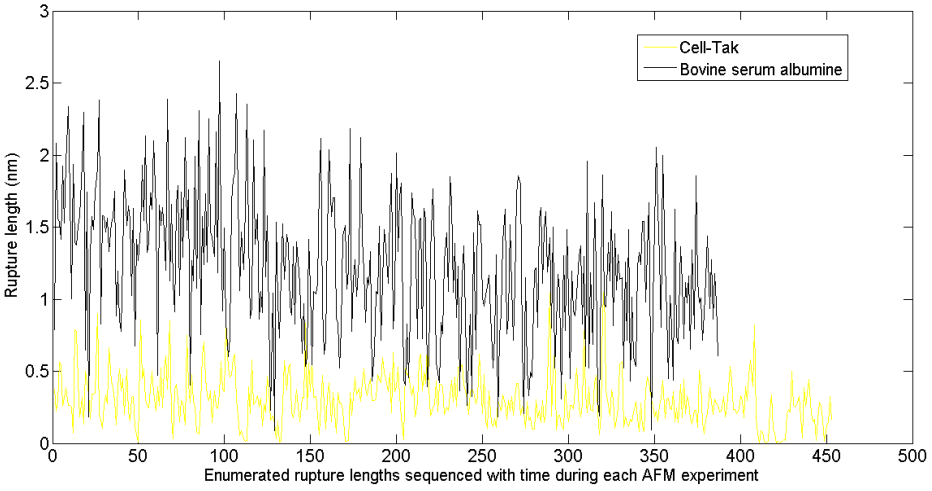

(B) Rupture forces (control) varying with time between the PDA coated AFM tip and BSA or Cell-Tak surfaces

FIGURE 6.13: Representative plots of the rupture forces (control) varying with time between the PDA coated AFM tip and the bacterial adhesive or repulsive surfaces

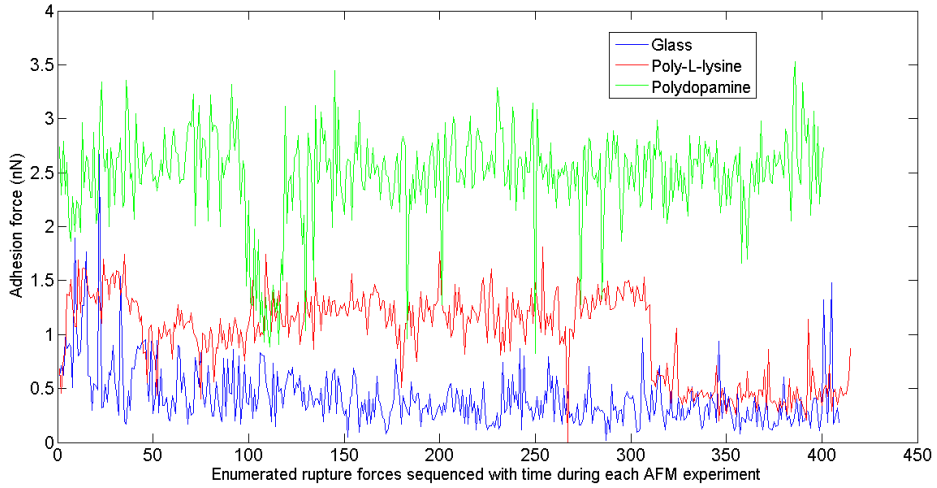

(A) Rupture forces (control) varying with time between the bare AFM tip and glass, PLL, or PDA surfaces

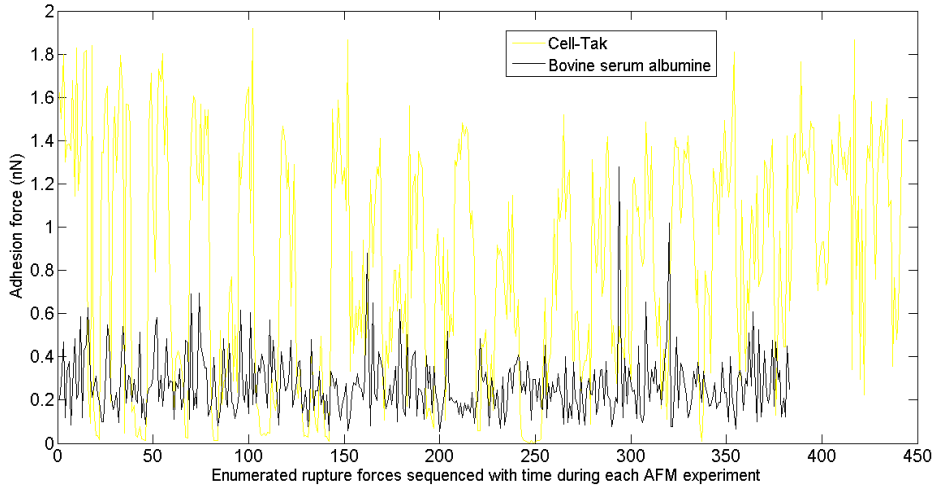

(B) Rupture forces (control) varying with time between the bare AFM tip and BSA or Cell-Tak surfaces

FIGURE 6.14: Representative plots of rupture forces (control) varying with time between the bare AFM tip and the bacterial adhesive or repulsive surfaces

As shown in table 6.2a and figure 6.11a, the interactions between bacterial *DH5alfa* coated AFM tip and PLL, PDA and Cell-Tak surfaces have a higher measured de-adhesion force than for BSA and glass surfaces. The PDA coated tip control measurements in table 6.2b and figure 6.11b show rupture forces that is close to the same value of ∼1.50nm. The bare tip control measurements in table 6.2c and figure 6.11c show to have rupture forces that is not close to the same value (Mean rupture forces: PDA; 2.48nN, PLL; 1.00nN, Cell-Tak; 0.83nN, Glass; 0.42nN, and BSA; 027nN).

Rupture forces tends to vary for, bacterial coated tip on PDA or Cell-Tak surfaces in figure 6.12a (PDA; from ∼0.50nN to ∼3.50nN, Cell-Tak; from ∼1.00nN to ∼3.00nN),

for PDA tip on BSA surface in figure 6.13b (BSA; from ∼0.50nN to ∼2.00nN), and for bare tip on PDA, PLL, glass or Cell-Tak surfaces in figure 6.14 (PDA; from ∼1.00nN to ∼2.50nN, PLL; from ∼0.50nN to ∼1.50nN, Cell-Tak; from ∼0.40nN to ∼1.40nN).

Rupture forces tend to decrease for PDA tip on BSA, PLL, PDA or glass surfaces in figure 6.13 (BSA; from ∼1.50nN to ∼1.00nN, PLL; from ∼2.00nN to ∼1.50nN, PDA; from ∼3.00nN to ∼2.00nN, Glass; from ∼2.00nN to ∼1.00nN). Rupture forces tends to be close to a certain value for, bacterial coated tip on PLL, BSA or glass surfaces in figure 6.12 (PLL; from ∼1.00nN, BSA; ∼0.25nN, Glass; ∼0.20nN), for PDA tip on Cell-Tak surface in figure 6.13b (Cell-Tak; ∼0.25nN) and for bare tip on PDA or BSA surfaces in figure 6.14(PDA; ∼2.50nN, BSA; ∼0.25nN). The SEM images of the AFM tip after the bacterial AFM measurements are shown in Appendix C.

6.2.3 Rupture length and control measurements

The rupture lengths are presented below in table 6.3 as well as in figure 6.15, 6.16, 6.17, and 6.18. Some rupture lengths obtained occurs as artifacts due to misinterpretation of force-distance curves in the analyzing procedure. These misinterpreted rupture lengths have negative values or values above 200nm and can be seen in figure 6.16, 6.17 and figure 6.18. The rupture lengths with negative values or values above 200nm are influencing the obtained histograms in figure 6.15 and mean rupture length values, which are discussed in Chapter 7.

Glass	Poly-L-lysine	Polydopamine	Cell-Tak	Bovine serum albumin
32 +/− 48	58 +/− 15	65 +/− 32	108 +/− 34	24 +/− 18

(A) Mean rupture length (nm) between the bacterial *DH5alfa* coated AFM tip and the bacterial adhesive or repulsive surfaces

Glass	Poly-L-lysine	Polydopamine	Cell-Tak	Bovine serum albumin
50 +/− 33	77 +/− 20	96 +/− 39	32 +/− 26	60 +/− 22

(B) Mean rupture length (nm) between the polydopamine coated AFM tip and the bacterial adhesive or repulsive surfaces

Glass	Poly-L-lysine	Polydopamine	Cell-Tak	Bovine serum albumin
21 +/− 21	58 +/− 30	135 +/− 31	67 +/− 70	14 +/− 9

(C) Mean rupture length (nm) between the clean and bare AFM tip and the bacterial adhesive or repulsive surfaces

TABLE 6.3: Mean and standard deviation of the rupture lengths between the bacterial *DH5alfa* coated AFM tip and the bacterial adhesive or repulsive surfaces including the control measurements. (+/−) Represents the standard deviation over the 350-450 ruptures lengths obtained of the different measurements

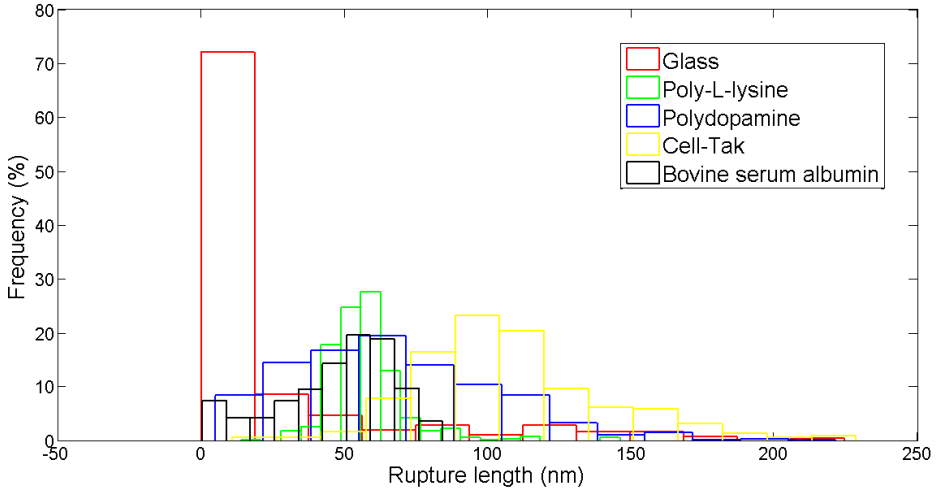

(A) Rupture length measurements between the bacterial *DH5alfa* coated AFM tip and the bacterial adhesive or repulsive surfaces

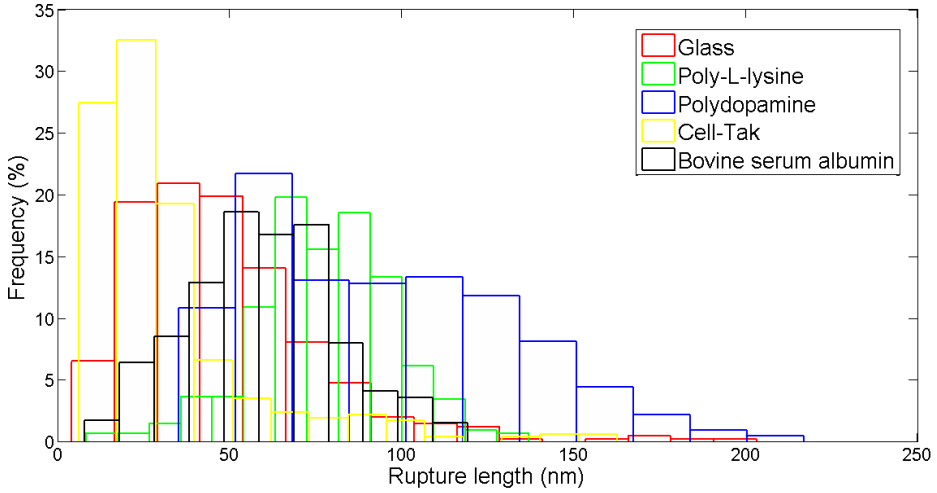

(B) Rupture length measurements (control) between the polydopamine coated AFM tip and the bacterial adhesive or repulsive surfaces

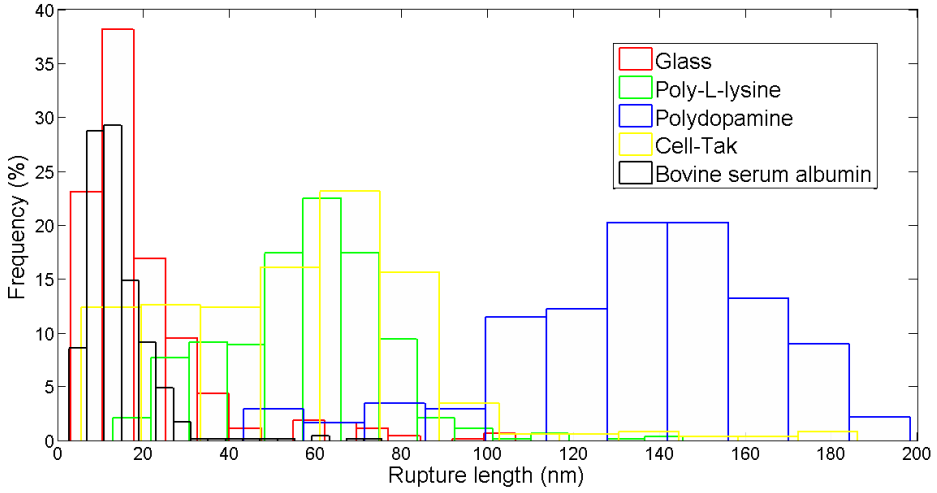

(C) Rupture length measurements (control) between the bare and clean AFM tip and the bacterial adhesive or repulsive surfaces

FIGURE 6.15: Representative histograms of the AFM rupture length measurements between bacterial *DH5alfa* coated AFM tip and the bacterial adhesive or repulsive surfaces including the control measurements

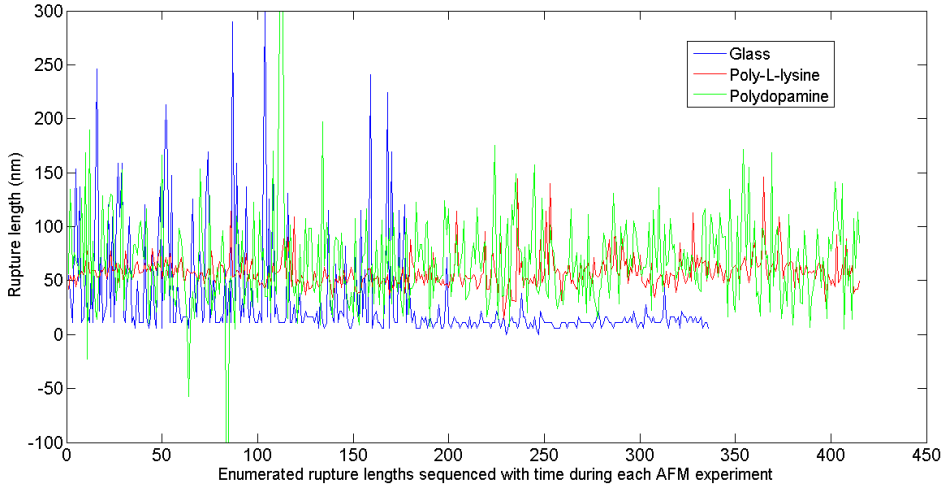

(A) Rupture lengths varying with time between the bacterial *DH5alfa* coated AFM tip and glass, PLL, or PDA surfaces

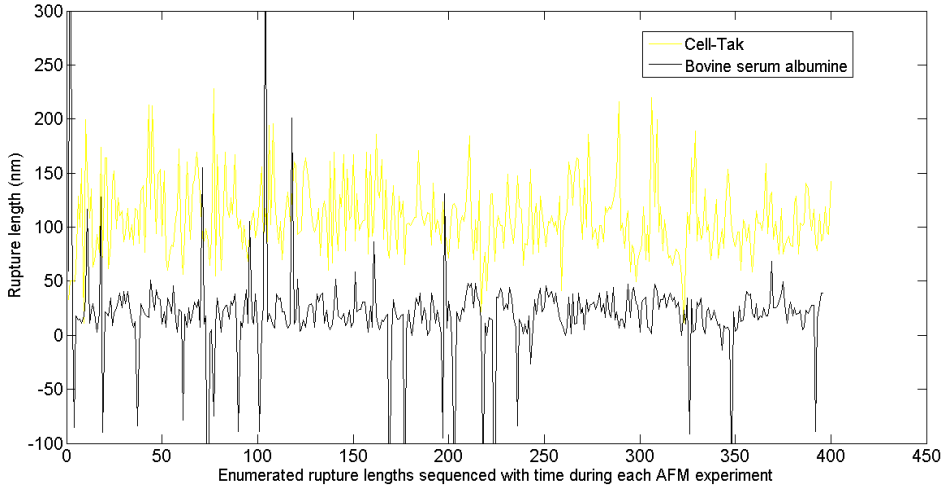

(B) Rupture lengths varying with time between the bacterial *DH5alfa* coated AFM tip and BSA or Cell-Tak surfaces

FIGURE 6.16: Representative plots of the rupture lengths varying with time between bacterial *DH5alfa* coated AFM tip and the bacterial adhesive or repulsive surfaces

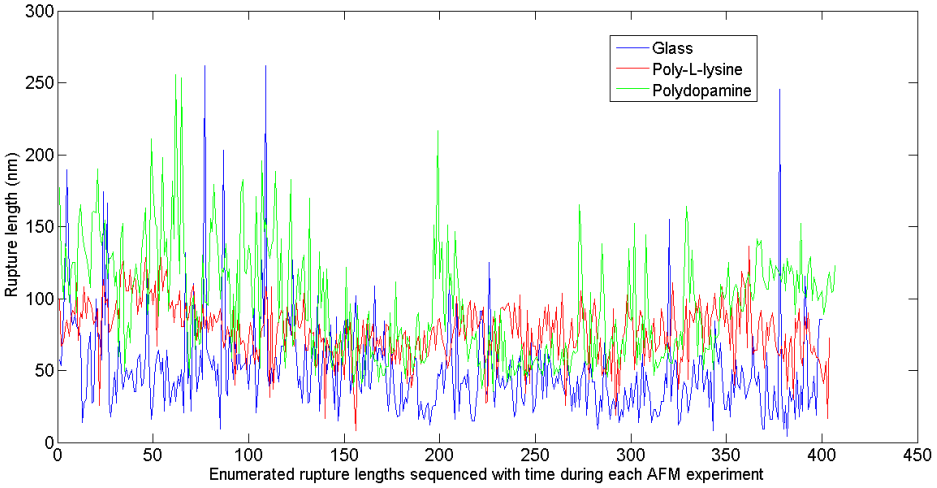

(A) Rupture lengths (control) varying with time between the PDA coated AFM tip and glass, PLL, or PDA surfaces

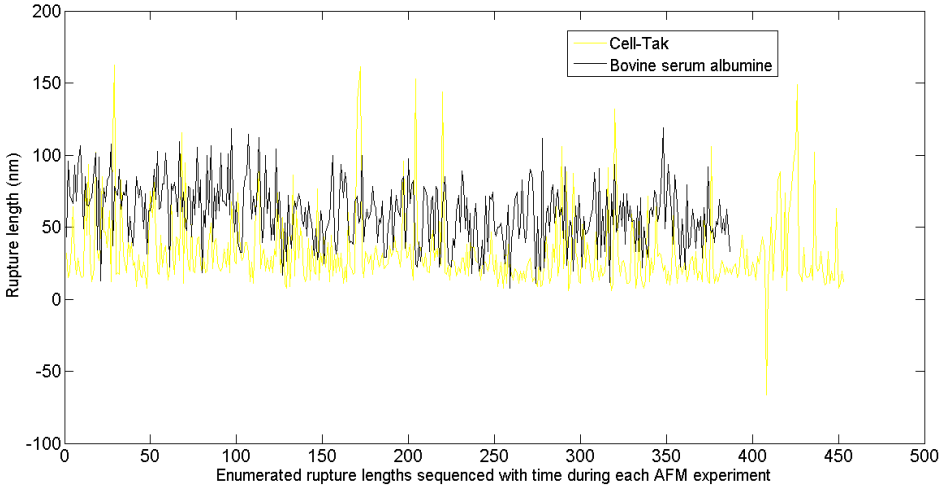

(B) Rupture lengths (control) varying with time between the PDA coated AFM tip and BSA or Cell-Tak surfaces

FIGURE 6.17: Representative plots of the rupture lengths (control) varying with time between the PDA coated AFM tip and the bacterial adhesive or repulsive surfaces

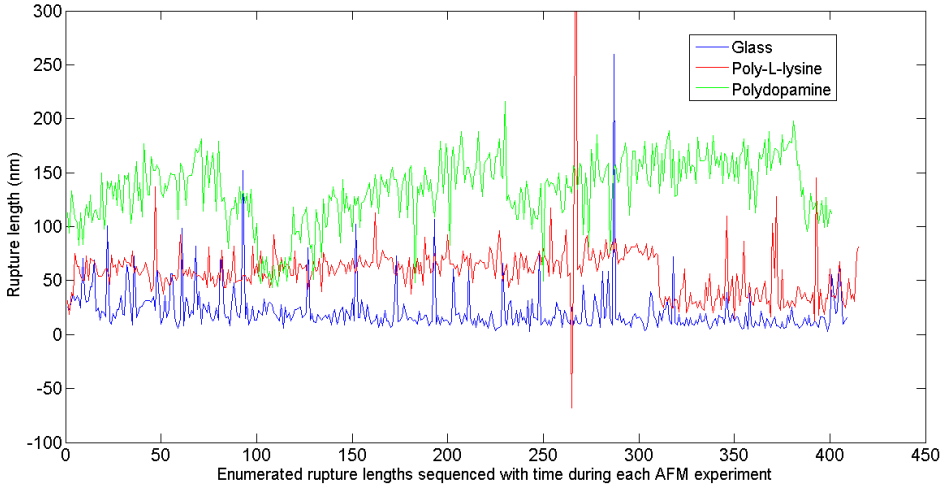

(A) Rupture lengths (control) varying with time between the bare AFM tip and glass, PLL, or PDA surfaces

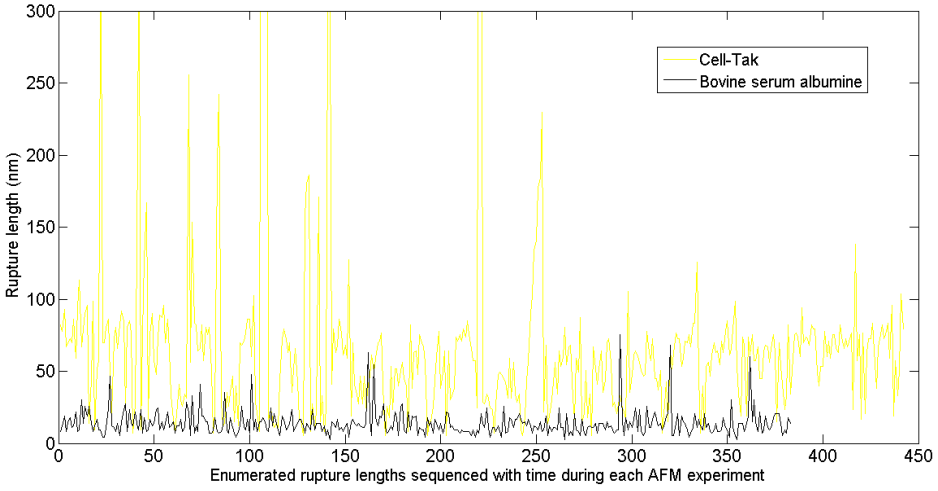

(B) Rupture lengths (control) varying with time between the bare AFM tip and BSA or Cell-Tak surfaces

FIGURE 6.18: Representative plots of rupture lengths (control) varying with time between the bare AFM tip and the bacterial adhesive or repulsive surfaces

As shown in the table 6.3a and figure 6.15a, the interactions between bacterial *DH5alfa* coated AFM tip and PLL or PDA surfaces have rupture lengths close to the same value of ∼60nm. The interactions between bacterial *DH5alfa* coated AFM tip and glass or BSA surface have rupture lengths close to the same value of ∼28nm. The rupture lengths obtained for bacterial *DH5alfa* coated AFM tip and Cell-Tak surfaces differentiates from the PDA and PLL values that is close to 60nm as well as the glass and BSA values that is close to 28nm (Cell-Tak; Mean rupture length of 108nm). The PDA coated tip control measurements in table 6.3b and figure 6.15b show rupture lengths that are close to the same value of ∼70nm. The rupture lengths obtained for PDA coated AFM tip and Cell-Tak or glass surfaces, are differentiating from the PDA, PLL, and BSA values that

are close to 70nm (Mean rupture lengths: Cell-Tak; 32nm, Glass; 50nm). The bare tip control measurements in table 6.3c and figure 6.15c show to have rupture lengths that are not close to the same value (Mean rupture length: PDA; 135nm, Cell-Tak; 67nm, PLL; 58nm, Glass; 21m, and BSA; 14nm).

Rupture lengths tend to vary for, bacterial coated AFM tip on PDA or Cell-Tak surfaces in figure 6.16 (PDA; from ∼20nm to ∼90nm, Cell-Tak; from ∼50nm to ∼100nm), for PDA tip on PDA surfaces in figure 6.17 (PDA; from ∼50nm to ∼180nm), and for bare tip on PDA, PLL and Cell-Tak surfaces in figure 6.18 (PDA; from ∼100nm to ∼200nm, PLL; from ∼10nm to ∼90nm, Cell-Tal; from ∼10nm to ∼90nm).

The force interactions are decreasing for PDA tip on BSA, PLL, PDA or glass surfaces in figure 6.17 (BSA; from∼80nm to ∼40nm, PLL; from ∼80nm to ∼50nm, PDA; from ∼125nm to ∼70nm, Glass; from ∼60nm to ∼25nm). For the interactions between bare AFM tip and the PDA surface in figure 6.18, the rupture lengths are increasing from ∼100nm to ∼200nm. The rupture lengths shows to be close to a certain value for, bacterial coated AFM tip on PLL, BSA or glass surfaces in figure 6.16 (PLL; ∼50nm, BSA; ∼20nm, Glass; ∼30nm), for PDA tip on Cell-Tak surface in figure 6.17b (Cell-TAk;∼25nm) and for bare tip on BSA or glass surfaces in figure 6.18 (BSA; ∼20nm, Glass; ∼30nm). The SEM images of the AFM tip after the bacterial AFM measurements are shown in Appendix C.

6.2.4 Correlation between the rupture forces and lengths

The correlation between rupture forces and lengths can be seen in figure 6.19, 6.20, and 6.21.

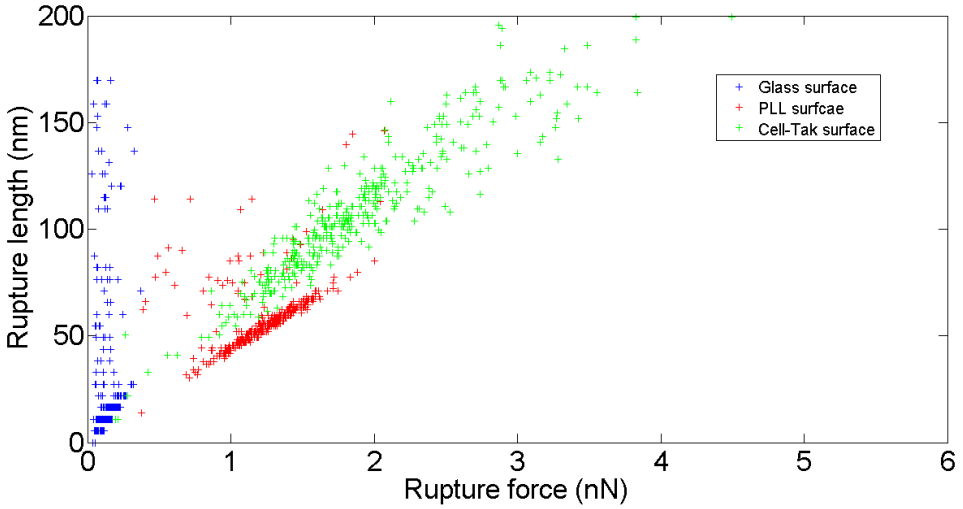

(A) Correlation between rupture forces and lengths for bacterial *DH5alfa* coated AFM tip and glass, PLL, or Cell-Tak surfaces

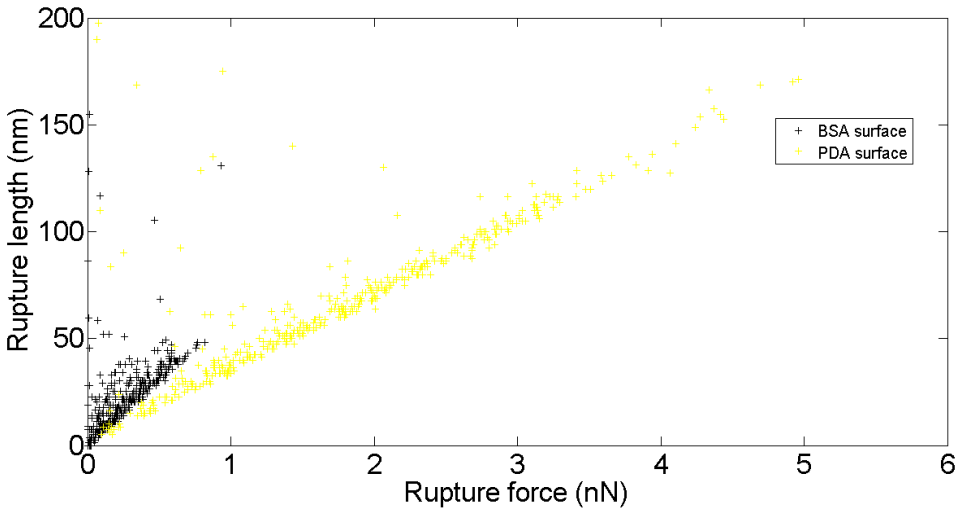

(B) Correlation between rupture forces and lengths for bacterial *DH5alfa* coated AFM tip and BSA or PDA surfaces

FIGURE 6.19: Representative data points of the correlation between rupture forces and lengths for bacterial *DH5alfa* coated AFM tip and the bacterial adhesive or repulsive surfaces

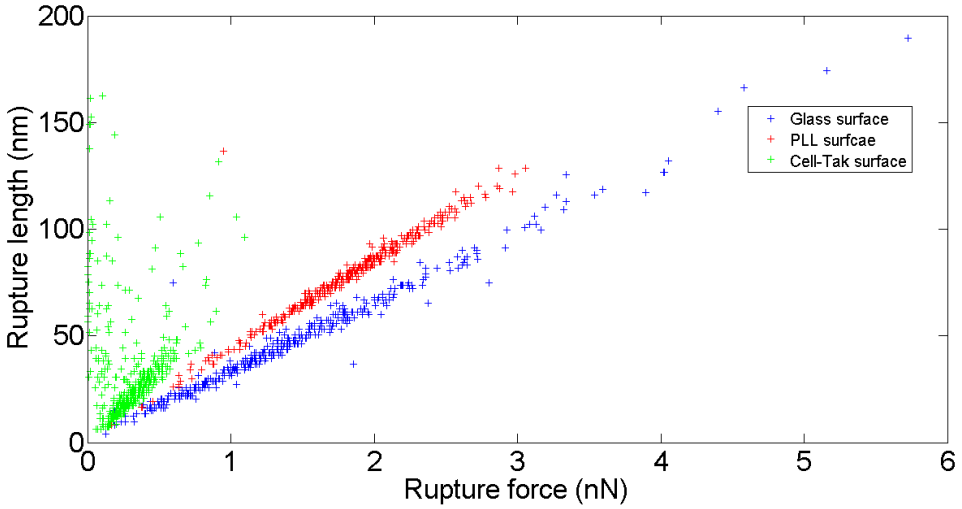

(A) Correlation between rupture forces and lengths for PDA coated AFM tip and glass, PLL, or Cell-Tak surfaces

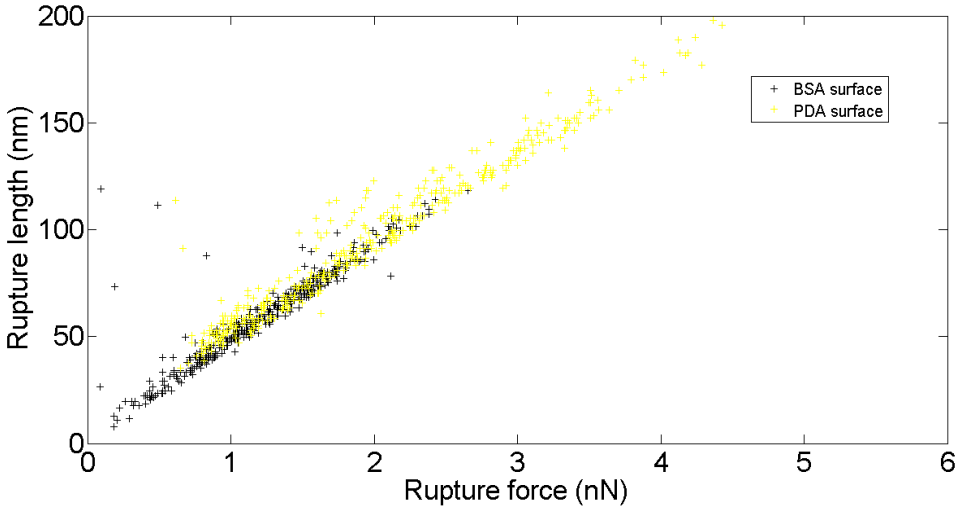

(B) Correlation between rupture forces and lengths for PDA coated AFM tip and BSA or PDA surfaces

FIGURE 6.20: Representative data points of the correlation between rupture forces and lengths for PDA coated AFM tip and the bacterial adhesive or repulsive surfaces

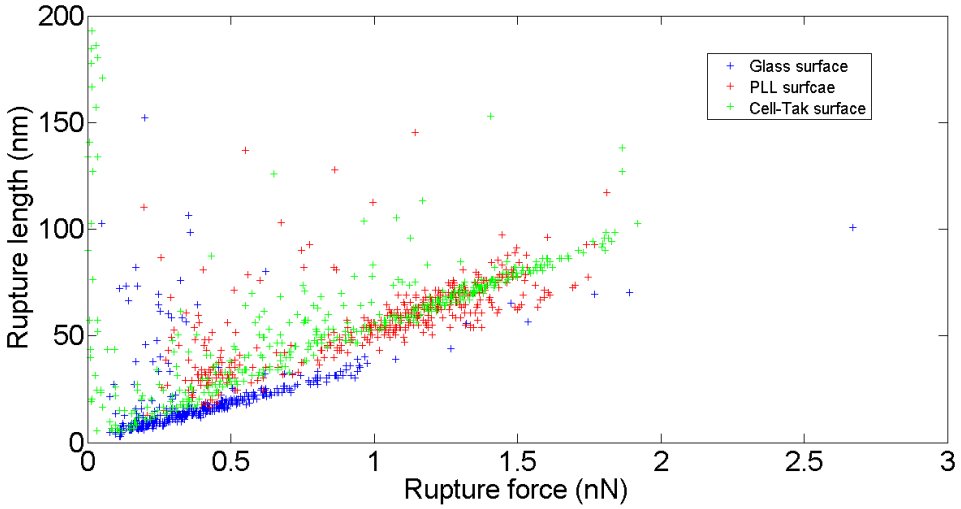

(A) Correlation between rupture forces and lengths for bare AFM tip and glass, PLL, or Cell-Tak surfaces

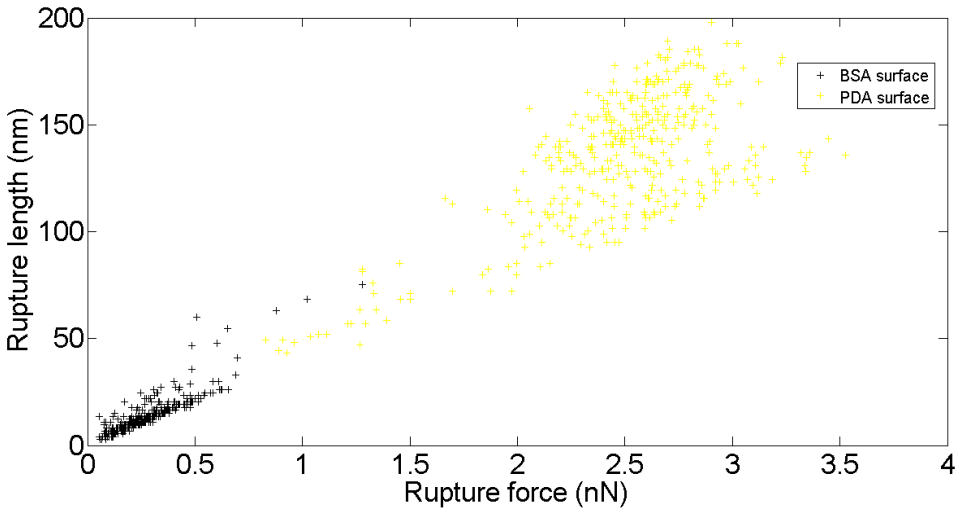

(B) Correlation between rupture forces and lengths for bare AFM tip and BSA or PDA surfaces

FIGURE 6.21: Representative data points of the correlation between rupture forces and lengths for bare AFM tip and the bacterial adhesive or repulsive surfaces

From figure 6.19, 6.20, and 6.21, a linear correlation can be seen between rupture forces and lengths for the bacterial interactions with bacterial adhesive or repulsive surfaces including the control measurements. Bacterial interactions with PDA, PLL or BSA surfaces have rupture force and length data points that is spread more than the rupture force and length data points for the the bacterial interaction with Cell-Tak or glass surfaces.

The PDA coated tip interactions with PLL, PDA or BSA surfaces have rupture force and length data points that is spread more than the rupture force and length data points for the PDA coated tip interactions with Cell-Tak surfaces

The bare tip interactions with BSA, Cell-Tak or glass surfaces have rupture force and length data points that is spread more than the rupture force and length data points for the bare tip interactions with PLL or PDA surfaces.

Chapter 7

Discussion

The project aimed for development and optimization of modified surfaces (glass) that will serve as repellents or adhesives for E. coli bacteria. The bacterial adhesive or repulsive layers of BSA or PDA was introduced on glass by μCP, while the bacterial adhesive layers of PLL and Cell-Tak was introduced on glass by regular incubation methods. The homogeneity of deposited layer was examined by imaging with AFM. AFM force spectroscopy was used to investigate the strength of interaction between the modified surfaces and bacteria. AFM tips coated with PDA was then used to immobilize bacteria on the tip. The immobilization of bacteria on the tip were validated before and after AFM force spectroscopy experiments by the use of fluorescence microscopy and SEM.

7.1 Experimental challenges in assessing bacterial interaction when using bacterial cells as a probe in AFM measurements

In the study of bacterial interactions with the different surfaces, bacteria were immobilized on the AFM tip and validated both before and after the AFM experiment as showed in Chapter 5 and 6. It was proven rather difficult to attach a single bacterial cell to the apex of AFM tip. The AFM tip monitoring before and after the interaction measurements demonstrated that clusters of individual bacterial cells were immobilized on the AFM tip. Simple immersion of the PDA-coated cantilever in bacterial suspensions were performed in order to attach bacteria . The immobilization of bacteria occurs randomly at the entire tip surface that is dipped into the bacterial suspension, which makes difficult to obtain a tip with sufficient enough amount of bacterial cells specifically at the apex of AFM tip. The distinct shape of single bacterial cells were not possible

to be observed either due to the high voltages used in the SEM, vacuum conditions, or the absorption of high energies. The heat or energy absorbed can be due to the gold sputtering process or the SEM imaging that are deforming or dissolving the bacterial cell shape. A high vacuum in the SEM imaging chamber might also result in deformation since water vapour are escaping the bacterial cell sample. As only voltages in range of 15-25kV resulted in SEM images with reasonable high contrast and resolution (obtained with SEM Tabletop), the secondary or backscattered electrons received by the electron detector have probably originated from a depth within the sample that exceeds the size of the bacteria. Namely, the shape of the bacterial cell did not become observable in SEM with voltages used in range of 15-25kV since the incoming electrons penetrates deep into the sample and generate secondary or backscattered electrons that will scatter or loose energy before reaching the electron detector. To solve this, a SEM with a possibility of achieving high resolution and contrast at lower voltages than 10kV should be used. If the sputtering process, electron energy, or vacuum conditions are the reason for not obtaining images of bacterial shapes in SEM, the fixation of bacteria before gold sputtering and SEM imaging is not sufficient enough to obtain stable bacterial cells. To preserve the bacterial cell shape for SEM imaging, it is suggested to choose another materials for the sputtering process or that other methods than glutaraldehyde treatment is used to fix the bacteria.

Since it seems that it is a cluster of bacteria that interacts with the bacterial adhesive or repulsive surfaces during the AFM experiments, multiple interactions are assumed to occur at the same time for each unbinding event. The relation between the unbinding events of the bacterial interactions and the number of bacterias present on the tip was not explored further and remains unclear. The immobilization of individual bacteria on an AFM probe shall minimize this effect. Choosing the proper cantilever spring constant for bacterial force measurements should be predicated upon on the behavior of the cantilever while performing the AFM interaction force measurements. Lower spring constant results in higher force sensitivity but also in higher noise as mentioned in Chapter 4. Other unwanted effects occurring when using cantilevers with low spring constant are the tendency of vertical or horizontal voltage drifting that is a result of the liquid medium being out of equilibrium or its hydrostatic pressure. Vertical drifting was common under the AFM force measurements performed within this study and manual adjustment of the vertical voltage to -2.00V during measurements was often necessary. To avoid drifting, cantilevers with higher spring constant can be used, although this results in a lower force sensitivity. Measurements with cantilever spring constants of 0.07-0.10 N/m instead of 0.02-0.03 N/m were tested but resulted also in vertical drifting. As drifting serves as an uncertain factor in the AFM measurements it is suggested to further optimise parameters such as the liquid medium, type of cantilever, or other

AFM instrumental factors to minimize vertical voltage drifting.

The parameters of contact time, loading rate, loading force and buffers used are also important to consider when assessing bacterial interactions. The loading rate was set to 96nN/m for all AFM measurements since the setting of different loading rates with intention to tilt the energy landscape of the unbinding events is often a very time consuming process. In this project, neither the rupture force dependency on loading rate nor contact time to find the dissociation or association rate constant were explored further. Neither the rupture force dependency on loading rate nor the contact time were explored since the unbinding forces itself was a sufficient enough indicator to assess type of molecules that would be suitable for bacterial micro arrays. However, finding the dissociation or association rate constant could be useful to determine the rate the bacteria are binding or unbinding in a micro array. The choice of buffers with a certain ionic concentration will also influence the interacting nature of the appendages of the bacteria with the molecules on the bacterial adhesive or repulsive surfaces. The electric double layer is also influenced by the ionic concentration as mentioned in Chapter 3. As all measurements were performed in milliQ water, that has a very low ionic concentration, a high repulsion and little adhesion should be observed for all measurements in theory. In this project adhesion forces were obtained for all bacterial adhesive or repulsive surfaces reflecting the fact that bacterial cells have the generic adhesive or repulsive molecular nature. Applied loading force seemed to overcome such electrostatic repulsion between the bacteria and the surfaces. A loading force of maximum 1nN was used since applying higher forces could result in damaging the bacterial cells. As the contact time was set to 0s, the bacterial adhesions obtained are assumed to be reversible. The use of different buffers than milliQ water with varying ionic concentration would affect the interacting nature of the bacteria with the bacterial adhesive or repulsive surfaces as well the viability of the bacteria. The use of a contact time longer than 0s would also influence the rupture forces and rupture lengths obtained from the AFM measurements as more appendages of the bacterias would bind the bacterial adhesive or repulsive surface. More appendages piercing the energy barrier and binding the surface indicates the initiation of the irreversible adhesion stage of the bacteria, which is mentioned in Chapter 3. The number of appendages binding the surface is however limited by the influence of thermal impulses as well as the geometry of the bacteria and the orientated state of the bacteria when in contact with the surface. Namely, for a high contact time range, the number of appendages binding the surface is saturated reaching a binding or unbinding equilibrium with the thermal impulses.

Specific reorientation of a single cell body to face it toward the sample surface when performing force spectroscopy has recently been demonstrated by Beaussart et al. and

Potthoff et al. as mentioned in Chapter 4 [28, 29]. Developing the force spectroscopy technique for bacteria in this direction gives results of unbinding events with a higher accuracy. This also gives more opportunities to explore the cell interactions as a function of buffers, contact time and loading rate as the immobilization and validation of a viable single cell on probes are achieved.

7.2 Analytical challenges in assessing bacterial interaction when using bacterial cells as a probe in AFM measurements

As presented in Chapter 6, SEM images were obtained of the bare, PDA-coated, and the bacterial-coated AFM tips. Bacterial immobilization can be confirmed by the observation of the cluster materials being observed on the AFM tip. Although for PDA-coated AFM tip it is not possible to distinguish any discriminating difference between the bare and the PDA-coated AFM tip. To distinguish and validate the presence of different materials on the AFM tips, control measurements were also obtained of the force interactions between the bare, PDA-coated, or the bacterial-coated AFM tip and the bacterial adhesive or repulsive surfaces. As seen from table 6.2 that represents the mean average rupture force from histograms in figure 6.11, it is possible to distinguish the rupture forces between the bare, PDA-coated, and the bacterial-coated AFM tips for most bacterial repulsive or adhesive surfaces. For bacteria- and PDA-coated AFM tip it is difficult to distinguish the rupture forces when interacting with PLL and PDA surfaces. Based on the control measurements, the presence of bacteria on the tip can not be unambiguously proven for PLL and PDA surfaces, even though based on the SEM images in Appendix C bacteria are attached on the tip. For bare and PDA-coated tip the rupture forces for all surfaces can be distinguished, which indicates that AFM tip has indeed a coating layer of PDA.

As seen from table 6.3 that represents the mean average rupture length from histograms in figure 6.15 it is possible to distinguish the rupture lengths between the bare, PDA-coated and bacteria-coated AFM tips for most bacterial repulsive or adhesive surfaces. For bacteria- and PDA-coated AFM tip it is difficult to distinguish the rupture lengths for the BSA and PDA surfaces. Based on the control measurements, the presence of bacteria on the tip cannot be concluded for BSA and PDA surfaces, even though from the SEM images in Appendix C showed bacteria on the tip. For bare and PDA-coated tip the rupture lengths for all surfaces can be easily distinguished, which indicates that PDA is a coating layer on the AFM tip.

Additionally, rupture force and rupture length were plotted as a function of time for each AFM experiment as shown in figure 6.12, 6.13, 6.14, 6.16, 6.17, and 6.18. This to observe the stability of the bonds between the bacteria and the PDA-coated AFM tip as well the stability of the bonds between the bacterial adhesive or repulsive molecules and the glass surface. It is assumed that a decrease or increase in the plotted data points of force interaction versus time can be seen when bacterias are detaching from the tip, when bacterial adhesive or repulsive molecules are attaching to the bacterial coated tip, or when bacterial adhesive or repulsive molecules are detaching from the glass surface during the AFM measurements. Some changes were observed as mentioned in Chapter 6. These factors should be considered when assessing the measured bacterial rupture forces and rupture lengths. The change in rupture force or length as a function of time can also be a result of a non-uniform topography of the bacterial adhesive or repulsive surfaces. The AFM images were presented in figure 6.2, 6.3, 6.4, and 6.5 showing topography, and the force interacting nature of these surfaces. Few aggregates can be seen for PLL and PDA surfaces, and the AFM phase image of the Cell-Tak surface shows to have non-uniform force interactions. Such lack of uniformity and presence of aggregates could influence the force measurements. It is suggested to further explore the bacterial interactions on Cell-Tak and PDA surfaces since the interactions decrease and increase during the AFM measurements, and if necessary, to further explore the control measurements for the PDA-coated tip and bare tip interactions with surfaces where the interactions decrease and increase during the AFM measurements as indicated in Chapter 6. Attachment of the final layer to the glass via intermediate step of silanization of the bacterial adhesive or repulsive molecules to the glass surface, or silanization of the PDA to the AFM tip should also be considered to produce a more stable and covalent bonds on the anchoring surfaces to assure that the molecules will not detach from the glass surface or from the AFM tip.

Considering the manual analysis of force-distance curves in the IDL program, some challenges occurred when determining rupture force and length in small values range. As mentioned in Chapter 5, determining force rupture or length was dependent on manually adjusting the derivative of the retracted force-distance curve with the smooth function as well the setting of range for the derivative function in the IDL program. For small rupture forces, the obtained rupture length tends to be unrealistically long since its determination is based on the analyzed adhesion work rupture of each retracted force-distance curve. The adhesion work analyzed was a result of integrating the area under the retracted force-distance curve at a range that does not represent genuine force ruptures. For histograms obtained in figure 6.15 or these artefacts can be seen typically

in the the bins for rupture length over 90 nm for bacterial and bare tip force measurements with glass and BSA surfaces. These unrealistically long rupture lengths can be set at approximately 0nm, since the rupture forces analysed were close to 0N.

Another factor to consider when assessing force-distance curves as mentioned in section 7.1, is unknown number of many interactions contributing to each unbinding event since it is a cluster of bacteria seems to interact with the different surfaces. Force jumps that reflected an enthalpic regime (rapid increase in force over a short displacement) with an exponential shape were not observable for the force-distance curves. The force-distance curves consisted mostly of force jumps with a linear rise of force with the displacement of cantilever tip, which indicates that multiple interactions are involved in the unbinding event. As the contact time was set to 0s, a small number of interactions is assumed be present. The distribution of rupture forces and lengths obtained in he histograms are similar to the shape of the Poisson distributed function . For experimental setups similar to the AFM setup used in this project, reports are suggesting that multiple bonds which are formed at a constant rate over a given time interval would have variables with a Poisson distribution [63–65]. The Poisson distribution models discrete random variables that are always positive and independent of the time since the last event. The variables should also be obtained from a large number of events. In this project rupture forces and lengths are always positive. The number of registered events is also relatively large, between 350 and 450 for each probe-surface configuration. The requirement of independence between subsequent events would be fulfilled mostly by the stability of the attachment of bacteria to the AFM tip and the attachment of bacterial adhesive or repulsive molecules to the glass surface. As mentioned above, the stability can be analyzed by observing the interaction variation as a function of time for each AFM experiment. The Poisson distributed shape of the histograms obtained from the rupture forces and lengths are suggested to be a result of the multiple interactions that are occurring for each unbinding event. Considering that the mean average of rupture forces and lengths values obtained are based on a Gaussian distribution, Poisson analysis were also performed for comparison. The Poisson-lambda values from the rupture forces and lengths obtained were however found to be approximately equal the Gaussian distributed mean values. The lambda values was found with the same function "fitdist" in Matlab as used for the mean values, even though the Poisson distribution were used instead on Gaussian distribution. The comparisons between Gaussian mean values and Poisson lambda values are shown in table 7.1 and 7.2.

Glass	Poly-L-lysine	Polydopamine	Cell-Tak	Bovine serum albumin
0.13 +/− 0.05	1.22 +/− 0.25	1.73 +/− 1.00	1.91 +/− 0.68	0.28 +/− 0.23

(A) Mean rupture force (nN) values obtained, based on the Gaussian distribution, between the bacterial *DH5alfa* coated AFM tip and the bacterial adhesive or repulsive surfaces

Glass	Poly-L-lysine	Polydopamine	Cell-Tak	Bovine serum albumin
0.13	1.22	1.73	1.91	0.28

(B) Lambda rupture force (nN) values obtained, based on the Poisson distribution, between the bacterial *DH5alfa* coated AFM tip and the bacterial adhesive or repulsive surfaces

Glass	Poly-L-lysine	Polydopamine	Cell-Tak	Bovine serum albumin
1.46 +/− 0.88	1.79 +/− 0.48	1.98 +/− 0.91	0.30 +/− 0.18	1.22 +/− 0.48

(C) Mean rupture force (nN) values obtained, based on the Gaussian distribution, between the polydopamine coated AFM tip and the bacterial adhesive or repulsive surfaces

Glass	Poly-L-lysine	Polydopamine	Cell-Tak	Bovine serum albumin
1.46	1.79	1.98	0.30	1.22

(D) Lambda rupture force (nN) values obtained, based on the Poisson distribution, between the polydopamine coated AFM tip and the bacterial adhesive or repulsive surfaces

Glass	Poly-L-lysine	Polydopamine	Cell-Tak	Bovine serum albumin
0.42 +/− 0.28	1..00 +/− 0.38	2.48 +/− 0.43	0.83 +/− 0.53	0.27 +/− 0.15

(E) Mean rupture force (nN) values obtained, based on the Gaussian distribution, between the clean and bare AFM tip and the bacterial adhesive or repulsive surfaces

Glass	Poly-L-lysine	Polydopamine	Cell-Tak	Bovine serum albumin
0.42	1..00	2.48	0.83	0.27

(F) Lambda rupture force (nN) values obtained, based on the Poisson distribution, between the clean and bare AFM tip and the bacterial adhesive or repulsive surfaces

TABLE 7.1: Comparisons between the rupture forces obtained with Gaussian and Poisson distribution, between the bacterial *DH5alfa* coated AFM tip and the bacterial adhesive or repulsive surfaces including the control measurements. (+/−) Represents the standard deviation over the 350-450 force ruptures obtained of the different measurements

Glass	Poly-L-lysine	Polydopamine	Cell-Tak	Bovine serum albumin
32 +/− 48	58 +/− 15	65 +/− 32	108 +/− 34	24 +/− 18

(A) Mean rupture length (nm) values obtained, based on the Gaussian distribution, between the bacterial *DH5alfa* coated AFM tip and the bacterial adhesive or repulsive surfaces

Glass	Poly-L-lysine	Polydopamine	Cell-Tak	Bovine serum albumin
29	58	68	108	47

(B) Lambda rupture length (nm) values obtained, based on the Poisson distribution, between the bacterial *DH5alfa* coated AFM tip and the bacterial adhesive or repulsive surfaces

Glass	Poly-L-lysine	Polydopamine	Cell-Tak	Bovine serum albumin
50 +/− 33	77 +/− 20	96 +/− 39	32 +/− 26	60 +/− 22

(C) Mean rupture length (nm) values obtained, based on the Gaussian distribution, between the polydopamine coated AFM tip and the bacterial adhesive or repulsive surfaces

Glass	Poly-L-lysine	Polydopamine	Cell-Tak	Bovine serum albumin
49	77	95	33	60

(D) Lambda rupture length (nm) values obtained, based on the Poisson distribution, between the polydopamine coated AFM tip and the bacterial adhesive or repulsive surfaces

Glass	Poly-L-lysine	Polydopamine	Cell-Tak	Bovine serum albumin
21 +/− 21	58 +/− 30	135 +/− 31	67 +/− 70	14 +/− 9

(E) Mean rupture length (nm) values obtained, based on the Gaussian distribution, between the clean and bare AFM tip and the bacterial adhesive or repulsive surfaces

Glass	Poly-L-lysine	Polydopamine	Cell-Tak	Bovine serum albumin
20	58	134	56	14

(F) Lambda rupture length (nm) values obtained, based on the Poisson distribution, between the clean and bare AFM tip and the bacterial adhesive or repulsive surfaces

TABLE 7.2: Comparisons between the rupture lengths obtained with Gaussian and Poisson distribution, between the bacterial *DH5alfa* coated AFM tip and the bacterial adhesive or repulsive surfaces including the control measurements. (+/−) Represents the standard deviation over the 350-450 ruptures lengths obtained of the different measurements

As mentioned in section 7.1, the reduction of control measurements and higher accuracy of unbinding events can be achieved by performing AFM techniques similar to that being demonstrated by Beaussart et al. where a single viable bacterial cell was used as a probe in force spectroscopy.

7.3 The use of other alternative methods than AFM based force spectroscopy to measure bacterial interactions

AFM force spectroscopy is based on using a force probe where molecules or cells are anchored to the cantilever. The cantilever can be steered precisely with piezo electric components enabling great control of the cantilever displacements. The molecules or cells interactions with a surface can be measured within a range of nanonewtons depending on the spring constant of the cantilever being used. Another state of the art

technique that also are a enables single molecule interaction studies is the Optical Tweezing (OT) technique. Here, typically functionalized polystyrene microbeads are optically trapped by a laser beam that has a Gaussion transversal intensity profile where the spring constant can be associated to the optical trap. In a similar signaling process to that arranged in the AFM, a quadrant photo diode is detecting voltage signals where the stiffness of the bead-optical trap and the displacement of the bead can be found. The force is then calculated using the voltage signal proportionality to the displacement and the spring constant of the optical trap. Typically, force measurements with OT are in the so called dual bead experiment reaching the ability to detect forces down to a fraction of a piconewton [15]. Bacterial interaction measurements have been performed in liquid with dual bead OT were two laser beams are used to trap two functionalized micro beads. One micro bead was used as a probe to anchor bacteria that is movable and another micro bead with a permanent position was used for anchoring molecules of interest. The movable bead was then approaching and retracting against the permanent bead in a controlled manner with a certain contact time, loading force and loading rate [66, 67]. A significant advantage of using OT instead of AFM is its ability to measure and apply smaller external forces than AFM, where the possible outer barriers of the energy landscape of the unbinding events becomes evident for the bacterial interactions. As the micro beads have a size in the order of bacteria, OT can be used to measure single bacterial interactions. However in dual beam experiments the bacterial interactions with molecules are occurring on a spherical bead and not on a flat surface. Fewer interactions are assumed to be involved in each unbinding event for the bacterial interactions in OT than for AFM force measurements as the micro beads are exposing only small amount of bacteria to a small amount of molecules. How the measuring of single molecule interactions reflects the ability of bacteria to bind and to be viable on bacterial adhesive or repulsive molecules is unclear. Since the reversible and irreversible bacterial adhesions often involve multiple interactions that constitutes between the bacterial surface, bacterial appendages and the substrate surface, including additive molecules as exopolymeric substances (EPS) (mentioned in section 4.1), the force measurements of multiple bacterial interactions with surfaces that occur simultaneously might reflect the adhesive nature of surfaces with a higher accuracy. Assuring bacterial viability might also be a challenge when performing OT. The laser beam trapping beads contains a high energy that could result in a heat transfer from the bead to the bacteria or in an energy transfer from the photons to the bacteria that would decrease its viability.

Bacterial interactions measured with OT might serve as an complementary technique to AFM as fewer interactions can be involved for each unbinding event. Applying and measuring forces in piconewton range with OT are favorable when assessing bacterial

interactions with surfaces to obtain information about the possible outer barriers of the energy landscape of the unbinding events.

7.4 Assessing the bacterial interactions

7.4.1 Biological interpretation and the optimization of bacterial micro arrays

AFM experiments were performed by using the *DH5alfa* bacteria as a probe to measure bacterial interactions with BSA, PLL, Cell-Tak, PDA and glass surfaces as presented in Chapter 6. The rupture forces or lengths were obtained with intention to optimize bacterial micro arrays in terms of assessing the bacterial adhesion and its stability in micro arrays. As mentioned in section 3.2.1, microbial cell development, cell viability, and metabolic activity have also shown to be strongly affected by cell adhesion, which also represents the initial step in biofilm formation [27]. From table 6.2a, the mean rupture force of the bacterial interactions with glass, PLL, PDA, Cell-Tak and BSA were found to be 0.13nN, 1.22nN, 1.73nN, 1.91nN, and 0.28nN respectively. The mean rupture force has then values in increasing order of $Bacteria(Force)_{\mathrm{Glass}} < Bacteria(Force)_{\mathrm{BSA}} < Bacteria(Force)_{\mathrm{PLL}} < Bacteria(Force)_{\mathrm{PDA}} < Bacteria(Force)_{\mathrm{Cell-Tak}}$. Note that the standard deviation is ± 1.00 for PDA and ± 0.23 for BSA surfaces that is 57% and 82% of their respective mean rupture force values. As the standard deviation are larger than the half of their mean values, it results in relatively wide distributions of obtained ruptures forces for PDA and BSA surfaces. For obtained unbinding events with a wide distribution, a force rupture or length is less likely to occur than for obtained unbinding events with a narrow distribution. From table 6.3a, the mean rupture length of the bacterial interactions with glass, PLL, PDA, Cell-Tak and BSA were found to be 32nm, 58nm, 65nm, 108nm, and 24nm respectively. The mean rupture length has then values in increasing order of $Bacteria(Length)_{\mathrm{BSA}} < Bacteria(Length)_{\mathrm{Glass}} < Bacteria(Length)_{\mathrm{PLL}} < Bacteria(Length)_{\mathrm{PDA}} < Bacteria(Length)_{\mathrm{Cell-Tak}}$. Note that the standard deviation is ± 47.8 for glass, ± 32.4 for PDA, and ± 17.7 for BSA surfaces, that is 148%, 50% and 73% of their respective mean rupture length values. As the standard deviation are larger than the half of the mean values, it results in relatively wide distributions of obtained rupture lengths for glass, PDA and BSA surfaces.

As expected, the bacteria *DH5alfa* are interacting stronger with PLL, PDA, and Cell-Tak surfaces than with glass and BSA surfaces, which reflects the bacterial adhesive and repulsive nature of these molecules, respectively. The BSA layer can be defined as a

bacterial repulsive surface because of its small interactions with the bacteria *DH5alfa*. The PLL, PDA, and Cell-Tak layers can be characterized as bacterial adhesive surfaces because of their relatively high interactions with the bacteria *DH5alfa*. The mean rupture force value of 1.91nN for the Cell-Tak layer are the highest value obtained from the bacterial force measurements. The mean rupture force value for the PDA layer are also close to the Cell-Tak value by having a difference of only 0.18nN. The bacterial rupture force distribution for PDA surfaces are though wider than the bacterial rupture force distribution for Cell-Tak surfaces. The Cell-Tak and PDA surfaces contain both certain amounts of the polyphenolic proteins secreted from the mussel *Mytilus edulis* as mentioned in section 4.3. Since the mean rupture force value for the PDA layer is close the mean rupture force value for the Cell-Tak layer, it indicates the importance of the polyphenolic proteins role in the interactions with the bacterias *DH5alfa*, which can be applied in the optimization of bacterial micro arrays. Although, the control measurements obtained should be considered for the PDA and Cell-Tak surfaces since there is a great difference between the mean rupture forces.

The type of interactions involved in the bacterial interactions can also be assessed by comparing the mean rupture force for the PDA and Cell-Tak surface values with the PLL surface values. As the positively charged PLL surface is assumed to form mostly electrostatic interactions with the negatively charged bacteria, it can be put into question whether PDA and Cell-Tak surfaces are exhibiting hydrophobic, hydrophilic, or hydrogen bond interactions with the bacteria since the mean rupture force values for the PDA and Cell-Tak layers are higher than the mean rupture force for the PLL layer. As mentioned in section 4.3, polyphenolic proteins consist mainly of L-DOPA that can exhibit zwitterionic properties dependent on the pH. When formed as a peptide its interaction potentials will mostly rely on the phenylene ring via its hydroxyl groups. The aromatic ring may then play a role in the bacterial interactions with the PDA and Cell-Tak surfaces.

Considering the rupture lengths obtained from the bacterial interactions, the PLL, PDA, and Cell-Tak layers have higher mean rupture lengths than glass and BSA layers. This also reflects the bacterial adhesive or repulsive nature of the surfaces, since BSA and glass surfaces have a smaller mean rupture length than PLL, PDA, and Cell-Tak surfaces. The Cell-Tak surface exhibits the highest value of the mean rupture length obtained from the bacterial force measurements. It should also be noted that the bacterial interactions with the Cell-Tak surface have a mean rupture length value of 108nm which is close to twice the value of the PLL or PDA surfaces. This might indicate the possibility that an extension of the Cell-Tak proteins or an extension of the appendages of the bacteria are occurring in the unbinding events. The extension of Cell-Tak proteins or appendages of

the bacteria would indicate a combination of non-covalent interactions being involved in the unbinding events (as Van der Waals, electrostatic, hydrophobic or hydrophilic, hydrogen bonds). It is unknown if these unbinding events can be considered as specific since multiple interactions are assumed to occur in each unbinding event, making it difficult to characterize individual interactions between a single bacterium and the Cell-Tak. Multiple interactions are generally assumed to occur since multiple bacteria are present on the AFM tip. It is suggested to further explore the bacterial interactions with Cell-Tak surfaces in terms of the force spectroscopy parameters, liquid medium or the Cell-Tak layer preparation as printing with PDMS stamp or regular incubation methods.

The bacterial interactions measured with relevance to the optimization of bacterial micro arrays indicate that the use of PDA or Cell-Tak as a bacterial adhesive layer would result in a higher bacterial adhesion with a higher stability than when using PLL. The bacterial viability is difficult to determine based on the rupture force or length. Although a bacterial cell death would occur if the bacterial adhesion in a micro array is limiting bacterial motility or is altering the cell membrane functions as proton pumps, transport through porins, or other biomolecular motors. How the bacterial adhesive nature of PDA and Cell-Tak influence the bacterial cell can be determined by observing its fluorescence as a function of the membrane integrity of the cell. The company "Life technologies" is already supplying LIVE/DEAD Baclight Viablility Kit (Invitrogen, kit L7012) for such purposes. The printed BSA on glass by the use of a flat PDMS stamp shows to function as a bacterial repulsive surface. Small rupture forces and lengths were measured for the BSA surface indicating that the surface is relatively inert to bacterial adhesions. The bacterial adhesion to BSA surfaces in bacterial micro arrays would be unstable and possibly detach from the BSA surface because of the bacterias motility, brownian motion, or simple washing procedures performed to remove excess bacterias when immobilizing bacterias in the micro arrays.

However, the experimental and analytical challenges mentioned in section 7.1 and 7.2 should be noted such that the bacterial interactions dependency on the number of bacterias present on the AFM tip are unknown and could be a significant factor in the measuring of bacterial rupture forces or lengths. Some suggestions were mentioned in section 7.1 how to measure bacterial interactions with a higher accuracy.

7.4.2 Comparison with other AFM force measurements of bacterial interactions

The obtained rupture forces or lengths are comparable to other reports and systems, even though other surfaces and other bacteria have been in focus when measuring bacterial interactions. Other reports have been using similar AFM force spectroscopy setup, by having bacteria immobilized on the tip and probing certain surfaces of interests. The force interaction between *Lactococcus lactis* bacteria and pig gastrin mucin reported by Dague et al [21] shows obtained forces in range under 1.00nN, while reports from Kang and Elimelech [24] showed force interactions obtained between different bacteria and quartz surface to be in range from 0.76nN to 2.79nN. Reports from Harimawan et al [22] explored also the bacterial interactions with stainless steel surface under a certain contact time from 0 to 60s. For 0s contact time the bacterial force interactions were in range from 0.65nN to 3.84nN, while for 60s contact time the bacterial interactions were in range from 1.44nN to 8.53nN. As these reports show bacterial adhesion forces to be in range from 0nN to 8.53nN, it indicates that a relatively wide range of rupture forces can be expected when performing AFM measurements between bacteria and surfaces.

Reports from Beaussart et al.[29] explore the bacterial interactions between the bacteria *Lactobacillus plantarum* and biotic (lectin monolayer) or abiotic (hydrophobic monolayer) surfaces. The bacterial interaction with the hydrophobic surface showed an adhesion force from 0.25nN to 2.5nN and rupture length from 100nm to 600nm, while the bacterial interaction with lectin monolayer showed a mean adhesion force of 0.25nN and rupture lengths from 25nm to 250nm. As bacterial interaction with Cell-Tak surfaces in this project shows a mean rupture force and length of 1.91nN and 108.4nm respectively, this might supports the indication that hydrophobic interactions are involved in the bacterial interaction with the Cell-Tak surface. In section 7.4.1 it was mentioned that hydrophobic interactions most likely are involved in the bacterial interactions with the Cell-Tak surface since the extended rupture lengths and multiple force peaks are consistent with the stretching and unfolding of cell surface proteins or Cell-Tak proteins. The bacterial interactions with the lectin monolayers show also that a specific bacterial interactions could exist in a range under 1.00nN with rupture length between 25-250nm. Such a range of rupture forces and length was not observable in the force-distance curves in this project, though. Beaussart et al [29] performed also bacterial force measurements on hydrophilic surfaces that showed an adhesion force of 0.2nN and rupture length from 250nm to 500nm, where the extended rupture length and well defined force peeks indicated that glycopolymers on the surface of the probiotic bacteria were stretched. The bacterial interactions with BSA surfaces obtained in this project had mean rupture force and length of 0.28nN and 24.1nm, respectively. Whether the bacterial interactions with

the BSA surface is small because of hydrophilic interactions are unknown, but similar experiments to Beaussart et al.[29] could be performed by using bacteria that express mostly glycopolymers on the cell surface to measure hydrophilic interactions with the BSA surface.

The comparison of the bacterial AFM experiments mentioned above helps to assess the validity and mechanisms behind the bacterial force measurements obtained in this project. There are still some mechanisms behind the bacterial adhesion to Cell-Tak, PDA and BSA that remain unclear and should be further explored. Characterizing the type and strength of the driving interaction forces behind the bacterial adhesion or repulsion to surfaces would be useful in the optimization of bacterial micro arrays. Bacterial AFM force measurements, PeakForce QNM AFM mode supplied by the company Bruker, or the MAPT technique mentioned in section 4.3.4 can be performed to uncover factors involved in the bacterial adhesion mechanisms to bacterial adhesive or repulsive surfaces.

Chapter 8

Conclusion

Bacterial force measurements were performed with AFM to investigate the interactions of *DH5alfa* bacterias with BSA, PDA, Cell-Tak and PLL layers on glass surfaces. The investigations were performed with intention to optimize bacterial micro arrays. The optimization is in terms of choosing the proper molecules for bacterial adhesion and repulsion. The mean rupture forces were found to be 0.13nN, 0.28nN, 1.22nN, 1.73nN, and 1.91nN for glass, BSA, PLL, PDA, and Cell-Tak surfaces respectively. The mean rupture lengths were found to be 32nm, 24nm, 58nm, 65nm, and 108nm for glass, BSA, PLL, PDA and Cell-Tak surfaces respectively. The presence of bacteria on the AFM tip were validated before and after AFM experiments by the use of fluorescence microscopy and SEM. Conclusively, the bacteria *DH5alfa* shows to interact stronger with PLL, PDA and Cell-Tak surfaces than for glass and BSA surfaces as seen from the mean rupture forces and lengths. Bacterial interactions with Cell-Tak and PDA surfaces show to exhibit mean rupture forces that is higher than the mean rupture force for PLL surfaces. The bacterial interactions with Cell-Tak surfaces show also to have mean rupture length value that is close to or larger than twice the mean rupture length value of bacterial interactions with glass, BSA, PDA, and PLL surfaces. PDA or Cell-Tak can be defined as optimal bacterial adhesive layers in bacterial micro arrays because of their larger mean rupture forces and lengths values than the PLL values. BSA can be characterized as a bacterial inert or repulsive layer because of its small mean rupture force and length. The bacterial viability on PDA and Cell-Tak surfaces was not explored in this project, but it can be assessed by the use of the LIVE/DEAD Baclight Viablility Kit (Invitrogen, kit L7012) supplied by the company Life Technologies.

Since a cluster of bacteria are interacting with the bacterial adhesive or repulsive surfaces, it is unknown if the bacterial interactions with surfaces are dependent on the

number of bacteria being immobilized on the tip. AFM force measurements of bacterial interactions with surfaces can be obtained with a higher accuracy by the use of a colloidal glass bead on the AFM tip as presented by Beaussert et al.[29]. This way of immobilizing and validating the presence of bacteria on the AFM tip minimize time consuming procedures of control measurements and SEM investigations of the AFM tip after the force measurements. The use of a simple, less time consuming and accurate AFM technique for bacterial force measurements would open up for the possibility to explore the bacterial interaction with the bacterial adhesive or repulsive surfaces as a function of the liquid medium, contact time or loading rate.

The bacterial interactions with Cell-Tak surface shows to have extended rupture lengths with multiple force peaks obtained that indicates stretching and unfolding of the Cell-Tak proteins or the bacterial cell surface proteins. The combination of non-covalent interactions behind this bacterial adhesion is not clear, but it is assumed to involve electrostatic and hydrophobic interactions. As the AFM images shows that the Cell-Tak layer is non-uniform, further force measurements of bacterial interactions with Cell-Tak surfaces are suggested to be investigated. The investigation of bacterial interactions with the Cell-Tak surface should also consist of using alternative preparation methods of Cell-Tak on glass surfaces as micro contact printing or other incubation methods. To further optimize bacterial micro arrays and to investigate the factors involved in bacterial adhesion to bacterial adhesive or repulsive surfaces, characterization techniques like PeakForce QNM AFM mode supplied by the company Bruker, mapping using accumulated probe trajectories (MAPT) technique, or bacterial AFM force measurements would have the possibility to facilitate such investigations.

Appendix A

Expressions from the extended DLVO theory

The extended DLVO theory is expressed in equation 4.1 in section 4.1 and the decay of these forces depends on the geometry of interacting bodies and the type of force.

Interaction energy terms used in XDLVO approach

Lifshitz–van der Waals interaction energy, $G^{LW}(H)$

Sphere–sphere
$$-\frac{A}{12}\left[\frac{y}{x^2+xy+x}+\frac{y}{x^2+xy+x+y}+2\ln\left(\frac{x^2+xy+x}{x^2+xy+x+y}\right)\right]\left(\frac{1}{1+1.77(2\pi H/\lambda)}\right),\quad \lambda = 1000\ \text{Å} \tag{7}$$

Sphere–flat plate
$$-\frac{A}{12}\left[\frac{2a(H+a)}{H(H+2a)}-\ln\left(\frac{H+2a}{H}\right)\right]\left(\frac{1}{1+1.77(2\pi H/\lambda)}\right),\quad \lambda = 1000\ \text{Å} \tag{8}$$

Electrostatic interaction energy, $G^{EL}(H)$

Sphere–sphere
$$\frac{\pi\varepsilon a_1 a_2(\zeta_1^2+\zeta_2^2)}{a_1+a_2}\left[\frac{2\zeta_1\zeta_2}{\zeta_1^2+\zeta_2^2}\ln\left(\frac{1+e^{-\kappa H}}{1-e^{-\kappa H}}\right)+\ln(1-e^{-2\kappa H})\right] \tag{9}$$

Sphere–flat plate
$$\pi\varepsilon a(\zeta_1^2+\zeta_2^2)\left[\frac{2\zeta_1\zeta_2}{\zeta_1^2+\zeta_2^2}\ln\left(\frac{1+e^{-\kappa H}}{1-e^{-\kappa H}}\right)+\ln(1-e^{-2\kappa H})\right] \tag{10}$$

Acid–base interaction energy, $G^{AB}(H)$

Sphere–sphere
$$\pi a\lambda\,\Delta G_{adh}^{AB}\,e^{[(d_0-H)/\lambda]} \tag{11}$$

Sphere–flat plate
$$2\pi a\lambda\,\Delta G_{adh}^{AB}\,e^{[(d_0-H)/\lambda]} \tag{12}$$

FIGURE A.1: Terms used in for the interaction energies in the extended DLVO approach [31, 32]

From the equations in figure A.1, H is separation distance, a is radius of solid particle, ζ is zeta-potential, κ is the double layer thickness^{-1}, A is the Hamaker constant, $x = \frac{H}{a_1+a_2}$, $y = \frac{a_1}{a_2}$, d_0 is the minimum separation between two surfaces, λ is the correlation length of molecules in liquid, and $\Delta G_{\text{adh}}^{AB}$ is the acid base component of the surface and interfacial free energies[31, 32].

Appendix B

Methods, procedures and analysis

B.1 Calibration of force measurements with Bioscope Catalyst

The first step of the calibration procedure in Bioscope Catalyst consisted of bringing the clean, polydopamine, or bacterial coated cantilever in contact with a clean glass surface. This to measure the linear readout of the photo detector to obtain the the deflection error sensitivity in nm/V. The image of Bioscope Catalyst program interface is shown in figure B.1.

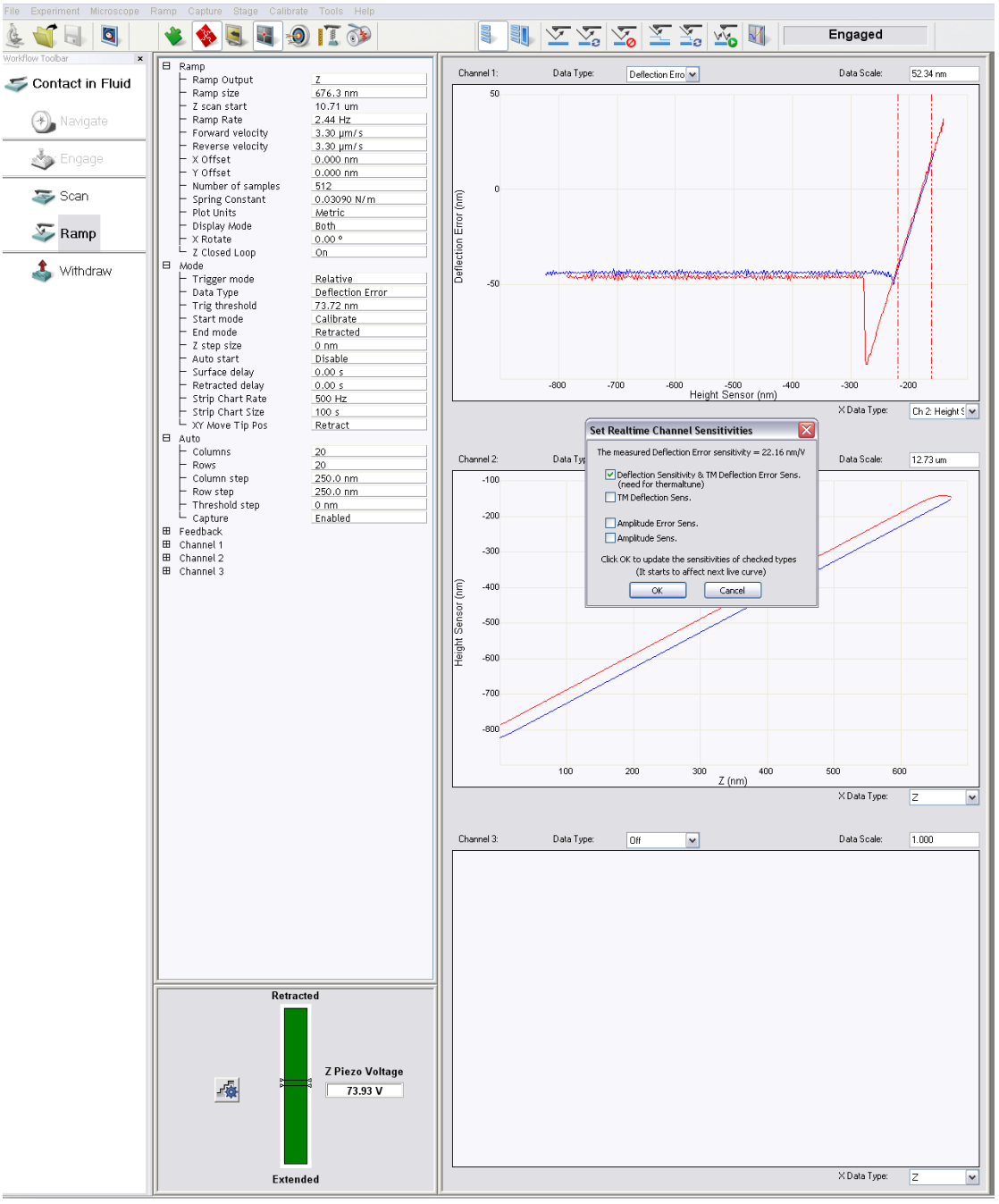

FIGURE B.1: The interface of the Bioscope Catalyst program. The deflection error-distance curve was labeled with two red lines to calculate the deflection error sensitivity with the Bioscope Catalyst program.

The linear readout in the deflection error-distance curve was labeled with two red lines to calculate the deflection error sensitivity with the Bioscope Catalyst program by using the function button close to the "engage" text.

Next step consisted of having the cantilever withdrawn from the surface and performing thermal tuning to find the spring constant of the cantilever. The thermal tuning is performed by exciting the cantilever at a certain frequency specter to find the resonance domains of the cantilever. The obtained frequency domain of the cantilever was then fitted with the Lorentzian function to obtain the spring constant. The image of the Bioscope Catalyst program interface is shown in figure B.2.

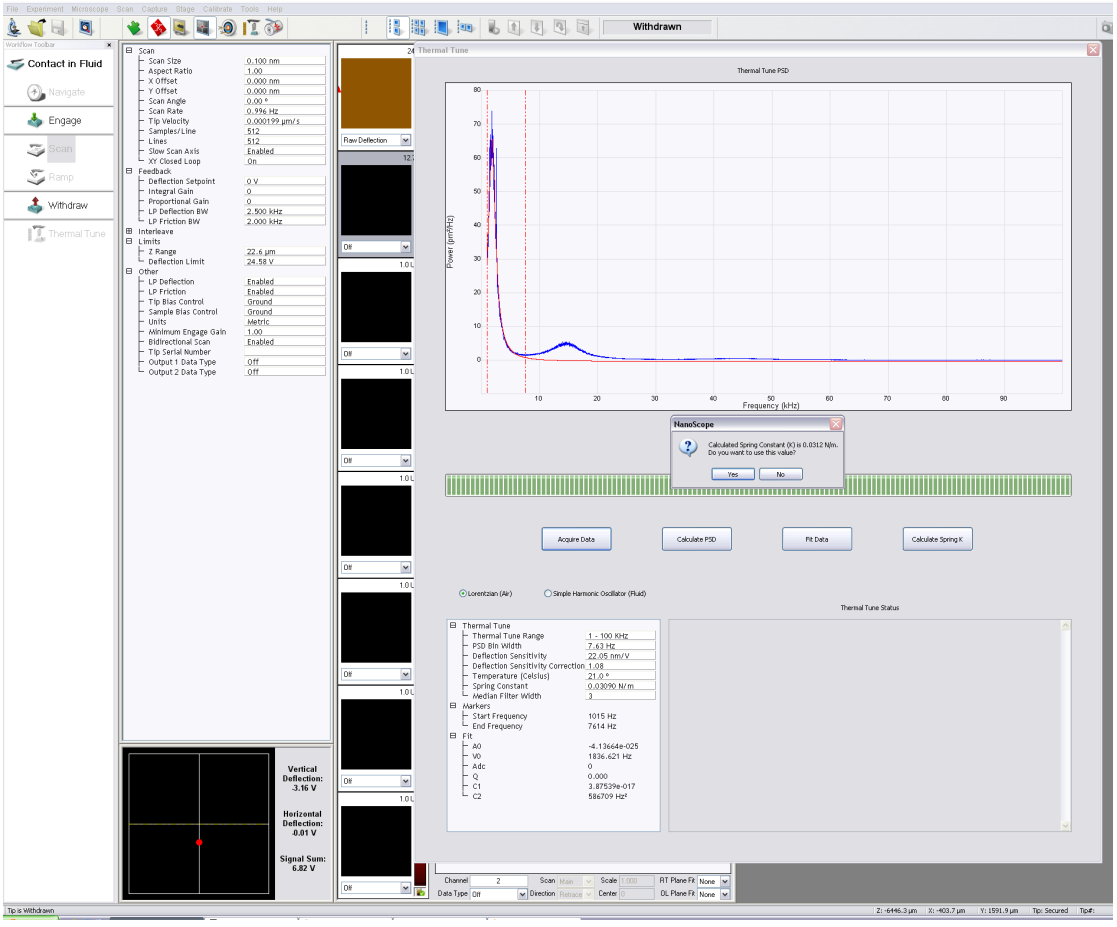

FIGURE B.2: The interface of the Bioscope Catalyst program. The obtained frequency domain of the cantilever was labeled with two red lines to fit the Lorentzian function and to calculate the spring constant of the cantilever with the Bioscope Catalyst program.

The obtained frequency domain from the thermal tuning was labeled with two red lines to fit the Lorentzian function and to calculate the spring constant of the cantilever with the Bioscope Catalyst program. The thermal tune function button are present above the instrument parameters.

B.2 Manual for the IDL and Matlab based analysis

B.2.1 IDL analysis

The IDL program "difordisveeco3.pro" enables collection of rupture forces and rupture lengths that are further analyzed and plotted in Matlab. The IDL program was developed to analyze the force-distance curves obtained from the Bioscope Catalyst and some simple factors needed to be taken into consideration when analyzing the force-distance curves. The user interface of the IDL program are shown in figure B.3.

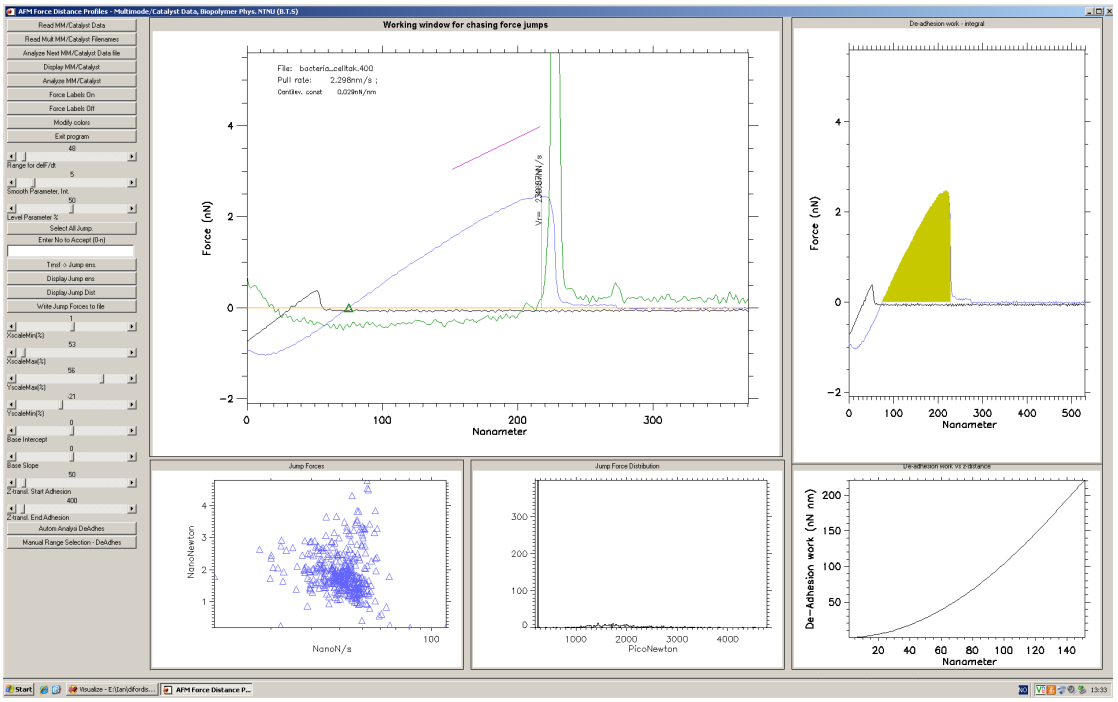

FIGURE B.3: The interface of the IDL program. The graphs on the top are showing the magnitude of the rupture force, and the graph at the bottom to the right show the de-adhesion work and rupture length of the magnitude of the rupture force.

The blue line in the top of figure B.3 shows the retracting force-distance curve, the black line shows the approaching force-distance curve, the green line shows the derivative of the retracting force-distance curve, and the yellow curve shows the baseline and force magnitude of the force-distance curve. The derivative curve were set for each force-distance curve by adjusting the smooth parameter and the setting of range for the derivative curve. The yellow base line was set at the same level as the non interacting range of the retracting force-distance curve to make sure the force ruptures are measured correctly. The base line was made by calculating an average value of a given range of the displacement range line were the interactions are less likely to occur. The yellow area in the top and right in figure B.3 shows the de-adhesion work obtained from the retracted force-distance curve. The de-adhesion work and rupture length are also plotted below

of this graph. The collection of rupture force, rupture length, and de-adhesion work data are transferred to a text file for each analysis and finally written when the set of force-distance curves are finished.

B.2.2 Matlab scripts and analysis

The histograms were made with a simple script that are plotting several histograms in the same graph labeled with colors and legends. The "ideal" number of bins were found as described in section 5.6.1. The function "calcnbins" used to calculate the " ideal" number of bins were found at the Matlab central[62]. The script are shown in figure B.4.

```
x1=load('histba_glass.txt'); % Load text files containing data of rupture forces or rupture lengths
x2=load('histba_pll.txt');
x3=load('histba_dpa.txt');
x4=load('histba_celltak.txt');
x5=load('histba_bsa.txt');

nb1=calcnbins(x1); % Calculate the "ideal" number of bins by the use of function calcnbins
nb2=calcnbins(x2);
nb3=calcnbins(x3);
nb4=calcnbins(x4);
nb5=calcnbins(x5);

pd1= fitdist(x1,'normal'); % Calculating and displaying the mean average and variance of the rupture forces and rupture lengths
pd2= fitdist(x2,'normal');
pd3= fitdist(x3,'normal');
pd4= fitdist(x4,'normal');
pd5= fitdist(x5,'normal');
display(pd1);
display(pd2);
display(pd3);
display(pd4);
display(pd5);

[n1,xout1]=hist(x1,nb1); % Get the values from the histograms
[n2,xout2]=hist(x2,nb2);
[n3,xout3]=hist(x3,nb3);
[n4,xout4]=hist(x4,nb4);
[n5,xout5]=hist(x5,nb5);

bar(xout1,(n1/sum(n1))*100,[min(x1),max(x1)],'hist'); % Plot the histograms in the same graph with frequency on the y-axis and measured values on the x-axis
hold on
bar(xout2,(n2/sum(n2))*100,[min(x2),max(x2)],'hist');
hold on
bar(xout3,(n3/sum(n3))*100,[min(x3),max(x3)],'hist');
hold on
bar(xout4,(n4/sum(n4))*100,[min(x4),max(x4)],'hist');
hold on
bar(xout5,(n5/sum(n5))*100,[min(x5),max(x5)],'hist');
hold off

h=findobj(gca, 'Type', 'patch');
set(h(5),'FaceColor','w','EdgeColor','r','LineWidth',1.7); % Get the histograms and plot them with colors
set(h(4),'FaceColor','w','EdgeColor','g','LineWidth',1.7);
set(h(3),'FaceColor','w','EdgeColor','b','LineWidth',1.7);
set(h(2),'FaceColor','w','EdgeColor','y','LineWidth',1.7);
set(h(1),'FaceColor','w','EdgeColor','k','LineWidth',1.7);
set (h, 'FaceAlpha', 0.8);

xlabel('Adhesion force (nN)','FontSize',20); % Label y-axis and x-axis
ylabel('Frequency (%)','FontSize',20);

h = legend([h(5) h(4) h(3) h(2) h(1)],'Glass','Poly-L-lysine','Polydopamine','Cell-Tak', 'Bovine serum albumin',5); % Make legends for the different histograms
set(h,'FontSize',20);
```

FIGURE B.4: Script of the plotting of histograms in Matlab

The mean average and standard deviation were also collected from the histograms by the use of "fitdist" function that is integrated in the Matlab program. "fitdist" are producing a mean average and standard deviation based on a Gaussian distribution of the data. The "fitdist" function have also the possibility to produce lambda values based on the Poisson distribution.

Appendix C

Results

All the obtained SEM images of the bacterial coated AFM tips after each experiment are presented in this section.

C.1 SEM images of bacterial coated AFM tips after each AFM experiment

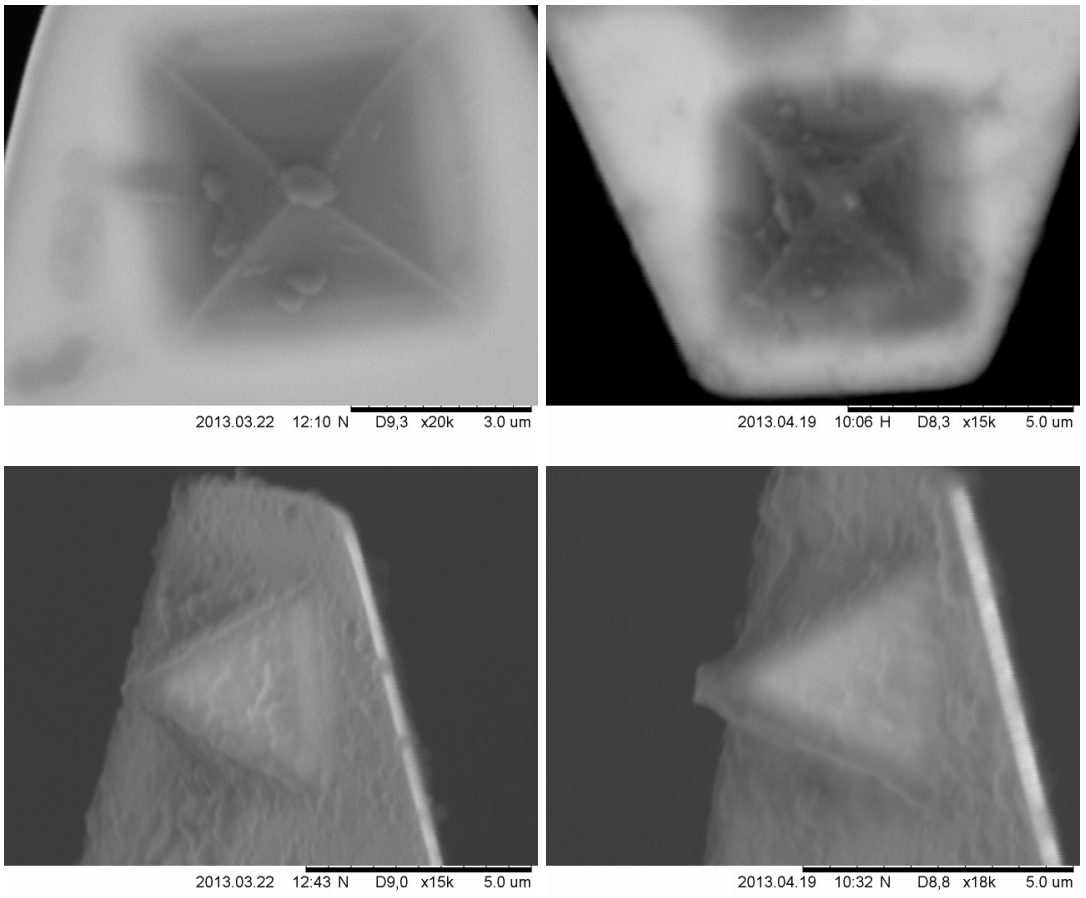

(A) Bacterial *DH5alfa* coated AFM tip after measuring interactions on glass

(B) Bacterial *DH5alfa* coated AFM tip after measuring interactions on PLL surface

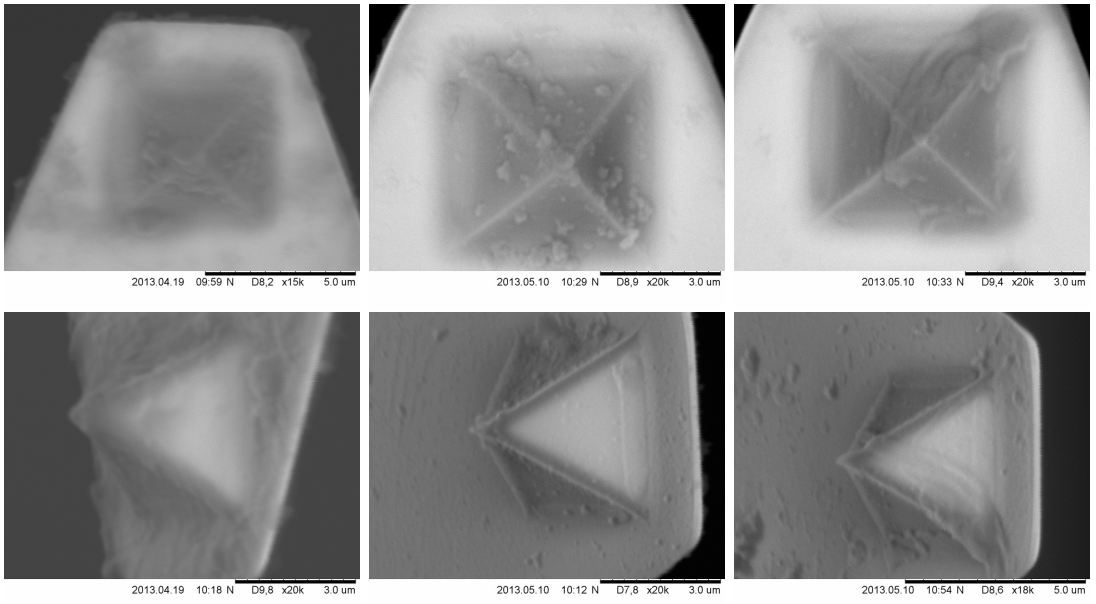

(C) Bacterial *DH5alfa* coated AFM tip after measuring interactions on PDA surface

(D) Bacterial *DH5alfa* coated AFM tip after measuring interactions on Cell-Tak surface

(E) Bacterial *DH5alfa* coated AFM tip after measuring interactions on BSA surface

FIGURE C.1: SEM images of bacterial *DH5alfa* coated AFM tips after each AFM experiment

References

[1] I. Barbulovic-Nad, M. Lucente, Y. Sun, M. Zhang, A. R. Wheeler, and M. Bussmann, "Bio-microarray fabrication techniquesa review," *Critical Reviews in Biotechnology*, vol. 26, no. 4, pp. 237–259, 2006.

[2] S. W. Howell, H. D. Inerowicz, F. E. Regnier, and R. Reifenberger, "Patterned protein microarrays for bacterial detection," *Langmuir*, vol. 19, no. 2, pp. 436–439, 2003.

[3] Y. Kuang, I. Biran, and D. R. Walt, "Living bacterial cell array for genotoxin monitoring," *Analytical Chemistry*, vol. 76, no. 10, pp. 2902–2909, 2004.

[4] I. Biran, D. M. Rissin, E. Z. Ron, and D. R. Walt, "Optical imaging fiber-based live bacterial cell array biosensor," *Analytical Biochemistry*, vol. 315, no. 1, pp. 106 – 113, 2003.

[5] E. Steager, J. Patel, C.-B. Kim, D. Yi, W. Lee, and M. Kim, "A novel method of microfabrication and manipulation of bacterial teamsters in low reynolds number fluidic environments," *Microfluidics and Nanofluidics*, vol. 5, pp. 337–346, 2008. 10.1007/s10404-007-0252-6.

[6] M. Kim and K. Breuer, "Microfluidic pump powered by self-organizing bacteria," *Small*, vol. 4, no. 1, pp. 111–118, 2008.

[7] M. J. Kim and K. S. Breuer, "Controlled mixing in microfluidic systems using bacterial chemotaxis," *Analytical Chemistry*, vol. 79, no. 3, pp. 955–959, 2007.

[8] S. Alom Ruiz and C. S. Chen, "Microcontact printing: A tool to pattern," *Soft Matter*, vol. 3, pp. 168–177, 2007.

[9] F. Yap and Y. Zhang, "Protein and cell micropatterning and its integration with micro/nanoparticles assembly," *Biosensors and Bioelectronics*, vol. 22, no. 6, pp. 775 – 788, 2007.

[10] I. Wong, X. Ding, C. Wu, and C.-M. Ho, "Accurate and effective live bacteria microarray patterning on thick polycationic polymer layers co-patterned with hmds," *RSC Adv.*, vol. 2, pp. 7673–7676, 2012.

[11] C. Thibault, C. Severac, E. Trvisiol, and C. Vieu, "Microtransfer molding of hydrophobic dendrimer," *Microelectronic Engineering*, vol. 83, no. 49, pp. 1513 – 1516, 2006.

[12] P. Krsko, J. B. Kaplan, and M. Libera, "Spatially controlled bacterial adhesion using surface-patterned poly(ethylene glycol) hydrogels," *Acta Biomaterialia*, vol. 5, no. 2, pp. 589 – 596, 2009.

[13] I. D. Muri, "Project report titled "atomic force microscope and confocal laser scanning microscope characterizations for optimization of microcontact printed patterns on surfaces for single bacterial micro arrays for gene expression studies"." Carried out at the Biophysics and Medical Technology research group, Department of Physics, Norwegian University of Science and Technology as a part of a Master thesis, 2012.

[14] N. B. Arnfinnsdottir, "Unpublished work and images obtained during the development and optimization of bacterial microarrays." Carried out at the Biophysics and Medical Technology research group, Department of Physics, Norwegian University of Science and Technoogy as a part of a Ph.D. thesis, 2013.

[15] M. S. Catharina de Lange Davies and B. T. Stokke, *Biophysical Nanotechnologies, Lecture notes TFY4265 and FY8906 Biophysical Microtechnologies*. Biophysics and Medical Technology, Dept. of physics, NTNU, 2011.

[16] P. information for Veeco AFM, "http://www.veeco.com/pdfs/library/spm_guide_0829_05_166.pdf and http://www.cigs.unimo.it/cigsdownloads/labs/afm2/manuali_letture/multimode_manual_revb.pdf."

[17] Roughness calculations with the AFM Nanoscope software, "Nanoscope software user guide."

[18] J. Helenius, C.-P. Heisenberg, H. E. Gaub, and D. J. Muller, "Single-cell force spectroscopy," *Journal of Cell Science*, vol. 121, no. 11, pp. 1785–1791, 2008.

[19] C. Yuan, A. Chen, P. Kolb, and V. T. Moy, "Energy landscape of streptavidinbiotin complexes measured by atomic force microscopy," *Biochemistry*, vol. 39, no. 33, pp. 10219–10223, 2000.

[20] T. A. Camesano, Y. Liu, and M. Datta, "Measuring bacterial adhesion at environmental interfaces with single-cell and single-molecule techniques," *Advances in Water Resources*, vol. 30, pp. 1470–1491, June 2007.

[21] E. Dague, D. T. L. Le, S. Zanna, P. Marcus, P. Loubiere, and M. Mercier-Bonin, "Probing in vitro interactions between lactococcus lactis and mucins using afm," *Langmuir*, vol. 26, no. 13, pp. 11010–11017, 2010.

[22] A. Harimawan, A. Rajasekar, and Y.-P. Ting, "Bacteria attachment to surfaces afm force spectroscopy and physicochemical analyses," *Journal of Colloid and Interface Science*, vol. 364, no. 1, pp. 213 – 218, 2011.

[23] Y.-L. Ong, A. Razatos, G. Georgiou, and M. M. Sharma, "Adhesion forces between e. coli bacteria and biomaterial surfaces," *Langmuir*, vol. 15, no. 8, pp. 2719–2725, 1999.

[24] S. Kang and M. Elimelech, "Bioinspired single bacterial cell force spectroscopy," *Langmuir*, vol. 25, no. 17, pp. 9656–9659, 2009. PMID: 19634872.

[25] D. Le, Y. Gurardel, P. Loubire, M. Mercier-Bonin, and E. Dague, "Measuring kinetic dissociation/association constants between lactococcus lactis bacteria and mucins using living cell probes," *Biophysical Journal*, vol. 101, pp. 2843–2853, Dec. 2011.

[26] V. Vadillo-Rodrguez, H. Busscher, W. Norde, J. De Vries, R. Dijkstra, I. Stokroos, and H. Van Der Mei, "Comparison of atomic force microscopy interaction forces between bacteria and silicon nitride substrata for three commonly used immobilization methods.," *Appl Environ Microbiol*, vol. 70, pp. 5441–5446–, Sept. 2004.

[27] Y. Bar-Or, "The effect of adhesion on survival and growth of microorganisms," *Experientia*, vol. 46, no. 8, pp. 823–826, 1990.

[28] E. Potthoff, O. Guillaume-Gentil, D. Ossola, J. Polesel-Maris, S. LeibundGut-Landmann, T. Zambelli, and J. A. Vorholt, "Rapid and serial quantification of adhesion forces of yeast and mammalian cells," *PLoS ONE*, vol. 7, p. e52712, 12 2012.

[29] A. Beaussart, S. El-Kirat-Chatel, P. Herman, D. Alsteens, J. Mahillon, P. Hols, and Y. Dufre'ne, "Single-cell force spectroscopy of probiotic bacteria," *Biophys J*, vol. 104, pp. 1886–1892, May 2013.

[30] J. Ubbink and P. Schr-Zammaretti, "Colloidal properties and specific interactions of bacterial surfaces," *Current Opinion in Colloid & Interface Science*, vol. 12, no. 45, pp. 263 – 270, 2007.

[31] P. Sharma and K. H. Rao, "Adhesion of paenibacillus polymyxa on chalcopyrite and pyrite: surface thermodynamics and extended {DLVO} theory," *Colloids and Surfaces B: Biointerfaces*, vol. 29, no. 1, pp. 21 – 38, 2003.

[32] K. Hori and S. Matsumoto, "Bacterial adhesion: From mechanism to control," *Biochemical Engineering Journal*, vol. 48, no. 3, pp. 424 – 434, 2010. ¡ce:title¿Invited Review Issue 2010¡/ce:title¿.

[33] A. Komaromy, R. I. Boysen, H. Zhang, I. McKinnon, F. Fulga, M. T. Hearn, and D. V. Nicolau, "Micro-structures modulate bacterial cell viability and attachment," *Microelectronic Engineering*, vol. 86, no. 46, pp. 1431 – 1434, 2009. ¡ce:title¿MNE 08¡/ce:title¿ ¡ce:subtitle¿The 34th International Conference on Micro- and Nano-Engineering (MNE)¡/ce:subtitle¿.

[34] C.-H. Choi, J.-H. Lee, T.-S. Hwang, C.-S. Lee, Y.-G. Kim, Y.-H. Yang, and K. Huh, "Preparation of bacteria microarray using selective patterning of polyelectrolyte multilayer and poly(ethylene glycol)-poly(lactide) diblock copolymer," *Macromolecular Research*, vol. 18, pp. 254–259, 2010.

[35] S. Rozhok, Z. Fan, D. Nyamjav, C. Liu, C. A. Mirkin, and R. C. Holz, "Attachment of motile bacterial cells to prealigned holed microarrays," *Langmuir*, vol. 22, no. 26, pp. 11251–11254, 2006.

[36] A. Cerf, J.-C. Cau, and C. Vieu, "Controlled assembly of bacteria on chemical patterns using soft lithography," *Colloids and Surfaces B: Biointerfaces*, vol. 65, no. 2, pp. 285 – 291, 2008.

[37] R. L. Meyer, X. Zhou, L. Tang, A. Arpanaei, P. Kingshott, and F. Besenbacher, "Immobilisation of living bacteria for afm imaging under physiological conditions," *Ultramicroscopy*, vol. 110, no. 11, pp. 1349 – 1357, 2010.

[38] A. Cerf, J.-C. Cau, C. Vieu, and E. Dague, "Nanomechanical properties of dead or alive single-patterned bacteria," *Langmuir*, vol. 25, no. 10, pp. 5731–5736, 2009.

[39] Y. Oh, W. Jo, J. Lim, S. Park, Y. Kim, and Y. Kim, "Micropatterning of bacteria on two-dimensional lattice protein surface observed by atomic force microscopy," *Ultramicroscopy*, vol. 108, no. 10, pp. 1124 – 1127, 2008.

[40] B. Rowan, M. A. Wheeler, and R. M. Crooks, "Patterning bacteria within hyperbranched polymer film templates," *Langmuir*, vol. 18, no. 25, pp. 9914–9917, 2002.

[41] J. Lee, J. Jung, K. Na, P. Heo, and J. Hyun, "Polypeptide-mediated switchable microarray of bacteria," *ACS Applied Materials & Interfaces*, vol. 1, no. 7, pp. 1359–1363, 2009. PMID: 20355934.

[42] M. Moccia, G. N. Roviello, E. M. Bucci, C. Pedone, and M. Saviano, "Synthesis of a l-lysine-based alternate alpha,epsilon-peptide: A novel linear polycation with

nucleic acids-binding ability," *International Journal of Pharmaceutics*, vol. 397, pp. 179–183, Sept. 2010.

[43] T. Kawai, T. Kubota, J. Hiraki, and Y. Izumi, "Biosynthesis of ε-poly-l-lysine in a cell-free system of streptomyces albulus," *Biochemical and Biophysical Research Communications*, vol. 311, pp. 635–640, Nov. 2003.

[44] I.-L. Shih, M.-H. Shen, and Y.-T. Van, "Microbial synthesis of poly(ε-lysine) and its various applications," *Bioresource Technology*, vol. 97, pp. 1148–1159, June 2006.

[45] L. M. Rzepecki, K. M. Hansen, and J. H. Waite, "Characterization of a cystine-rich polyphenolic protein family from the blue mussel mytilus edulis l," *The Biological Bulletin*, vol. 183, pp. 123–137, Aug. 1992.

[46] R. Jensen and D. Morse, "The bioadhesive of phragmatopoma californica tubes: a silk-like cement containing l-dopa," vol. 158, no. 3, pp. 317–324, 1988.

[47] http://www.bdbiosciences.com/ptProduct.jsp?prodId=362331&catyId=775673&page=product, "Bd biosciences, cell-tak manual."

[48] M. Weinhold, S. Soubatch, R. Temirov, M. Rohlfing, B. Jastorff, F. S. Tautz, and C. Doose, "Structure and bonding of the multifunctional amino acid l-dopa on au(110)," *J. Phys. Chem. B*, vol. 110, pp. 23756–23769, Nov. 2006.

[49] C. Xu, M. Tian, L. Liu, H. Zou, L. Zhang, and W. Wang, "Fabrication and properties of silverized glass fiber by dopamine functionalization and electroless plating," *Journal of The Electrochemical Society*, vol. 159, no. 4, pp. D217–D224, 2012.

[50] http://www.sigmaaldrich.com/etc/medialib/docs/Sigma/Product_Information_Sheet/a7906pis.Par.0001.File.tmp/a7906pis.pdf, "Product information on bovine serum albumine from sigma-aldrich."

[51] K. A. Majorek, P. J. Porebski, A. Dayal, M. D. Zimmerman, K. Jablonska, A. J. Stewart, M. Chruszcz, and W. Minor, "Structural and immunologic characterization of bovine, horse, and rabbit serum albumins," *Molecular Immunology*, vol. 52, pp. 174–182, Oct. 2012.

[52] S. H. Lee and E. Ruckenstein, "Adsorption of proteins onto polymeric surfaces of different hydrophilicitiesa case study with bovine serum albumin," *Journal of Colloid and Interface Science*, vol. 125, pp. 365–379, Oct. 1988.

[53] S. B. Ken A.Dill, *Molecular Driving Forces, Statistical Thermodynamics in Chemistry and Biology*. Garland Science, 2002.

[54] R. Walder, N. Nelson, and D. K. Schwartz, "Super-resolution surface mapping using the trajectories of molecular probes," *Nat Commun*, vol. 2, pp. 515–, Nov. 2011.

[55] R. Walder, M. Kastantin, and D. K. Schwartz, "High throughput single molecule tracking for analysis of rare populations and events," *Analyst*, vol. 137, no. 13, pp. 2987–2996, 2012.

[56] M. J. Skaug and D. K. Schwartz, "Using the dynamics of fluorescent cations to probe and map charged surfaces," *Soft Matter*, vol. 8, no. 48, pp. 12017–12024, 2012.

[57] H.-W. Chien, W.-H. Kuo, M.-J. Wang, S.-W. Tsai, and W.-B. Tsai, "Tunable micropatterned substrates based on poly(dopamine) deposition via microcontact printing," *Langmuir*, vol. 28, no. 13, pp. 5775–5782, 2012.

[58] *Labwork and images obtained during Ian Damm Muri's Master project "Atomic force microscope measurements for surface and interaction characterization to optimize the surface patterning for bacterial micro arrays"*, 2013.

[59] D. Freedman and P. Diaconis, "On the histogram as a density estimator:l 2 theory," *Zeitschrift fr Wahrscheinlichkeitstheorie und Verwandte Gebiete*, vol. 57, no. 4, pp. 453–476, 1981.

[60] D. W. SCOTT, "On optimal and data-based histograms," *Biometrika*, vol. 66, no. 3, pp. 605–610, 1979.

[61] H. A. Sturges, "The choice of a class interval," *Journal of the American Statistical Association*, vol. 21, no. 153, pp. pp. 65–66, 1926.

[62] http://www.mathworks.com/matlabcentral/fileexchange/21033-calculate-number-of-bins-for-histogram, "Calculate number of bins for histogram (function "calcnbins")."

[63] T. Erdmann, S. Pierrat, P. Nassoy, and U. S. Schwarz, "Dynamic force spectroscopy on multiple bonds: Experiments and model," *EPL (Europhysics Letters)*, vol. 81, no. 4, p. 48001, 2008.

[64] C. Zhu, "Kinetics and mechanics of cell adhesion.," *J Biomech*, vol. 33, pp. 23–33–, Jan. 2000.

[65] A. Pierres, D. Touchard, A.-M. Benoliel, and P. Bongrand, "Dissecting streptavidin-biotin interaction with a laminar flow chamber," *Biophysical Journal*, vol. 82, no. 6, pp. 3214 – 3223, 2002.

[66] E. Fallman, S. Schedin, J. Jass, M. Andersson, B. E. Uhlin, and O. Axner, "Optical tweezers based force measurement system for quantitating binding interactions: system design and application for the study of bacterial adhesion," *Biosensors and Bioelectronics*, vol. 19, pp. 1429–1437, June 2004.

[67] J. Jass, S. Schedin, E. Fallman, E.llman, J. Ohlsson, U. J. Nilsson, B. E. Uhlin, and O. Axner, "Physical properties of escherichia coli p pili measured by optical tweezers," *Biophysical Journal*, vol. 87, pp. 4271–4283, Dec. 2004.